Characterization and Simulation of the Deformation and Failure Behavior of Printed Circuit Boards (PCB)

Dissertation

by

Peter Filipp Fuchs

prepared at the

Polymer Competence Center Leoben GmbH

and the

Chair of Materials Science and Testing of Polymers

submitted to the

Montanuniversität Leoben

Academic Advisor

Univ.-Prof. Dipl.-Ing. Dr. Gerald Pinter
Montanuniversität Leoben, Austria

Supervisor

Univ.-Prof. Dipl.-Ing. Dr. Zoltan Major
Johannes Kepler University Linz, Austria

Referees

Univ.-Prof. Dipl.-Ing. Dr. Gerald Pinter
Montanuniversität Leoben, Austria

Univ.-Prof. Dipl.-Ing. Dr. Zoltan Major
Johannes Kepler University Linz, Austria

Leoben, April 2012

I declare in lieu of oath, that I wrote this dissertation and performed the associated research myself, using only the support indicated in the acknowledgements and literature cited.

Leoben, April 2012 Dipl.-Ing. Peter Fuchs

ACKNOWLEDGEMENTS

First, I would like to thank Prof. Gerald Pinter and Prof. Zoltan Major for being my advisors and for the thorough reviewing of my dissertation and the associated papers. To Prof. Zoltan Major I am especially grateful for offering me the possibility to work in this interesting field of research and for having kept supporting me, in spite of difficult ancillary conditions, during the last years. His ideas and the various fruitful discussions contributed considerably to the success of this work. Prof. Gerald Pinter on the other hand, enabled, in a time of numerous personnel changes, a smooth continuation of the dissertation. Due to his personal commitment, he became acquainted with this topic very quickly and his guidance was an important element for the completion of this work.

I am indebted to AT&S Austria Technologie & Systemtechnik Aktiengesellschaft (Leoben, A) for acting as a project partner, for supplying the materials investigated in this dissertation and for performing complementary tests and analyses. Particularly I would like to thank Dr. Manfred Riedler and DI Markus Leitgeb for their valuable contribution to my understanding of printed circuit boards and their support during the last years. Special thanks go to the AT&S coworkers performing accurate and reliable measurements, being the basis of some of the papers within this thesis.

I am also very grateful to Prof. Thomas Antretter, who supported me in the field of finite element simulations. His expert knowledge and ideas were very helpful and important in several cases.

I would like to thank my former fellow students Irena Bergant, Maximilian Tonjec, and Klaus Fellner, who conducted numerous experimental tests within their bachelor thesis or master thesis. Their work has been an essential contribution to the dissertation.

I also would like to express my gratitude to my colleagues (Daniel Tscharnuter, Michael Jerabek, Michael Berer and Andreas Hausberger) who were always happy to discuss challenging tasks with me. Their help and support from the professional and human point of view were important for the progress of this work.

Last but not least, my gratitude goes to my girlfriend Lenka Lampl, who always gave me the necessary support and trust I needed to complete my thesis. She was the one who picked me up when I was desperate about one of the smaller or bigger problems which I encountered during the last years.

The research work of this dissertation was performed at the Polymer Competence Center Leoben GmbH (PCCL, Austria) within the framework of the COMET-program of the Austrian Ministry of Traffic, Innovation and Technology with contributions by the University of Leoben and by the AT&S Austria Technologie & Systemtechnik Aktiengesellschaft. The PCCL is funded by the Austrian Government and the State Governments of Styria and Upper Austria.

ABSTRACT

In this thesis a systematic approach for the lifetime assessment of printed circuit boards (PCB) under drop impact is shown. While current procedures are based on a standardized board level drop test (BLDT), where PCB are repeatedly dropped under defined conditions till failure is detected, it was tried to develop alternative methods applying finite element simulations. Doing so, it was aimed for the reduction of necessary complementary experiments, which are time consuming and expensive. For example, conducting BLDT, including the PCB production, the assembling and the actual test can last up to months and can cause significant personal and material costs, while preliminary simulations can be performed much faster without extensive financial effort. However, in order to simulate a drop test, the experiments boundary conditions and the behaviour of the modelled materials had to be known. Thus, the BLDT was analysed in detail.

Therefore, instrumented BLDT tests, featuring a high speed camera, strain gauges and an acceleration sensor were performed. A precise analysis of the acting loads and the PCB deformation behaviour was carried out. The PCB material behaviour was characterised by a dynamic mechanical analysis and a linear viscoelastic material law was determined. Based on the gained results a simulation model of the test was set up. In order to verify the model, the simulation outcome was compared with the experimental results of a BLDT. To a large extend, a good correlation could be observed, but with respect to some important parameters, it appeared, that the boundary conditions of the BLDT were too complex to properly map them in the simulation.

Thus, and due to other drawbacks of the BLDT, an alternative testing method, a board level cyclic bend test (BLCBT) was developed in a consecutive step. The test was based on the fact, that due to the repeated drops, PCBs are exposed to a cyclic loading condition in a BLDT. In a BLCBT, instead of individual drops, a load similar to the BLDT load was applied continuously. Thereby, the PCBs are deflected displacement controlled with a sinusoidal load. The BLCBT and BLDT test were compared on the basis of six test PCBs and a very good agreement, approving the experiments correlation, could be shown. The main advantages of

the BLCBT were that it was faster to perform, less sensitive to operator influences, better adaptable and easier to model in a finite element simulation. Hence, the simulation of the BLCBT was realized without further difficulties in this study. In order to use the model for a lifetime assessment, simulated loading parameters had to be correlated to–to-failure. As the size of failures, leading to malfunction in a PCB, are in the range of 10 μm compared to a total board size of about 100 mm, evaluating the critical failure driver, it was crucial to take into account local stress concentrations.

As all analyzed boards were state of the art multilayer PCBs, the material behavior of the individual layers had to be characterized in order to be able to analyze the local conditions. The anisotropic material behavior of the insulating (glass fiber woven fabric reinforced epoxy) and conducting (copper structure/epoxy composites) PCB layers was determined by a combination of both, an experimental characterization and a micromechanics approach. Thus the direction dependent mechanical properties, important to describe the local stress states accurately, were described accurately. As not only the deformation behavior, but also the damage behavior was of interest, also fracture mechanics approaches were evaluated and applied. An in-plane and out-of-plane cohesive zone model, applicable to describe failure initiation and propagation, was determined for the insulating layers.

Using the generated material data, a simulation model of the BLCBT was used to determine local loading parameters, which were supposed to correlate with the PCBs lifetime. Thereby a sub-modeling technique allowing a detailed local analysis at reasonable computation times was applied. Dependent on the failure mode (three predominant failure modes were observed for the in this study analyzed PCBs), either a fracture mechanics parameter, a strain based or stress based parameter was used. In order to be able to perform a PCB lifetime assessment, BLCBT results and the local loading parameter simulations were correlated. So called ‘characteristic failure curves’, describing the correlation were generated performing BLCBT at different set-ups (amplitudes). Doing so, a desired range of local loading conditions was associated to the respective resulting lifetime. Thus the prediction of the expected lifetime of unknown PCB types, with respect of the regarded failure type was enabled. For the lifetime assessment only

a local loading parameter had to be simulated and evaluated using the characteristic failure curve. A sample lifetime assessment was performed for three PCBs and an excellent accuracy of prediction could be found.

The methodology shown represents a powerful design and optimization tool for PCBs. As only the analysis of one PCB type is necessary for the generation of a characteristic failure curve, the procedure is fast and easy to perform. Once knowing the correlation between lifetime and local loading parameters for a defined failure mode, only a single simulation has to be run, in order to be able to estimate the reliability with respect to the analyzed failure type. This study only dealt with PCBs with surface mounted components under impact load, while my developed procedure, including failure analysis, material characterization, the definition of a critical failure parameter, a corresponding finite element simulation and a failure curve generation, should be applicable for a broad field of different loading conditions and failure modes.

KURZFASSUNG

In dieser Arbeit wurde ein systematischer Ansatz zur Lebensdauerabschätzung von Leiterplatten unter Impactbelastung dargestellt. Während aktuelle Ansätze auf standardisierte Falltests ganzer Leiterplatten beruhen, wobei die Platten (wiederholt definiert und bis ein Fehler detektiert wird) fallengelassen werden, wurde versucht eine alternative Methode basierend auf Finite Elemente (FE) Simulationen zu entwickeln. Ziel dabei war, die notwendigen Experimente auf Leiterplattenebene, die teuer und zeitaufwendig sind, zu reduzieren. Falltests können z.B. mit Berücksichtigung der Leiterplattenherstellung, dem Bestücken und der Testdurchführung gegebenenfalls Monate in Anspruch nehmen und dabei hohe Personal- und Materialkosten verursachen, während entsprechende Simulationen ohne großen finanziellen Aufwand wesentlich schneller durchgeführt werden können. Um jedoch einen Falltest zu simulieren, müssen die Randbedingungen des Experiments und das Verhalten der modellierten Materialen bekannt sein.

Deswegen wurde in der Arbeit zuerst eine detaillierte Analyse des Falltests durchgeführt. Eine Hochgeschwindigkeitskamera, Dehnmessstreifen und ein Beschleunigungssensor wurden verwendet um die wirkenden Kräfte und das Deformationsverhalten der Leiterplatten genau zu bestimmten. Das Materialverhalten wurde in einer dynamisch mechanischen Analyse bestimmt und mit Hilfe eines linear viskoelastischen Materialmodells beschrieben. Basierend auf den Ergebnissen wurde ein Simulationsmodell erstellt. Die Simulationen wurden mit den Experimenten abgeglichen um das Modell zu evaluieren. Dabei wurde eine weitgehend gute Übereinstimmung gefunden, aber im Hinblick auf einige wichtige Parameter zeigte sich, dass die komplexen Randbedingungen des Falltests in der Simulation nicht vollständig richtig abgebildet werden konnten.

Deswegen, und wegen anderer Nachteile des Falltests, wurde im nächsten Schritt ein Ersatztest, ein zyklischer Leiterplattenbiegeversuch, entwickelt. Der Test basiert auf der Tatsache, dass die Leiterplatten durch die sich wiederholenden Stöße ähnlich einer Kurzzeitermüdung belastet werden. Im zyklischen Biegeversuch werden die Leiterplatten, statt durch einzelne Stöße, mit einer

ähnlichen Last wie beim Falltest, kontinuierlich belastet. Die Platten werden dabei wegkontrolliert mit sinusförmiger Belastung gebogen. Die Tests wurden anhand von sechs Testleiterplatten verglichen. Es zeigte sich eine sehr gute Übereinstimmung bei den Ergebnissen, wodurch die Korrelation der beiden Tests gezeigt und bestätigt werden konnte. Die wichtigsten Vorteile des zyklischen Biegeversuchs sind, dass er schneller durchzuführen, weniger sensibel auf Bedienereinflüsse, besser adaptierbar und leichter in einer Simulation modellierbar ist. Der zyklische Biegeversuch konnte ohne weitere Probleme in einer Simulation umgesetzt werden. Um die Simulation jedoch in einer Lebensdauerabschätzung zu verwenden, mussten simulierte Belastungsparameter mit den entsprechenden Fehlerzeiten korreliert werden. Weil aber die Fehler, welche zu Fehlfunktionen in Leiterplatten führen können, im Vergleich zur ungefähren Größe einer Leiterplatte von 100mm in der Größenordnung von 10 μm liegen, müssen, wenn der kritische Belastungsparameter bestimmt wird, die lokalen Spannungskonzentrationen berücksichtigt werden.

Um die lokalen Bedingungen zu simulieren, musste das Materialverhalten der Einzelschichten (alle untersuchten Leiterplatten waren Vielschichtleiterplatten) charakterisiert werden. Das anisotrope Materialverhalten der isolierenden (glasfasergewebeverstärktes Epoxidharz) und leitenden (Kupfer Struktur/Epoxidharz Verbund) Leiterplattenschichten wurde durch eine Kombination von experimentellen Versuchen und mikromechanischen Ansätzen bestimmt. Dadurch konnten die richtungsabhängigen Materialeigenschaften, die bei der Bestimmung der richtigen lokalen Spannungsverhältnisse essentiell sind, korrekt beschrieben werden. Des Weiteren, weil neben dem Deformationsverhalten auch das Schädigungsverhalten von Bedeutung war, wurden bruchmechanische Ansätze verwendet und evaluiert. Kohäsivzonenmodelle, verwendbar um Bruchinitierung und Bruchwachstum in einer Simulation zu beschreiben, wurden für die isolierenden Schichten für Belastungen in der Ebenen und aus der Ebene bestimmt.

Mit Hilfe der bestimmten Materialdaten wurde ein Simulationsmodell des zyklischen Biegeversuches dazu verwendet, die lokalen Belastungsparameter, welche mit der Leiterplattenlebensdauer korrelieren sollten, zu bestimmen. Dabei wurde eine Simulationstechnik mit Untermodellen genützt, um im gewünschten

Bereich detailliert aufgelöste Ergebnisse zu erhalten ohne die dafür notwendigen Berechnungszeiten übermäßig zu verlängern. Abhängig vom untersuchten Fehlermodus (drei unterschiedliche Fehlertypen wurden für die in dieser Arbeit untersuchten Leiterplatten festgestellt), wurde entweder ein bruchmechanischer Parameter, ein Spannungsparameter oder ein Dehnungsparameter verwendet. Um schließlich eine Lebensdauerabschätzung durchzuführen, wurden die lokalen Belastungsparameter mit den Ergebnissen aus den zyklischen Biegeversuchen korreliert. Sogenannte charakteristische Fehlerkurven, welche den entsprechenden Zusammenhang beschreiben, wurden durch die Durchführung von zyklischen Biegeversuchen bei unterschiedlichen vorgegebenen Amplituden ermittelt. Dabei wurde ein gewünschter Bereich von lokalen Belastungsbedingungen mit der sich dadurch jeweils ergebenden Lebensdauer in Verbindung gesetzt. Dadurch wurde die Vorhersage der zu erwartenden Lebensdauer von unbekannten Leiterplattentypen in Bezug auf den berücksichtigten Fehlermodus ermöglicht. Dazu war nur die Simulation des lokalen Belastungsparameters, welcher mit Hilfe der charakteristischen Fehlerkurve einer Lebensdauer zugeordnet werden konnte, notwendig. Eine exemplarische Lebensdauerabschätzung wurde anhand von drei Leiterplatten durchgeführt und eine sehr gute Vorhersagequalität konnte gezeigt werden.

Die gezeigte Methodik repräsentiert ein wertvolles Werkzeug zur Auslegung und Optimierung von Leiterplatten. Da nur die Analyse eines einzelnen Leiterplattentyps notwendig ist, um eine charakteristische Fehlerkurve zu erstellen, ist die Methode schnell und einfach durchzuführen. Wenn der Zusammenhang zwischen Lebensdauer und lokalen Belastungsparametern für einen bestimmten Fehlermodus bekannt ist, dann ist nur mehr eine einzelne Simulation durchzuführen um die Zuverlässigkeit in Bezug auf den untersuchten Fehler abzuschätzen. Die präsentierte Arbeit kann auch als Grundlage für die Evaluierung unterschiedlicher Lastfälle, Fehlerpositionen und Fehlerarten, die von Interesse sind, gesehen werden, da die Methodik unabhängig vom untersuchen Fehlerfall anwendbar ist.

TABLE OF CONTENT

STRUCTURE

The results are presented in two main parts. Part I provides an overview of the work, briefly describing the overall objectives and background along with a summary of the methodology and the major results. Part II consists of a collection of papers published or prepared for publication in scientifically related journals. Following the overall approach of a reliability evaluation and optimization method for a PCB under impact loads **paper 1** (P. F. Fuchs, Major, & Lang, 2009), describes the characterization and simulation of the global deformation behavior of a PCB in a standardized reliability impact test. In **paper 2** (P. Fuchs & Major, 2010), an alternative, advantageous testing method is presented. Based on this test a finite element simulation lifetime prediction method was developed. Therefore, a detailed material characterization, taking into account the deformation behavior (**paper 3** (P. F. Fuchs, Pinter, & Tonjec, 2012)) and the damage behavior (**paper 4** (P. F. Fuchs & Major, 2010) and **paper 5** (P. F. Fuchs, Pinter, & Fellner, 2012)) was performed. In **paper 6** (P. F. Fuchs, Pinter, & Major, 2012) the overall approach and an actual lifetime evaluation and prediction was shown exemplarily for three PCB types. The papers are entitled as follows:

Paper 1: Characterization of the deformation behavior of PCBs under dynamic loading conditions
Paper 2: Cyclic bend tests for the reliability evaluation of printed circuit boards under dynamic loads
Paper 3: Determination of the Orthotropic Material Properties of Individual Layers of Printed Circuit Boards
Paper 4: Experimental Determination of Cohesive Zone Models for Epoxy Composites
Paper 5: Local damage simulations of printed circuit boards based on determined in plane cohesive zone parameters
Paper 6: PCB drop test lifetime assessment based on simulations and cyclic bend tests

PART I: OUTLINE AND SUMMARY

1. CONTENT AND BACKGROUND

Printed Circuit Boards (PCB) are the linking part of almost all electronic devices. As mechanically supporting and electrically connecting applied electronic components they are representing the devices backbone. While some decades ago PCBs were single sided boards, state of the art PCBs are multilayer boards with up to 22 conductive copper layers separated by epoxy based, glass fibre reinforced dielectric layers. The conductive copper layers are structured in an etching process and additionally introduced microvias (laser drilled and copper platted holes) connecting the individual layers with each other enable a three dimensional design. These complex procedures are necessary to map the circuits of advanced devices (Coombs, 2008).

Nevertheless, due to intentions of miniaturization parallel to the request of the integration of more features, PCB related research is focused on a further increase of the interconnection density. Thus, the microvia diameters, the conducting path widths and the layer thicknesses are continuously downsized. However, these adaptions counteract the effort of improving the PCB reliability, which is a key issue and the main quality criteria for the related industry. In the case of electronic devices used for safety related tasks, where human life can depend on a proper function, the importance of reliable PCBs is apparent. But also for products only used in the entertainment industry, an ensured lifetime is important, as any failure directly affects the image of the respective company and can additionally cause high warranty costs.

The purpose of this work was to find methods to evaluate and consequently improve the reliability of PCBs. Due to the wide field of applications of electronic devices, a wide field of different loads, like impact, temperature, vibration and fatigue loads had to be regarded. To develop appropriate methods a load case to start off had to be chosen. As the market of mobile devices is, due to extensive expansion rates, currently of increasing interest, the focus was set on loads especially important for them. Thus, as mobile devices are known to be especially prone to be dropped, impact loads were chosen for a detailed analysis.

The most common failures of PCBs due to impact loads, taken into account in this study, were cracks in, or at the vicinity of the solder bumps which are connecting the boards with the components mounted on the surface. The solder bumps for one component are arranged in a regular structure, representing the so called ball grid area (BGA).

Evaluating the deformation and damage behavior of a PCB, the quite different thermo-mechanical behavior of the materials (e.g. copper, epoxy, glass fibers, solder…) applied has to be taken into account. Mutual deformation interferences can be the reason for local stress concentrations, being again the reason for crack initiation and propagation. Furthermore, already small local failures can cause malfunction of a whole device. Crack length of 10 μm, compared to a total size of a mobile device PCB in the order of 100 mm, are sufficient, if a conducting path is affected. Thus, analytical methods are difficult to apply, as the loading conditions are too complex to describe.

Current reliability evaluation methods are based on experimental tests, as e.g. the board level drop test (BLDT) for impact loads (“Board level drop test method of components for handheld electronic products,” 2003), (Wong, Seah, & Shim, 2008). Thereby a defined impact load (1500g in 1ms) is applied repeatedly. Failures are detected by measuring the electrical resistance of a daisy chain going through the BGA of the individual components. A failure is defined as an electrical discontinuity of resistance greater than 1000 ohms lasting for 1 microsecond or longer. The resulting number of drops to failure can be taken as a parameter for the drop performance. But only the failing component of the analyzed PCBs, not the actual failure position and failure pattern, is determined. In order to get more information on the damage behavior, cross sections of the individual solder bumps have to be prepared and evaluated with the help of light microscopy. Consequently, the reliability tests are time consuming and expensive. In order to obtain lifetime and failure mode estimations, the boards have to be produced, assembled, tested, and analyzed in detail. Thus, in order to keep up with the short development periods, new methods are developed and evaluated. A promising approach is finite element simulations where the global deformation behavior (e.g. (Jeng, S, Yeh, Lai, & Wu, 2007), (John, Pang, Che, & Xiong, 2005),(Bai, Qin, &

An, 2007) and (Luan et al., 2006)) and the resulting local effects (e.g. (T. Tee, Ng, C. Lim, Pek, & Zhong, 2004a),(Qu, Chen, Qi, Lee, & Wang, 2007),(Le Coq, Tougui, Stempin, & Barreau, 2011) and (T. Tee, Ng, C. Lim, Pek, & Zhong, 2004b)) are predicted. However, in the quoted literature the number of necessary complementary experiments on manufactured PCBs is still relatively high. For example, assembled boards had to be analyzed in order to describe their damping behavior – the oscillation simulations could not be run on the basis of a material analysis only. Also, in order to associate local loading conditions to the reliability performance of PCBs and to define a proper correlation, a lot of different board types had to be analyzed experimentally.

Hence, the aim of this study was to further improve existing methods and alternative procedures were proposed. The focus was set on the generation of predictive PCB simulation models based on detailed preliminary material analyses in combination with a significantly reduced number of experiments on completed boards. To do so an alternative experimental testing procedure, a board level cyclic bend test (BLCBT) (P. Fuchs & Major, 2010), enabling the adjustment of different loading levels and advantageous for the realization as finite element model, was developed and local failure parameters were calculated. These local loading parameters were tried to be correlated to the measured lifetimes, whereby a PCB performance prediction should be enabled. The correlation function can be generated based on the tests of only one PCB type, as different load levels can be carried out by an adaption of the BLCBT test set up, allowing to describe the whole lifetime region of interest without extensive testing and specimen manufacturing effort.

2. SUMMARY OF DEVELOPED METHODS AND MAJOR RESULTS

The current industry wide standard for the evaluation of the impact performance of printed circuit boards is the so called board level drop test (BLDT) ("Board level drop test method of components for handheld electronic products," 2003). Based on this test an alternative, less time and cost intensive, reliability and lifetime evaluation method was developed. Therefore, in a first step the drop test was analyzed in detail in **paper 1**. The test was recorded using a high speed camera (Ultima 512, Photron Inc., SanDiego, CA, USA) to analyze the PCBs deformation due to the impact load. Furthermore, an acceleration sensor was mounted on the drop table to measure the acting load and strain gauges were applied to the PCBs to determine the resulting maximum strain of the outermost layer. In Fig. 1 the experimental drop test set up and the corresponding instrumentation is depicted. Failure is recorded using a so called event detector (256 STD, Analysis Tech, Wakefield, US), which is monitoring all conducting connections.

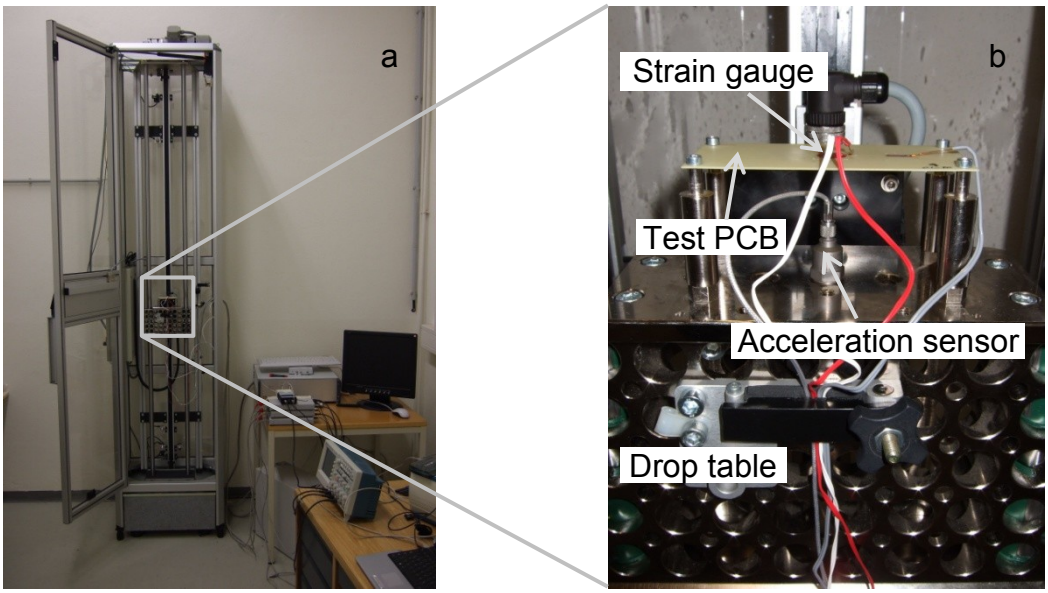

Fig. 1 The experimental set up of a board level drop test (a) and the additional applied acceleration sensor and strain gauges (b).

The test analysis revealed that during the impact the center of the PCB is deflected by about 3mm towards the drop table and starts to oscillate due to stored elastic energy. Within about 0.3 s the sinusoidal oscillation fades out due to damping effects. Results of the high speed camera measurement and the strain

gauge evaluation (maximum principal strain of the outer fiber at the center of the board) are depicted in Fig. 2. Experimental studies showed that changes of the PCB built-up did not significantly affect the initial deflection, but had an influence on the amplitude decay. The damping of the oscillation of boards without reinforcement of the outermost layers was much more pronounced than of boards with glass fiber reinforcement in the outermost layers for example.

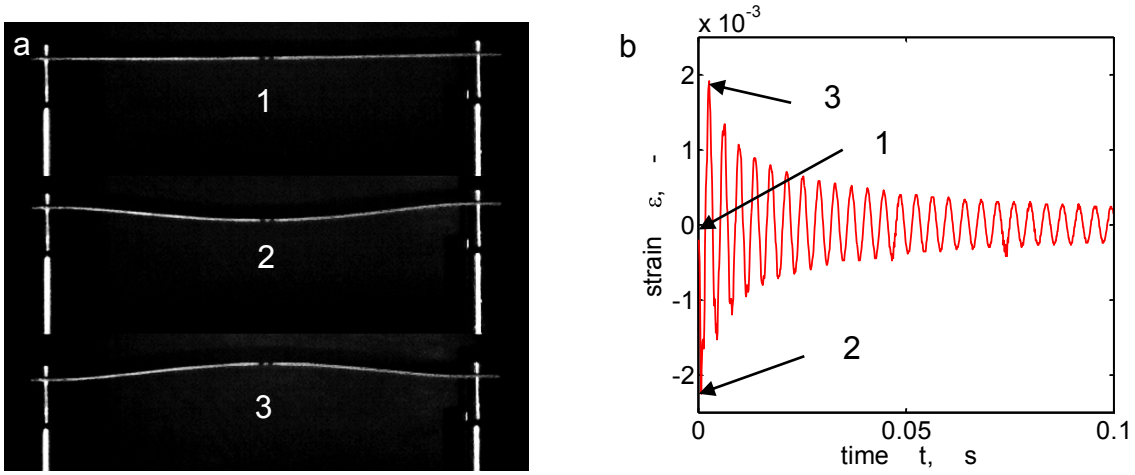

Fig. 2 High speed camera images taken right before (1) at (2) and right after (3) the impact (a). In (b) the corresponding oscillogram of the maximum principal strain of the outer fiber at the center of the board is shown. (P. Fuchs & Major, 2010)

In order to describe the global deformation behavior of a PCB during a BLDT in a simulation model the material behavior was characterized. As at this point of time, only the global deformation was of interest, the measurements were performed on complete boards and a homogenized material law was determined. The board behavior was described using a linear viscoelastic law, whereby it was possible to describe the pronounced time dependent material behavior of the polymeric matrix (epoxy) used in the insulating layers. The viscoelastic material parameters were determined on the basis of the results of a dynamic mechanical analysis (DMA) performed under a three point bending load. The DMA measurements were performed at different frequencies and temperatures, and a mastercurve was generated using a time-temperature superposition principle. The master-curve was fitted using a Prony-series (Tschoegl, 1989). The applied method is described in **paper 1** in greater detail. The material law described by the Prony-series was

used to model the BLDT in a finite element simulation. No artificial damping had to be applied, as in the viscoelastic law the material damping is integrated (Tschoegl, 1989). Results of the simulation are shown in Fig. 3. The measurement results represent the strain gauge measurement evaluations. The amplitude-strain correlation was calibrated using the high speed camera images. Fig. 3 (a) compares a fit through the positive deflection maxima of the oscillation of the measurement and the simulation for a selected PCB. A good agreement could be observed, approving the applicability of a viscoelastic material law to describe the PCB damping behavior. On the other hand, the frequency development, shown in Fig. 3 (b), revealed a significant discrepancy. Even if the frequency development trend was described reasonably well in the simulation, the frequency level was not in accordance.

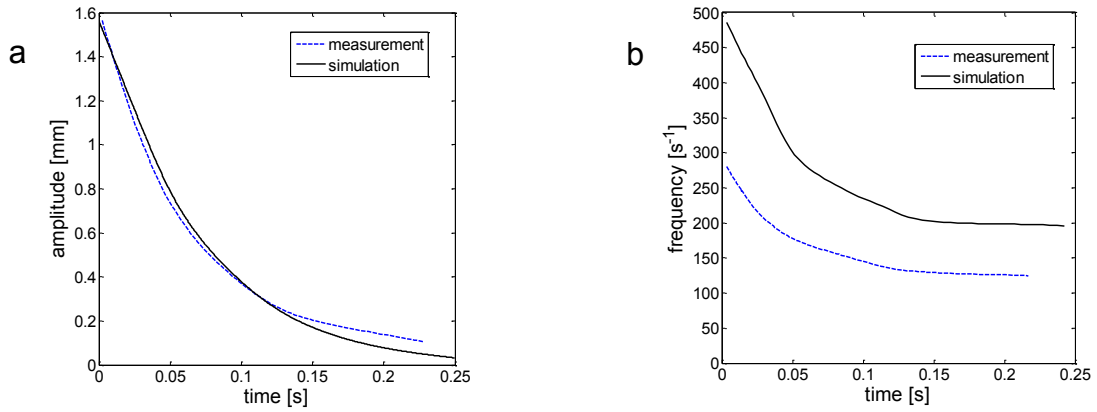

Fig. 3 The comparison of the positive deflection maxima of the oscillation (a) and the frequency development (b) of a sample PCB during a BLDT experiment and simulation. (P. F. Fuchs et al., 2009)

Further test simulations indicated that a proper idealization of the boundary conditions, the fixation of the board with screws at its four corners, is crucial for an accurate description of the frequency behavior. Variations of the constraint definitions in the simulation model had a significant influence on the frequency and amplitude level. However, despite some considerable effort, modeling the relevant fixation, the frequency level could not be reproduced in agreement with the experimental results without affecting the agreement of the amplitude results. As too many, hardly accurately determinable, influence factors, partly changing for every performed test, (e.g. the test operator dependent actual tightening torque of

the screws, the exact position of the PCBs, the compliance of the pillars carrying the PCBs during the drop test, possible measurement imprecisions in the determination of the experimental deflection, …) did affect the simulation, a further improvement was not in conformity with the purpose of this work, an easy and fast method to describe the deformation and damage behavior, as the repetitive effort would have exceeded the benefit. Nevertheless, the simulations could be used to relatively compare different board built-ups and damping behaviors and for the determination of the maximum short term load the board has to endure during the test.

Knowing the drawbacks of the BLDT, further work was focused on the development of an alternative experimental testing method, combining the advantages of both, a simplified procedure and precisely defined boundary conditions, which enable an exact finite element modeling. The development is introduced in **paper 2**. The test, a so called board level cyclic bend test (BLCBT), was based on the observation, that in a BLDT, due to the repeated drops, the PCBs are loaded correspondingly to cyclic loading conditions. Thus, a test, applying a load similar to the BLDT load through a three point bending fixture, was set up. Thereby, the PCBs are deflected sinusoidal and displacement controlled. Furthermore, in contrast to the BLDT in a BLCBT the load is applied continuously.

A similar test procedure has successfully been applied in a published work (Wong et al., 2008). To evaluate the BLCBT, different PCB types have been analyzed with both methods. Due to machine limits, the bending frequency in the BLCBT (25 Hz) was significantly lower than in the BLDT (280 Hz), what had to be regarded analyzing the results. Different loading rates affect the material behavior and thus the loading conditions. Nevertheless, a good agreement between the respective event detector results was observed, indicating that the stain rate influence is not pronounced and approving the applicability of the test as an alternative for the BLDT. In Fig. 4 an overview of the comparison of the experiments is given. The correlation of the BLDT and BLCBT results for six different PCB types is shown.

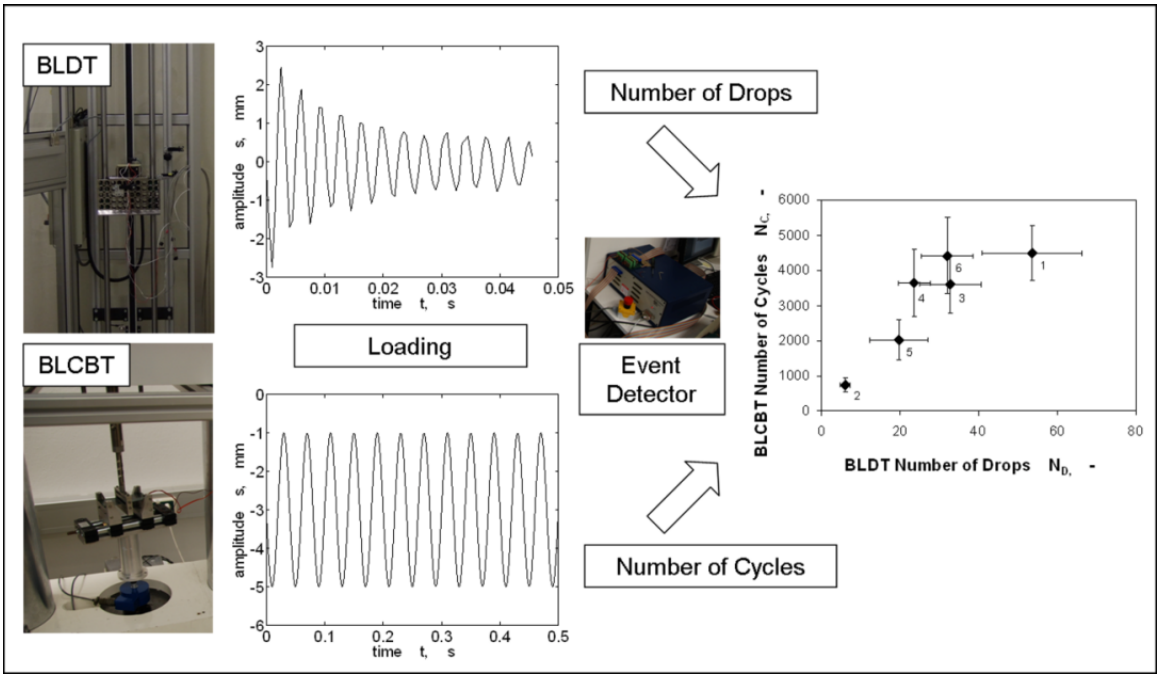

Fig. 4 Comparison of the board level drop test (BLDT) and the board level cyclic bend test (BLCBT). (P. Fuchs & Major, 2010)

The advantages of a BLCBT are summarized in **paper 2** as follows:"

- The BLCBT testing time is significantly shorter than the BLDT testing time (The factor between the method testing times depends on the board performances. The better a board performs, the faster is the BLCBT compared to the BLDT. In our case the BLCBT was about two times faster than the BLDT. The reason for the testing time differences is an approximate break of 5 seconds between each drop in the BLDT.)
- The BLCBT can be performed considering different influence parameters (e.g. temperature, frequency or amplitude) by default. In contrast the BLDT under temperature influence is costly, as the temperature has to be applied on a large testing space. Furthermore, in the BLDT only the initial amplitude can be controlled. As this is done by adapting the impact energy, an adjustment to predefined amplitudes is difficult. The frequency in BLDT can hardly be varied at all.
- The BLCBT can be performed on basically every dynamic testing machine which is capable of applying the desired displacement and frequency.
- The BLCBT can be simulated at lower computing times than the BLDT using the Finite Element Method. Simulations of the BLDT are difficult, as the load

application and the definition of the boundary conditions are challenging ([14], [15] and [16]). The simplest way to simulate the BLDT is the 'Input-G method' ([17], [18], [13] [20] and [21]), where an acceleration signal is applied directly to the board, which is still computationally expensive.

" (P. Fuchs & Major, 2010)

The BLCBT was implemented in a simulation model in good agreement with the experiments (results are given together with results of local simulations within the summary of **paper 5** and **paper 6** in a later section). However, applying the BLCBT instead of the BLDT, it had to be kept in mind that the influence of the different loading conditions can vary significantly, analyzing PCBs failing in other modes.

In a next step, the local loading conditions were analyzed. Thereby, as the regarded PCB built-ups consisted of numerous different layers (In Fig. 5 the schematic built-up of a typical eight layer PCB is shown), the individual layers had to be characterized (**paper 3**).

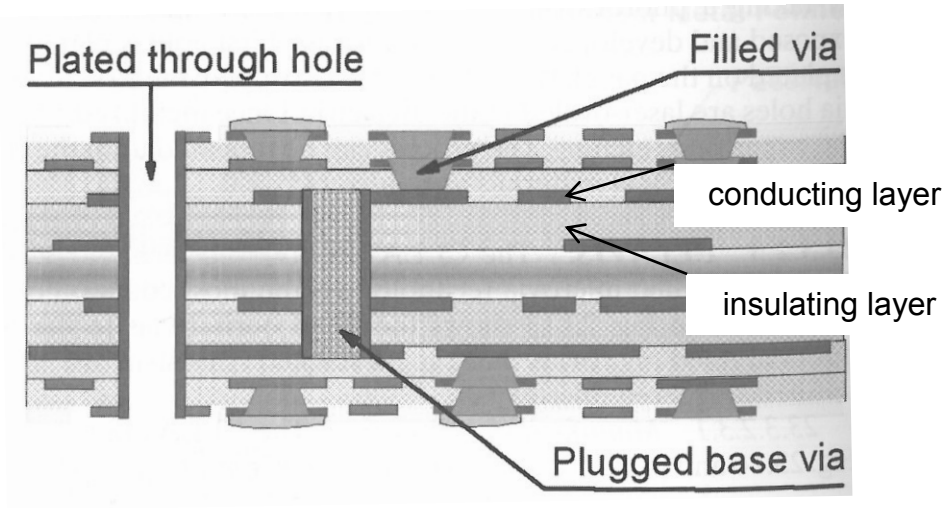

Fig. 5 Schematic representation of an eight layer PCB (alternating conducting and insulating layers). Different possibilities (plated through hole, filled via and plugged base via) to electrically connect the individual layers with each other are indicated. (Coombs, 2008)

In order to describe the local situation, instead of a homogenized material model for the whole board, sufficient to describe the global loads, the properties of the single layers had to be known. The insulating layers were neat (unreinforced) and

glass fiber reinforced epoxy resins. The optional glass fiber reinforcements were different standardized ("Specification for Finished Fabric Woven from 'E' Glass for Printed Boards," 2008) types of woven fabrics. The fibers were orientated in 0° and 90° directions and differences between warp and weft were regarded. The conducting layers were structured copper foils, designed according to customer requirements. In the regarded test PCB the structure was regular, as it had no actual technical function. The free volumes, originating from the copper removal, were filled with the epoxy matrix of the next insulating layer, applied during the production process. In order to idealize the layers in a finite element simulation model, the glass fibers and copper paths could have been modeled according to their geometry, but the necessary model resolution would have let it exceed a computable size.

Thus, homogenized material models, common models to efficiently map heterogeneous materials on a macroscopic level (Böhm, 2008), were applied for the individual layers and, due to the direction dependent reinforcements, anisotropic material behavior was taken into account. Furthermore, as for the evaluation of the local stress situation, the out-of-plane stresses were of major importance, a complete, three-dimensional characterization had to be performed. Both, the glass fiber woven fabric/epoxy (insulating) layers and the copper structure/epoxy (conductive) layers were identified to have an orthotropic material behavior. As a consequence, nine, in most cases independent, engineering constants had to be determined, in order to describe the direction dependent linear elastic material behavior. A classical, exclusively experimental approach (e.q (Daniel, Luo, & Schubel, 2008), could not be applied, as the individual layers were very thin (thickness: conducting layers 18 μm, insulating layers 70 to 160 μm), whereby no out-of-plane specimen could be prepared. The conducting layers were not available for testing at all, as the actual layer only came into being during the production process. Hence, alternative approaches were applied. The orthotropic material parameters of the insulating layers were determined using a combination of experimental tests and micromechanics simulations. The in-plane parameters were measured in tensile tests applying a digital image correlation system (Aramis HS, GOM mbH, Braunschweig, D) (Fig. 6), whereas a mean-field theory based micromechanics approach (Benveniste, 1987), using the software digmat-MF 4.2.1

(e-Xstream engineering SA, Louvain-la-Neuve, BE), enabled the determination of the missing out-of-plane parameters.

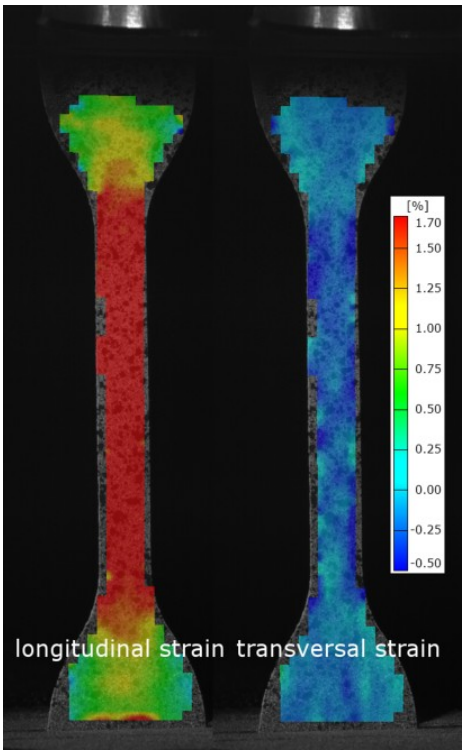

Fig. 6 Digital image correlation (Aramis HS, GOM mbH, Braunschweig, D) tensile test strain overlay plots of a specimen, of an individual woven glass fiber fabric reinforced insulating layer, just before breaking. (P. F. Fuchs, Pinter, & Tonjec, 2012)

The properties of the conducting layers were determined based on an almost exclusively numerical approach. Only the isotropic material parameters of copper were determined in preliminary tests. Representative volume elements (RVE), analyzed in finite element simulations, have been used to determine the homogenized copper structure/epoxy composite behavior (described e.g. by (Sun & Vaidya, 1996) or (Böhm, 2008)). Thereby, defined load cases were taken into account, in order to obtain the orthotropic material data. The regular structure of the layers simplified the generation of the necessary finite element models (Abaqus 6.9, Simulia, Daussault Systèmes, Providence, RI, USA). Periodic boundary conditions were applied using an automated process (Antretter, 1998). To estimate the influence and the importance of the anisotropic material behavior, additional test simulations were conducted in **paper 3**. A chosen region of interest,

corresponding to known critical failure positions in PCB, was evaluated. It was shown, that taking into account the copper structure, instead of full copper layers, has only small effects on the regarded area, whereas the consideration of the direction dependent influence of the glass fiber reinforcement in the insulating layers had considerable effects on the local stress situation. Thus, all further simulations were based on proper orthotropic material data for the reinforced layers.

As not only the deformation behavior, but also the failure behavior, should be simulated in this work, additional research dealt with the modeling of damage. In order to describe the damage, a fracture mechanics approach was applied. A 'cohesive zone model' (CZM), introduced in the 1960's ((Dugdale, 1960) and (Barenblatt, 1962)), was used. The advantage of this phenomenological model was that its implementation in several finite element codes (e.g. Abaqus 6.10-1, Daussault Systèmes Simulia Corp., Providence, USA) enables the simulation of crack initiation and crack propagation without having to define a crack path. Currently there is no other material law available, which can be used as alternative. However, the determination of the CZM parameters is challenging and no generally accepted methodology or standard exists. The model describes the correlation between crack opening displacement (separation) and cohesive stress (traction). While the crack opening displacement can be measured experimentally, no direct measurement method for the determination of the cohesive stress exists. In **paper 4**, in preliminary tests it was tried to determine the shape of the cohesive stress graph, due to in-plane loads, using a 'J-Integral approach' e.g. (Sørensen & Jacobsen, 2003). Thereby, the cohesive stress was calculated by the derivation of the determined J-Integral over the crack opening displacement. A novel test set-up, including a digital image correlation system (Aramis HS) was used to measure the crack opening displacement with high accuracy. Furthermore, the influence of different specimen geometries and the effect of the loading direction, with regard to warp and weft of the glass fiber woven fabric reinforcement, were analyzed. It was shown, that the determined CZM parameters were mostly specimen geometry independent, but were influenced significantly by the loading direction. The shaping of the traction-separation curve changed with the analyzed direction. However, applied in a finite element model, the results showed that a solely

experimental approach was not applicable for a predictive simulation. The results were highly sensitive to the fitting of the J-Integral curve, performed within the calculation of the cohesive stress. Small changes of the fitting parameters already implicated large changes of the maximum cohesive stress. As a consequence, in continuative work, a combination of both, experiments and matching of corresponding simulations, as proposed for example by Schwalbe et. al (Schwalbe, Scheider, & Cornec, 2009), were applied.

In **paper 5** a CZM describing fracture due to out-of-plane loading was determined. Therefore, double cantilever beam (DCB) tests of insulating layers, pressed to a required thickness of 5 mm, were conducted. Thereby, the behavior of a crack propagating in the epoxy resin, or at the interface between epoxy and glass fiber, was analyzed. In this case a linear damage behavior was assumed (according to literature data the influence of the shape of the damage function is minimal (Schwalbe et al., 2009)) and the maximum cohesive stress was determined, matching the force-displacement curves of the experiments to the results of corresponding simulation models (see **paper 5**). Thus, as the energy release rate was known from the measurements, the CZM was fully described. In Fig. 7 (a) the matching of the simulation to the measurement results is indicated. The cohesive stress was adapted in order to minimize the discrepancies. Fig. 7 (b) shows the evaluation of the determined CZM parameters on the basis of a comparison of additional experiments and simulations of thinner specimen (2 and 0.65 mm). The excellent correlation proved the applicability of the proceeding. However, so far only the mode I fracture was taken into account. This had to be considered applying the CZM in simulation models.

A PCB lifetime prediction methodology is described in **paper 5** and **paper 6**, and is summarized on their basis. The lifetime prediction is based on the fact that failure in a PCB during a BLCBT or a BLDT is usually not resulting from of a global damage but from very small cracks compared to the global board size. At boards with surface mounted components, as analyzed in this work, such cracks can predominantly be found at the vicinity of the solder bumps connecting the mounted components with the board (P. Fuchs & Major, 2010). In Fig. 8 (a) a test PCB with

surface mounted components is shown. The solder bumps are arranged in a regular structure and represent the BGA (Fig. 8 (b) and (c)).

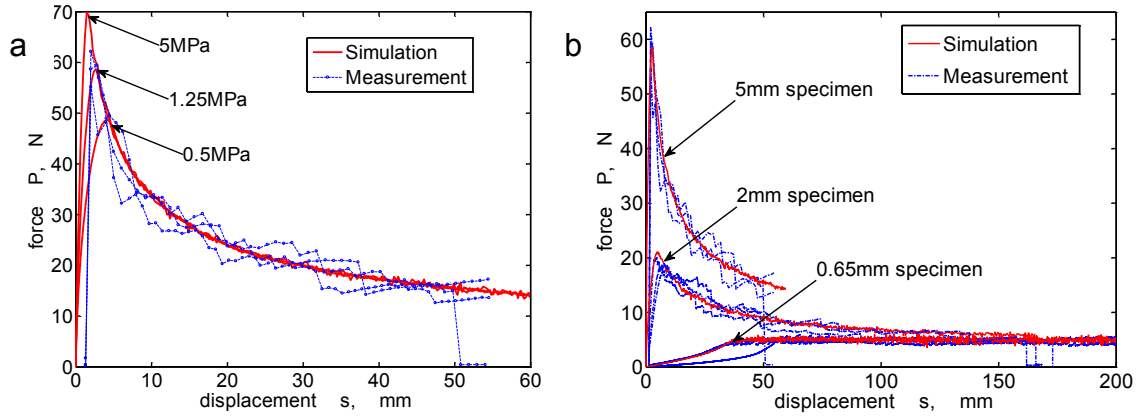

Fig. 7 The matching of the simulation results to the experimental results of a DCB test by the adaption of the maximum cohesive stress of a cohesive zone model is indicated in figure (a). In figure (b) the determined cohesive zone model was evaluated on the basis of a comparison of additional experiments and simulations of thinner specimen (2 and 0.65 mm). (P. F. Fuchs, Pinter, & Fellner, 2012)

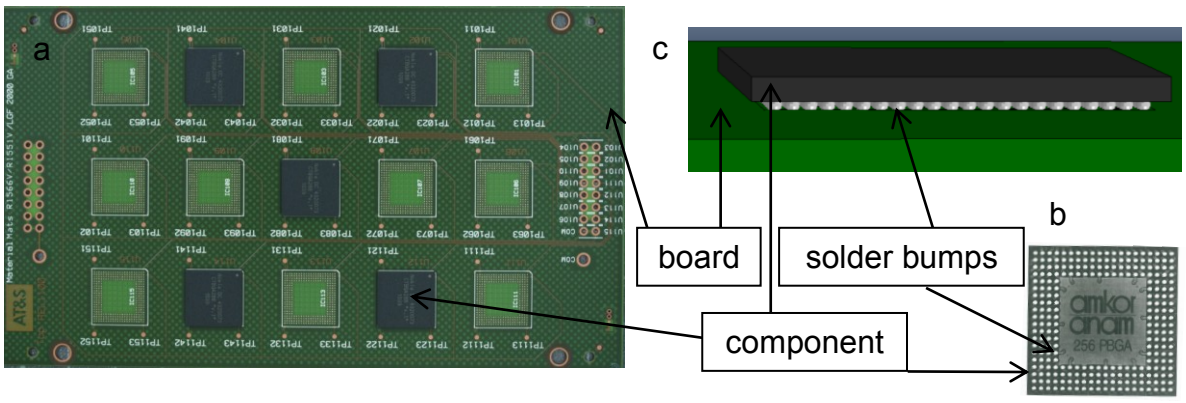

Fig. 8 Surface mounted compenents on a test PCB (a). Additonally, the backside of a typical component with the BGA (b) and its implementation as CAD model (c) is shown. (Coombs, 2008) and (P. F. Fuchs et al., 2012)

Typical failures of PCBs with surface mounted components are schown in Fig. 9. The figures show individual solder bumps with the board on the upper side and the component on the lower side. The arrows inidicate the respective cracks being the reason for malfunction. In Fig. 9 (a) a crack was initiated at the corner between solder bump, copper pad and outermost epoxy layer. It grew towards the copper

via and thus caused failure. In Fig. 9 (b) a crack went through the solder bump, while in Fig. 9 (c) it was initiated at the interface between copper pad and solder bump. Whatever failure type was predominant depended on the local loading situation, which again was affected by the PCB built-up and the materials used for the individual layers. Failure in PCBs were detected using a so called event detector (256 STD, Analysis Tech, Wakefield, US) during a BLCBT or a BLDT. Thereby, an electrical discontinuity of 1000 ohms, lasting for 1 microsecond or longer, in a daisy chain (seriel circuit of all connections between component and board of an individual component) is recorded as malfunction.

However, as observed failures were very small compared to the global board, the local loading situation is decisive for the PCB reliabilty. Thus, as the local conditions could not be determined experimentally, finite element simulations were used to evaluate the local stress and deformation field. In order to rate the local situation, a parameter, corresponding to the regarded failure mode, was defined. For example, in published studies for failure type b (Fig. 9 (b) – failure in the solder bump) the maximum plastic strain has been used (Le Coq et al., 2011), while for failure type a (Fig. 9 (c) – interface solder copper pad) a maximum peel stress was determined (T. Tee, Ng, C. Lim, Pek, & Zhong, 2004a). Approaches for failure type c (Fig. 9 (a) – outermost epoxy layer) have not been published yet and were taken into account in **paper 5**.

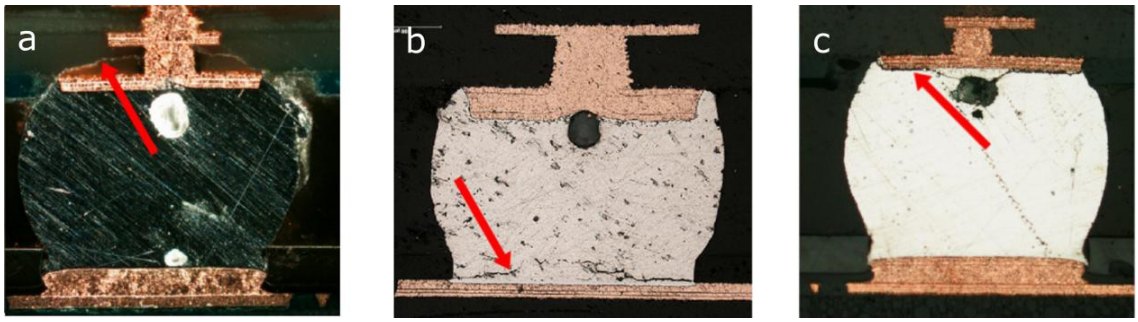

Fig. 9 Typical failure patterns of PCBs during a BLDT or BLCBT:(a) Failure in the outermost epoxy layer, (b) Failure in the solder bump, close to the component, (c) Failure at the interface between solder bump and copper pad. (P. F. Fuchs et al., 2012)

For example, in published works for failure type b (Fig. 9 (b) – failure in the solder bump) the maximum plastic strain has been used (Le Coq et al., 2011), while for

failure type a (Fig. 9 (c) – interface solder copper pad) a maximum peel stress was determined (T. Tee, Ng, C. Lim, Pek, & Zhong, 2004a). Approaches for failure type c (Fig. 9 (a) – outermost epoxy layer) have not been published yet and were taken into account in **paper 5**.

The local loading conditions were analyzed for the maximum deflection of a BLCBT (The BLCBT was chosen for the reasons which were mentioned above). In order to gain the required detailed local information a submodeling technique was applied. Using this technique, a global model, featuring a rough mesh, is simulated, and its results are used as boundary conditions for the simulation of a local submodel. Thus, a fine mesh has to be used for a small area only, keeping the computing times low, while detailed results can be generated in the area of interest. A representation of the finite element model is shown in Fig. 10. The solder ball exhibiting the highest loads in the global model was chosen for the submodel analysis. From the results the local loading parameters were determined.

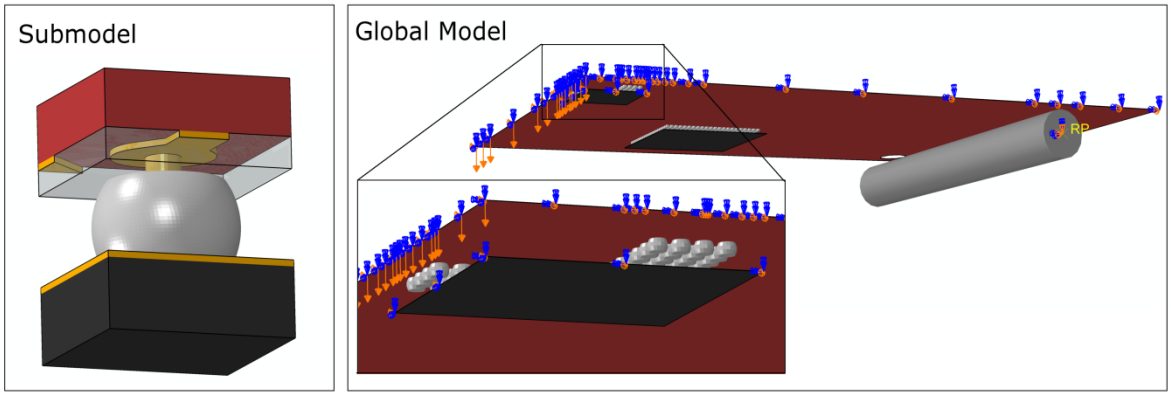

Fig. 10 Simulation model for the evaluation of the local loading situation of a test PCB in a BLCBT. The submodel allows for a detailed analysis. (P. F. Fuchs et al., 2012).

For failure type a an even more detailed simulation model (a ‘subsubmodel’) was generated in **paper 5**. With it a fracture simulation using the determined cohesive zone law in an enriched finite element (X-FEM) simulation, was conducted. Thereby, the crack initiation and propagation was predicted in agreement with experimental failure analyses. Furthermore, as a single parameter was needed for the correlation with the PCB lifetime, a fracture mechanics value (J-Integral) was

determined. The J-Integral was calculated for a short initial crack positioned corresponding to the experimental failure analysis and the X-FEM simulation.

Being able to determine local loading parameters, in dependence of the PCB built-up, the materials used for individual layers and the applied global load, a characteristic failure curve was generated. This curve correlates the PBC lifetime to a local loading parameter for a given failure type. In order to determine the curve, tests at different local loading situations had to be conducted. Different local loading situations were carried out changing the set-up (amplitude) of the BLCBT. Thus, in order to generate a correlation, compared to other approaches, a considerable advantage was gained, as only one PCB type had to be analyzed. The resulting curve was used to estimate the lifetime of unknown PCBs with respect to the analyzed failure type. Therefore, only the corresponding local loading parameter had to be determined in a simulation. A schematic representation of the methodology is given in Fig. 11. As the BLCBT is correlating with the BLDT, also conclusions regarding the BLDT lifetime can be drawn from the results.

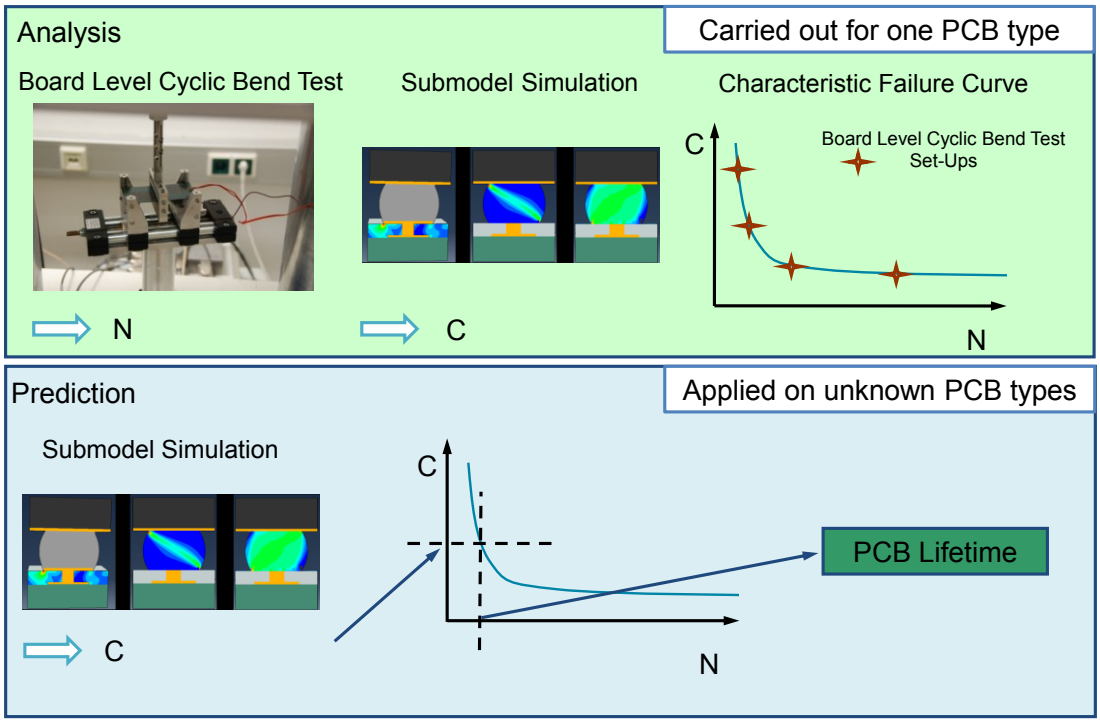

N…Cycles to failure C…Local loading parameter

Fig. 11 Schematic representation of the PCB BLCBT lifetime assessment methodology.

In **paper 6** an example lifetime prediction was conducted. Therefore, three test PCBs (PCB 1, PCB 2 and PCB 3) were characterized in a BLCBT. The boards differed regarding the materials for the built-up. A failure analysis of the tested boards exhibited a failure mode corresponding to type b. Thus, the maximum equivalent plastic strain was used as local loading parameter. A characteristic failure curve, based on BLCBT results and submodel simulations of PCB 1, was fitted using a Manson-Coffin equation, a common model to describe low cycle fatigue of metals (Manson & Halford, 2006). The fit again, was used to predict the BLCBT lifetime of PCB 2 and PCB 3. In Fig. 12 a double logarithmic plot of the Manson – Coffin fit is shown. The experimental BLCBT results for PCB 2 and PCB 3 were added to the plot. An excellent correlation between the predicted and the measured lifetime is indicated, as the experimental results of PCB 2 and PCB 3 lie close to the Manson-Coffin fit.

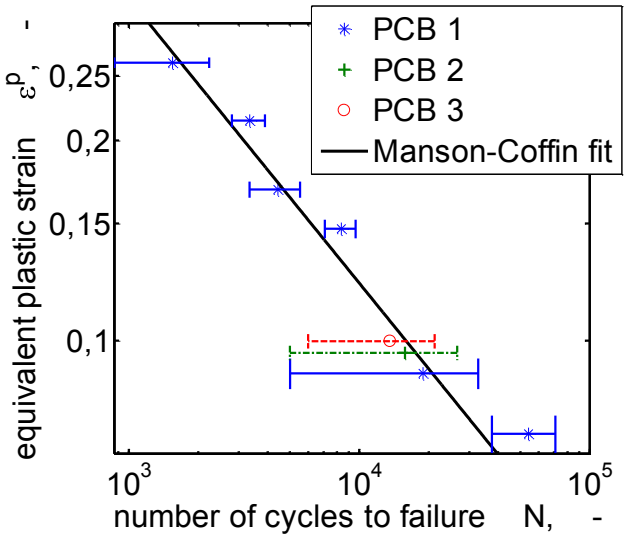

Fig. 12 Comparison of the predicted and measured BLCBT lifetime. The measured results of PCB type 2 and 3 lie close to the predictive characteristic failure curve (Manson-Coffin fit) based on results of PCB 1. (P. F. Fuchs et al., 2012)

The experimental BLDT results also went very well with the predictions, further supporting the applicability of the lifetime prediction methodology. Nevertheless, it had to be taken into account, that the differences between the analyzed PCBs types were statistically not significant. Thus, future work will take into account

boards with distinct differences, with respect to the local loading situation, in order to properly evaluate the characteristic failure curve. However, already yet the presented method provides a powerful tool to predict the reliability of unknown PCBs. Once a characteristic failure curve is generated, only the properties of the individual layers, planned to be used in the PCB have to be defined for a PCB type of interest. Thus, numerous costly experiments and development time can be saved.

3. CONCLUSION AND OUTLOOK

The characterization and simulation of the deformation and failure behavior of PCBs under dynamic loads and a corresponding reliability assessment have been performed in a systematic way. The state of the art methodology, an experimental test, was analyzed and an alternative approach was developed. Finite element models based on an adapted experiment, featuring advanced material models, were used to predict the PCB lifetime.

Doing so, the detailed analysis of the current industry wide standard test for the evaluation of the PCB reliability, the board level drop test (BLDT), enabled the generation of a corresponding finite element model. The determined boundary conditions and the linear viscoelastic material behavior of the PCBs, studied in a dynamic mechanical analysis, were used to describe the experiment in the simulation. The amplitude decay of the board oscillation in the test could be mapped by the simulation. Thus, a relative comparison of different PCB types was possible. However, due to given uncertainties in the test procedure, a proper reproduction of the experimental results, with respect to the frequency level, was difficult. The frequency level in the simulation model was too high, but the discrepancy could not be led back to the material model, as simulations featuring simplified linear elastic models (the linear elastic models, neglecting the damping effects, were verified in monotonic tests and simulations before), led to the same initial frequencies. That is, not the material behavior, but the complex boundary conditions of the BLDT did aggravate an accurate simulation.

Thus, the board level cyclic bend test (BLCBT), developed in a consecutive step, was used as alternative. It was shown that it led to the same results as the BLDT, but was faster to perform and easier to reproduce in a finite element simulation. Despite the advantages of the BLCBT, using it, it had to be regarded that the loading conditions, with respect to the loading rate, were different from the BLDT. Possible influences on failure modes, not yet regarded in this study, have to be taken into account. However, the BLCBT was modeled and simulated in accordance with the experiments and showed an excellent correlation with the BLDT for the yet analyzed PCBs and regarded failure types.

The local loading analyses, performed applying the BLCBT model, were done using detailed material models of the individual conductive and insulating layers. The importance of taking into account the anisotropic material behavior was shown in comparative simulations. Characterizing the anisotropic behavior, only the application of a combination of both, experimental methods and micromechanical approaches, enabled the determination of the out of plane behavior.

The damage behavior of the epoxy layers was described using a cohesive zone model (CZM). The determination of the CZM parameters was challenging and different methods were applied. The combination of an experimental approach and corresponding simulations gave good results which were successfully used to simulate the initiation and propagation of a crack in the PCB outermost epoxy layer in accordance with an experimental failure analysis. As a result, the failure development and influence factors could be studied. Understanding the failure mode was important, as it enables a proper adaption, with respect to a reliability improvement, of the PCB built-up and design.

The lifetime prediction methodology was performed applying the BLCBT at different set-ups and corresponding local loading analyses. The approach was based on the definition of a single local loading parameter for the correlation (described by a characteristic failure curve) with the respective PCB lifetime. Three failure types were regarded in this study, and different parameters were proposed for them, but only the lifetime assessment of one failure type was experimentally verified yet. However, the results were promising and revealed an excellent correlation between predicted and measured BLCBT lifetimes. The correlation with the BLDT was also given. Nevertheless, the verification was based on three PCB types only and will have to be extended.

It can be concluded, that a potential tool to improve the reliability of PCBs under BLDT loads was developed, but further work will have to be done to verify and if necessary adapt and enhance it. First results for one chosen failure type revealed excellent results, but it will have to be checked based on a statistically relevant number of PCB types. Furthermore, the proposed single loading parameters for the other predominant failure modes will have to be applied and evaluated. Doing

so, it should be possible to develop a methodologically sound approach. Further study will also take into account different load cases, e.g. temperature, applying the same systematics. Finally different load cases should be combined in the approach, and it should be possible to predict the failure location, the failure mode and the lifetime.

4. REFERENCES

Antretter, T. (1998). *Micromechanical modeling of high speed steel*. University of Leoben.

Bai, J., Qin, F., & An, T. (2007). Dynamic Stress of Solder Joints under Board-Level Drop/Impact. *International Conference on Electronics Packaging Technology*.

Barenblatt, G. I. (1962). The Mathematical Theory of Equilibrium Cracks in Brittle Fracture. *Advanced Applied Mechanics*, *7*, 55-129.

Benveniste, Y. (1987). A new approach to the application of Mori-Tanaka's theory in composite materials. *Mechanics of Materials*, *6*(2), 147–157. Elsevier.

Board level drop test method of components for handheld electronic products. (2003). *JEDEC Standard JESD22-B111*, (July).

Böhm, H. J. (2008). *A short introduction to basic aspects of continuum micromechanics* (Vol. 80124).

Coombs, C. F. (2008). *Printed Circuit Handbook* (6th ed.). The McGraw-Hill Companies.

Le Coq, C., Tougui, A., Stempin, M.-P., & Barreau, L. (2011). Optimization for simulation of WL-CSP subjected to drop-test with plasticity behavior. *Microelectronics Reliability*, *51*(6), 1060-1068.

Daniel, I., Luo, J., & Schubel, P. (2008). Three-dimensional characterization of textile composites. *Composites Part B: Engineering*, *39*(1), 13-19.

Dugdale, D. S. (1960). Yielding of steel sheets containing slits. *Journal of the Mechanics and Physics of Solids*, *8*(2), 100-104.

Fuchs, P. F., & Major, Z. (2010). Experimental Determination of Cohesive Zone Models for Epoxy Composites. *Experimental Mechanics*, *51*(5), 779-786.

Fuchs, P. F., Major, Z., & Lang, R. W. (2009). Characterization of the deformation behaviour of PCBs under dynamic loading conditions. *Journal of Physics: Conference Series*, *181*, 012065.

Fuchs, P. F., Pinter, G., & Fellner, K. (2012). Local damage simulations of printed circuit boards based on determined in plane cohesive zone parameters. *submitted to Engineering Fracture Mechanics*.

Fuchs, P. F., Pinter, G., & Major, Z. (2012). PCB drop test lifetime assessment based on simulations and cyclic bend tests. *submitted to Microelectronics Reliability*.

Fuchs, P. F., Pinter, G., & Tonjec, M. (2012). Determination of the Orthotropic Material Properties of Individual Layers of Printed Circuit Boards. *to be published in Microelectronics Reliability*.

Fuchs, P., & Major, Z. (2010). Cyclic bend tests for the reliability evaluation of printed circuit boards under dynamic loads. *Frattura ed Integrità Strutturale*, *15*(15), pages–64.

Jeng, S. T., S, S. H., Yeh, C.-L., Lai, Y.-S., & Wu, J.-D. (2007). High-G drop impact response and failure analysis of a chip packaged printed circuit board. *International Journal of Impact Engineering*, *34*, 1655-1667.

John, H. L., Pang, F. X., Che, B. S., & Xiong, L. X. (2005). Drop Reliability Performance Assessment for PCB Assemblies of Chip Scale Packages (CSP). *Electronics Packaging Technology Conference*.

Luan, J.-E., Tee, T. Y., Pek, E., Lim, C. T., Zhong, Z., & Zhou, J. (2006). Advanced Numerical and Experimental Techniques for Analysis of Dynamic Responses and Solder Joint Reliability During Drop Impact. *Transactions on components and packaging technologies*.

Manson, S. S., & Halford, G. R. (2006). *Fatigue and durability of structural materials* (p. 456). ASM International.

Qu, X., Chen, Z., Qi, B., Lee, T., & Wang, J. (2007). Board level drop test and simulation of leaded and lead-free BGA-PCB assembly. *Microelectronics Reliability*, *47*(12), 2197-2204.

Schwalbe, K. H., Scheider, I., & Cornec, A. (2009). *The SIAM method for applying cohesive models to the damage behaviour of engineering materials and structures*.

Specification for Finished Fabric Woven from “E” Glass for Printed Boards. (2008). *IPC - 4412A Amendment 1*.

Sun, C. T., & Vaidya, R. S. (1996). Prediction of composite properties from a representative volume element. *Composites Science and Technology*, *56*(2), 171-179.

Sørensen, B. F., & Jacobsen, T. K. (2003). Determination of cohesive laws by the J integral approach. *Engineering Fracture Mechanics*, *70*(14), 1841-1858.

Tee, T., Ng, H., Lim, C., Pek, E., & Zhong, Z. (2004a). Impact life prediction modeling of TFBGA packages under board level drop test. *Microelectronics and Reliability*, *44*(7), 1131-1142.

Tee, T., Ng, H., Lim, C., Pek, E., & Zhong, Z. (2004b). Impact life prediction modeling of TFBGA packages under board level drop test. *Microelectronics and Reliability*, *44*(7), 1131-1142.

Tschoegl, N. W. (1989). *The Phenomenological Theory of Linear Viscoelastic Behavior: An Introduction* (p. 769). Springer-Verlag.

Wong, E., Seah, S., & Shim, V. (2008). A review of board level solder joints for mobile applications. *Microelectronics Reliability*, *48*(11-12), 1747-1758. Elsevier Ltd.

PART II: COLLECTION OF PAPERS

PAPER 1: CHARACTERIZATION OF THE DEFORMATION BEHAVIOR OF PCBS UNDER DYNAMIC LOADING CONDITIONS

P.F.Fuchs[a], Z.Major[b], R.W. Lang[c]

[a] Polymer Competence Center Leoben GmbH, Roseggerstrasse 12, 8700 Leoben, Austria

[b] Institute of Polymer Product Engineering, Johannes Kepler University Linz, 4040 Linz, Austria

[c] Institute of Polymeric Materials and Testing, Johannes Kepler University Linz, 4040 Linz, Austria

published in *Journal of Physics: Conference Series*, *181*, 012065 (2009)

Journal of Physics: Conference Series **181** (2009) 012065 doi:10.1088/1742-6596/181/1/012065

Characterization of the deformation behaviour of PCBs under dynamic loading conditions

P. F. Fuchs[1], Z. Major[1, 2], R.W. Lang[1, 3]

1 Polymer Competence Center Leoben GmbH, Leoben, A

2 Institute of Polymer Product Engineering, University of Linz, Linz, A

3 Institute of Materials Science and Testing of Plastics, University of Leoben, Leoben, A

E-mail: fuchs@pccl.at

Abstract. Printed circuit boards (PCBs) are frequently exposed to a complex combination of external and internal thermo-mechanical loads (static, cyclic and impact loads superimposed by local and global temperature effects). In this study, instrumented impact tests of the PCBs were performed and characterized. In addition to the acceleration measurement of the impact, the deformation behaviour was analyzed using a high speed camera and strain gauges. To reduce the testing effort for future PCB design the oscillation behavior of the PCB after impact was simulated using a finite element (FE)-software. Dynamic mechanical analysis experiments were performed and a linear viscoelastic material model was defined. Furthermore, the results of the simulation were compared to the measured values. In spite of the difference in the measured and simulated frequency values over the time, the viscoelastic effects including the damping behaviour were reflected accurately in the simulation.

1. Introduction and Objectives

Printed circuit boards (PCBs) are the heart of all common electronic devices. The area of application of these electronic devices is wide spread. Consequently, the PCBs are exposed to various application dependent complex loads. To meet the increasing demands on the PCBs the build ups and the materials used have to be optimized [1].

In this study the impact loading situation was selected for detailed analysis. Impact is a frequent failure initiator in PCBs and therefore of high practical interest [2] [3]. Due to the load the PCBs are exited to a damped oscillation which was examined and characterized.

To accelerate the optimization process, a finite element (FE) - software was used to simulate the impact. In order to describe the deformation behaviour in the simulation, the material properties had to be determined. Unlike previous studies on the drop test simulation, e.g. [4], which used either elastic or elastic-plastic material models, in this case a viscoelastic material model was chosen. Thus the time dependent damping of the oscillation amplitude and the frequency development could be simulated. Finally the results from the simulation were compared to the experimental results.

The objectives of this paper are to:

- conduct instrumented impact tests on PCBs identifying the loading situation.
- determine the material properties (time dependent modulus values).
- perform a data reduction identifying the parameters for the material model.
- simulate the instrumented impact test.
- compare the simulation with the experiment.

2. Experimental

The specimen characterized was a simplified PCB plate consisting of glass fiber reinforced epoxy layers without intermediate copper layers.

2.1. Instrumented Impact test

Instrumented impact tests were performed using a drop tower and subsequently analyzed. The loading was recorded by an acceleration sensor and the deformation behaviour was characterized by strain gauges applied on the surface of the plates and by a high speed camera (Photron Ultima 512, San Diego, CA, USA). Figure 1 shows the tested plate mounted on the impact fixture with the strain gauges applied. To measure the impact loading the acceleration sensor was fixed at the base plate.

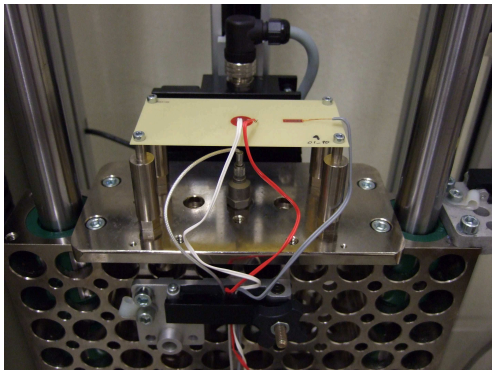

Figure 1. Instrumented impact test with specimen and applied strain gauges and acceleration sensor.

The PCB deformed and the post-impact oscillations measured by the high speed camera are shown in figure 2a. The deformation amplitude is determined at various deformation stages and plotted over the time in figure 2b.

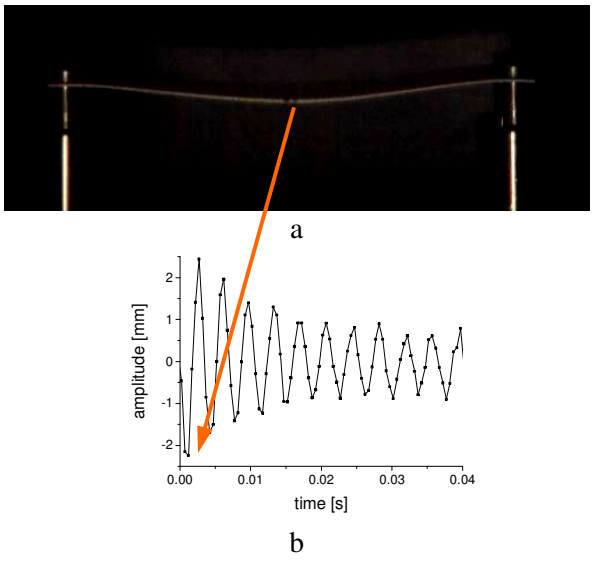

Figure 2. High speed camera image at a deformation stage selected (a) and the oscillogram related to the post-impact oscillations (b).

Due to the limited optical resolution of the high-speed camera, the amplitude decrease could be monitored only during the first 50 ms after the impact. Data from strain gauges was used to cover larger times.

Furthermore, the strain gauges provided information on the local strains. The strain gauges were applied both at the center of the plate and at the half distance between the edge and the mid of the plate. The strain gauge at the center was a biaxial type and additionally to the longitudinal strain the transversal strain was measured.

2.2. Mechanical Analysis

The plate specimen consists of fiber reinforced epoxy resin layers and was therefore supposed to show viscoelastic deformation behavior. To determine an adequate viscoelastic material model for the FE simulation, dynamic mechanical analysis (DMA) experiments were performed under bending load over a wide frequency and temperature range (from 0.01 up to 10 Hz and at the temperatures of -40,-20, 0, 23, 60, 125 °C). The plate was mounted on a 3 point bending fixture and exposed to sinusoidal oscillations by the actuator of the dynamic testing machine (figure 3). An electrodynamic testing machine (BOSE 3450, BOSE Co, MN, USA) was used for these tests.

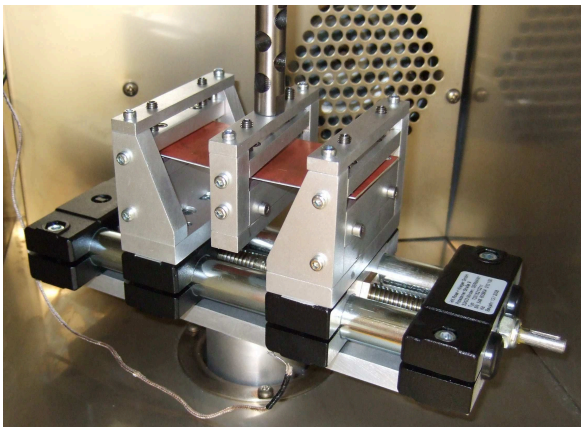

Figure 3. Bending fixture for the dynamic mechanical analysis with clamped plate specimen.

2.3. Data Reduction

The data obtained from the DMA is the dynamic bending modulus over the frequency for the different temperatures. To get the parameters for the linear viscoleastic material model used in the FE simulation, the following steps were performed:

- Creation of a master-curve using the time (frequency)-temperature shift principle. The master-curve approach is well defined and described in the polymer science literature e.g. [5], [6].
- Calculation of the dynamic tensile modulus from the dynamic bending modulus considering the plate stiffness.
- Usage of the linear elastic equations to determine the dynamic shear modulus from the dynamic tensile modulus assuming a constant bulk modulus and a Poisson's ratio value from the literature [7].
- Transformation of the frequency basis to a time basis [8].
- Prony series fit for the dynamic shear modulus master-curve. A detailed description on the physical and mathematical background of the Prony series can be found in literature [8].

2.4. Simulation

The deformation behavior during the impact process of the test plate was simulated using commercial FE software Abaqus 6.7.1 (Simulia, Providence, RI; USA). The plate was modelled as a homogenous solid and the boundary conditions were set corresponding to the mounting situation on the impact fixture (see figure 1). The specimen was loaded directly by the acceleration values measured using the acceleration sensor. The material model was assumed as linear viscoelastic and defined by the Prony series parameters calculated from the DMA data. The deformation amplitude as a function of time was determined in the simulation and compared to the experimental results.

3. Results and Discussion

First, the data measured in the DMA experiments for the generation of the material model is presented. The frequency dependence of the dynamic bending modulus values for three different temperatures over the frequency range investigated (from 0.01 up to 10Hz) are shown in figure 4.

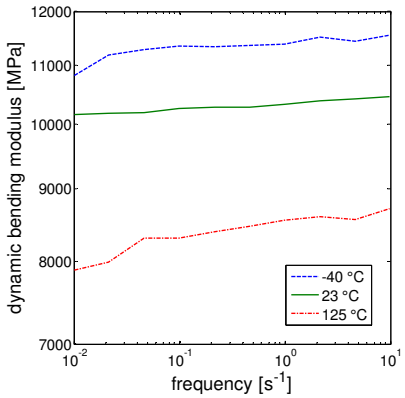

Figure 4. The frequency dependence of the dynamic bending modulus for three different temperatures (-40°C, 23°C and 125°C).

As the experimentally determinable frequency range is limited, to obtain dynamic modulus values for higher frequency ranges, a reference temperature was selected (in this case it was the room temperature, 23 °C) and a master-curve was created.

The master-curve was generated by shifting the dynamic modulus measured at higher temperatures to lower frequencies and the dynamic modulus measured at lower temperatures to higher frequencies. The concept is based on the physical effect, that the influence on the material behavior is similar regarding a change of the loading time and a change of the temperature.

The time-dependent dynamic shear modulus was calculated from the frequency-dependent dynamic bending modulus. The resulting master-curve was shown in figure 5. A Prony series measured was fitted to the data and the relaxation time values and the modulus values were calculated.

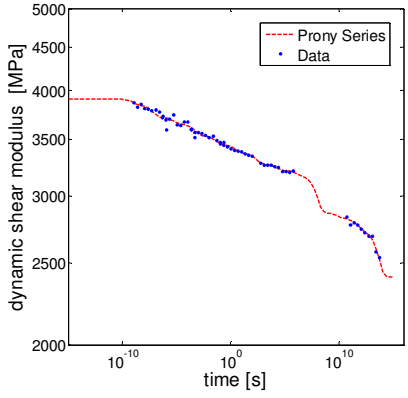

Figure 5. Master-curve of the dynamic shear modulus with the Prony series fit.

The envelop curves of both the measured deformation amplitudes and the simulated deformation amplitudes at the center of the plate over the time were shown in figure 6.

The deformation amplitude was calculated from the longitudinal strain measured by the strain gauge applied at the center of the specimen. The maximum value of the deformation measured by the high speed camera to the maximum value of the longitudinal strain was taken as proportionality factor. The second curve shows the results of the FE simulation. Over the measured time range of 0.25s, the experimental and the simulated envelop curves reveal only small, nearly negligible differences. It is concluded that the damping behaviour of the material in terms of amplitude decay is accurately described by the Prony series and by the master curves generated using the DMA experiments.

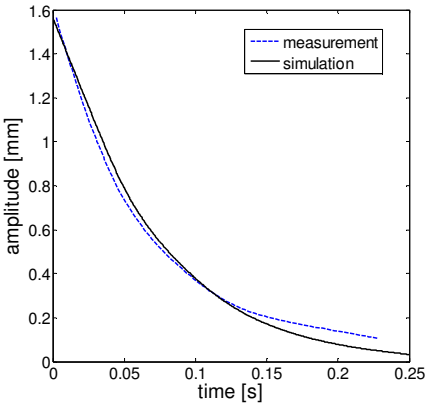

Figure 6. Deformation amplitude development of the post impact oscillation.

The frequency of the damped oscillation was found to decrease with increasing time both in the experiments and in the simulation. For comparison the results are shown in figure 7. Along with the amplitude, the loading rate is also decreasing over the time. Due to the viscoelastic properties of the epoxy matrix, the decline of the loading rate leads to a lower stiffness. As the frequency of the oscillation depends on the specimen stiffness [9], this effect could possibly explain the sinking frequency.

However, the experimental results reveal significantly smaller values over the entire time range than the simulation (the initial values are at about 300 Hz and 500 Hz respectively). No plausible reason for this discrepancy was found up to now. One reason of the difference between the experiments and the simulation could be measurement errors due to the very small forces at the dynamic bending test which were difficult to record. To adress this problem, further experiments will be performed and theoretical considerations regarding the viscoelastic model used will be done.

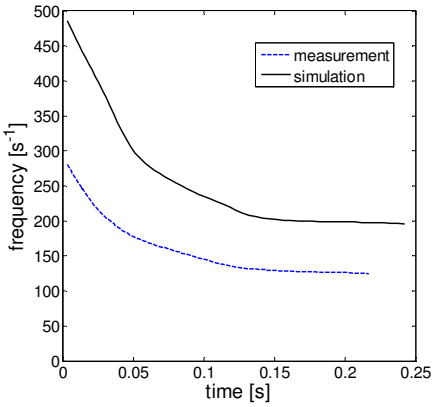

Figure 7. Frequency development over the time of the post impact oscillation.

4. Summary and Conclusion

Instrumented impact tests were performed on PCB plates and the subsequent oscillations were recorded by optical devices and by strain gauges over a wide time range.

To characterize the material behavior and to determine material parameters for FE simulation dynamic mechanical analysis (DMA) tests were carried out. A linear viscoelastic material model was defined by the parameters of a Prony series and applied.

FE simulations were performed on PCB plates using the viscoelastic material models and the results of the simulation in terms of amplitude and frequency were compared.

While the results of the simulation reveal a good correlation to the experimental results regarding the amplitude of the deformation behaviour, significant difference was found between the measured and the calculated frequency range for the damped oscillations.

To gain more insight into the frequency change during the damped oscillations, both further experiments will be performed and theoretical considerations regarding the viscoelastic material model and the FE model used will be done.

References

[1] Ehrler S 2002 Properties of new printed circuit board base materials *Circuit World* **28/**4 38
[2] Jeng S T, Sheu H S, Yeh C L, Lai Y S, Wu J D 2007 High G drop impact response and failure analysis of a chip packaged printed circuit board *International journal of impact engineering* **34** 1655
[3] Liu F, Meng G, Zhao M 2007 Viscoelastic influence on dynamic properties of PCBs under drop impact *Journal of electronic packaging* **129** 266
[4] Wang Y, Low K H, Pang H L J, Hoon K H, Che F X, Yong Y S 2006 *Modeling and simulation for a drop-impact analysis of multi-layered printed circuit boards* Microelectronics Reliability **46** 558
[5] Wineman A S, Rajagopal K R 2000 *Mechanical Response of Polymers An Introduction* (Cambridge:University Press)
[6] Schwarzl F R 1990 *Polymermechanik* (Berlin: Springer)
[7] Walter H 2003 *Morphologie-Zähigkeitskorrelation von modifizierten Epoxidharzsystemen mittels bruchmechanischer Prüfmethoden an Miniaturprüfkörpern* (Halle-Wittenberg: Martin-Luther-Universität)
[8] Tschoegel N W 1989 *The Phenomenological Theory of Linear Viscoelastic Behavior* (Berlin: Springer)
[9] Pilkey W K 1994 *Formulas for Stress, Strain, and structural Matrices* (New York: Wiley–Interscience)

PAPER 2: CYCLIC BEND TESTS FOR THE RELIABILITY EVALUATION OF PRINTED CIRCUIT BOARDS UNDER DYNAMIC LOADS

P.F.Fuchs[a], Z.Major[b]

[a] Polymer Competence Center Leoben GmbH, Roseggerstrasse 12, 8700 Leoben, Austria

[b] Institute of Polymer Product Engineering, Johannes Kepler University Linz, 4040 Linz, Austria

published in *Frattura ed Integrità Strutturale*, *15*(15), pages–64 (2010)

Cyclic bend tests for the reliability evaluation of printed circuit boards under dynamic loads

P.F.Fuchs
Polymer Competence Center Leoben GmbH, Roseggerstrasse 12, 8700 Leoben, Austria

Z. Major
Institute of Polymer Product Engineering, Johannes Kepler University, Altenbergerstrasse 69, 4040 Linz, Austria

ABSTRACT. The reliability of printed circuit boards under dynamic loads is a key issue in the handheld electronic products industry. In order to predict the performance of the boards in their application lifetime, different tests were developed. The current industry-wide standard testing method is a board level drop test. In this test, the boards are dropped under defined conditions until a failure in the board is detected. The main failure driver is a flexural oscillation of the board due to the impact event. As this test method has a number of drawbacks, an alternative test method was evaluated in this study. A board level cyclic bend test was used and the results of both tests were compared. A very good correlation between the methods could be observed, supporting the suitability of the board level cyclic bend test for the determination of the drop test performance. The advantages of the alternative test method were shorter testing times, better adaptability and test simulations at lower computing time. In future analysis, test simulations will be used to generate Wöhler curves related to the local stresses.

KEYWORDS. Printed Circuit Board; Reliability; Drop Test; Cyclic Bend Test; Fatigue.

INTRODUCTION

The performance of printed circuit boards (PCBs) under dynamic loads is of significant interest due to the increasing market for handheld electronic products. Because of their size and application, handheld electronic products are especially prone to be dropped, i.e. exposed to an impact load during their useful service life. These impact loads can result in serious damage of the PCB interconnections and thus in the malfunction of the product. To evaluate the drop performance and to develop reliable designs, different board level test methods were introduced. Wong et al. reviewed the development of the methods in their work [1]. A standardized board level drop test (BLDT) JESD22-B111 was defined under the Joint Electronic Device Engineering Council (JEDEC) [2]. In this test defined drops of the PCBs are repeated until failure is detected. The rather complex test set-up and load application affect the test robustness. Drawbacks of the standardized BLDT are discussed in literature e.g. by Wong et. al [1, 3] and Luan et. al [4]. Apart from the poor reproducibility, the main criticisms are the slow test throughput and the lack of relevance to the product drop impact performance.
Thus, in this work an alternative test to determine the drop performance was performed and evaluated. Flexing of the circuit board, due to input acceleration created from dropping, is the primary driver for PCB failure. Therefore, a board level cyclic bend test (BLCBT), applying a repeated and well defined flexure, was used to reproduce the loading situation.

The simplified and accelerated load application should result in a more robust test method, providing faster and more reliable results.
In this study, conventional BLDT and BLCBT were performed for a set of PCBs. The results were compared to evaluate the suitability of cyclic bend tests as an alternative test method.
The test method applied was based on similar ideas to the high speed cyclic bend test (HSCBT) [5, 6], but was realized under different loading conditions. The specimens were loaded under three-point bending and significantly higher deflection amplitudes were used.

MATERIALS AND SPECIMENS

PCBs with different layer build-ups, expected to differ significantly regarding their BLDT performance, were tested. The aim was to simplify the comparison of the testing methods by covering a wide range of BLDT performances.
The analyzed specimens were eight layer PCBs and six different layer build-ups were tested. These build-ups differed regarding the intermediate epoxy layers which are glass-fibre reinforced in most cases. Only for the surface layers it can in some cases be advantageous to use neat epoxy resin. Thus, variations in the reinforcement of the surface layers were considered in the test plan. Additionally, different epoxy resin types were analyzed. A detailed summary of the materials used in the different layers (Core, IL1, IL2 and IL3) of the tested PCB designs is provided in Tab. 1. The abbreviations M1, M2, M3 and M4 represent different manufactures and epoxy resin types respectively, PP indicates a Prepreg layer (glass fibre reinforced) and R stands for an unreinforced and neat epoxy resin layer. PP1 and PP2 differ regarding the glass fibre mat used for reinforcement. The layers marked with b are the low dielectric constant versions of the layers marked with a. A schematic representation of the layer assignments in the build-up, including the epoxy layer thicknesses, is shown in Fig. 1. All copper layers had a thickness of 18 μm.

Design Nr.	Core	IL1	IL2	IL3
	Material			
1	*M1 a*	*M1 PP 1a*	*M1 PP 2a*	*M3* R
2	*M1 a*	*M1 PP 1a*	*M1 PP 2a*	*M1 PP 2a*
3	*M1 a*	*M1 PP 1a*	*M1 PP 2a*	*M4* R
4	*M2*	*M2 PP1*	*M2 PP2*	*M3* R
5	*M2*	*M2 PP1*	*M2 PP2*	*M2 PP2*
6	*M1 b*	*M1 PP1 b*	*M1 PP2 b*	*M3* R

Table 1: An overview of the chosen materials for the specified layers in the six PCB designs tested.

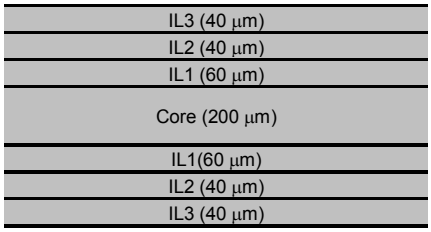

Figure 1: A schematic representation of the layer assignments in the PCB build-up.

The PCB geometry was chosen following the JEDEC standard, but was adapted according to customer requirements. The defined board geometry is shown in Fig. 2. The darker squares at the board centre represent the mounted components. Only two components instead of 15 were used to simplify the test. The two most failure-prone components, with regard to the PCB manufactures experience, were chosen. The components were daisy chained according to the standards.

BOARD LEVEL DROP TEST ANALYSIS

Before the development of an alternative test method, it was necessary to analyze the acting loads and resulting PCB deformation in a standard BLDT. The drawn conclusions should help designing a reasonable test.
Except for some adapted parameters, the analyzed BLDT was performed according to the JEDEC standard. An

alternative board geometry, described in *Materials and specimens* chapter, and a different board fixation (longer standoffs) were used. The drop height and strike surface were adjusted to achieve a specified G level of 1500 g peak acceleration and a pulse duration of 1 ms.
Drops were repeated until first failure was detected. Failure was defined as an electrical discontinuity in the daisy chains of resistance greater than 1000 ohms lasting for 1 microsecond or longer. To measure the very short lasting electrical discontinuities a special event detector (256STD, Analysis Tech, Wakefield, US) was used.
For the BLDT analysis a high-speed camera (Fastcam SA1.1, Photron Inc., San Diego, US) was used. In Fig. 3 the BLDT set-up is shown. The board is fixed with four screws at its corners on the drop table. The test, i.e. the impact of the drop table on the strike surface was filmed with the high-speed camera.

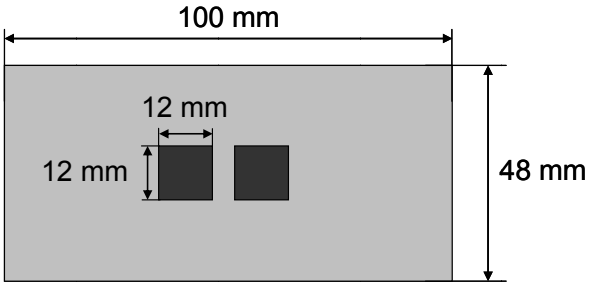

Figure 2: A schematic presentation of the used PCB geometry. The darker squares represent the mounted components.

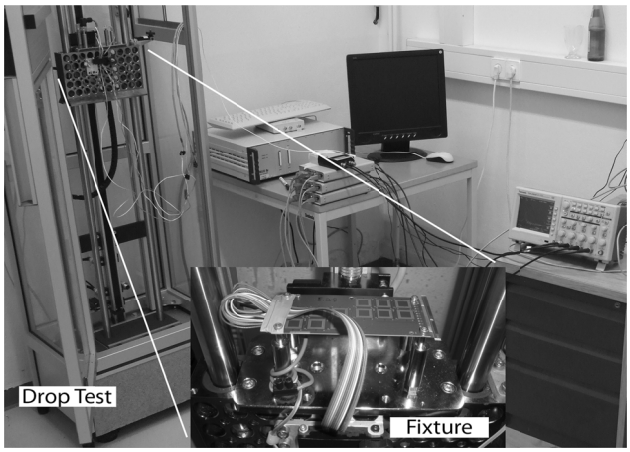

Figure 3: The test set-up of the JESD22-B111 board level drop test.

In Fig. 4a), starting from the top, three consecutive high-speed camera images show the impact of the PCB. The board is set in a damped bending-oscillation, which can be recorded by a camera. Using image analysis software (Viana 3.64, Thomas Kersting, Institute for Didactics and Physics, University of Essen, DE), an oscillogram of the PCB centre deflection could be generated (Fig. 4b). The initial oscillation frequency was determined as 280 Hz.
Furthermore, strain gauges were placed at the PCB surface centre to measure the maximum occurring longitudinal strains. The observed longitudinal strain values at the first deflection were 2×10^{-3}.
From the analysis results it could be concluded that the main deformation mechanism and consequently failure driver is the bending-oscillation. Knowing this, it seemed reasonable to expect correlating results from a BLCBT, where a sinusoidal cyclic bending load is applied.

BOARD LEVEL CYCLIC BEND TEST DEVELOPMENT

For the load generation an electro-dynamic testing machine (Bose ElectroForce 3450, Bose Corporation, Eden Prairie, US) was used. This machine has the advantage of a very precise force and displacement control and was used to apply a sinusoidal displacement amplitude.

For the board fixation a three-point bending fixture was constructed, where the board is placed centred on support rollers (Ø 5 mm) which have a distance of 90 mm to each other. The load is applied by a fin, which consists of two rollers (Ø 5 mm), clamping the board at half length. The clamping force was applied over spring plungers to have a defined load. A schematic representation of the fixation is shown in Fig. 5.

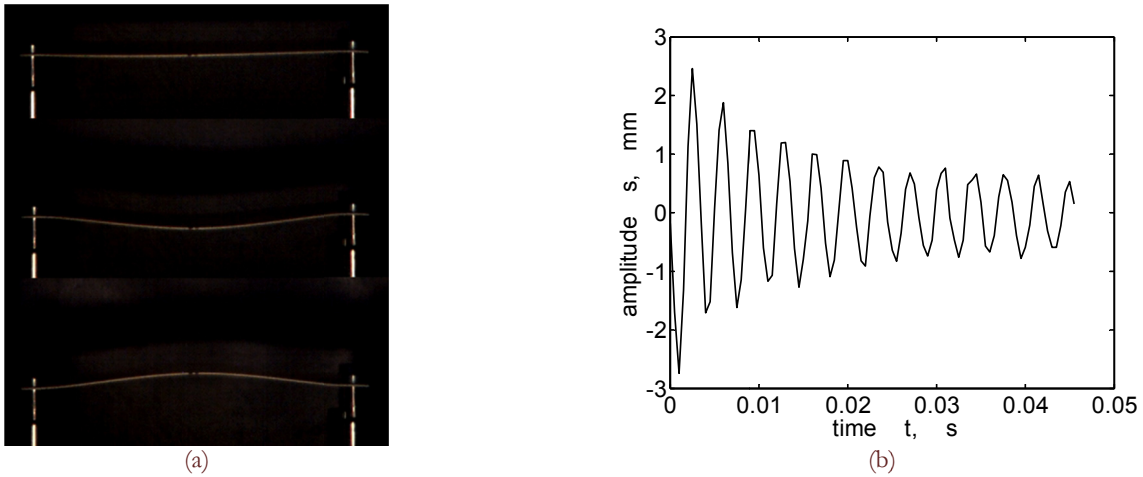

(a) (b)

Figure 4: The results of the JESD22-B111 board level drop test high-speed camera analysis. In a) chosen consecutive high-speed camera pictures show the development of the PCB deflection right after the impact. In b) the according amplitude oscilloagram is presented.

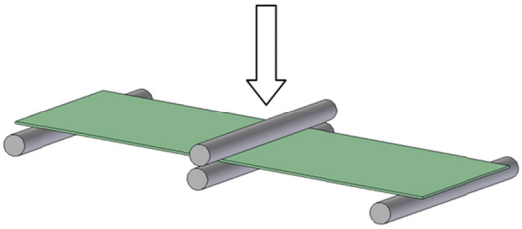

Figure 5: A schematic representation of the three-point bending fixture used in the board level cyclic bend test.

It needs to be considered that the board is not clamped at the position of the support rollers, implicating that the load can only be applied in one direction. A set-up with clamps at the support rollers would have resulted in an overconstrained system. Robustness and reproducibility of the test would have been affected, counteracting previous efforts. Therefore, it was accepted that in contrast to the actual BLDT alternating loads could not be applied.

The test parameters were derived from the BLDT analysis. The maximum peak-to-peak oscillation amplitude in the BLDT was about 5 mm and the maximum fibre strain was about 2 x 10^{-3}. For the BLCBT peak-to-peak amplitudes of 4mm with a mean deflection of 3mm (BLCBT Set-Up 1) and 3mm with a mean deflection of 2.5mm (BLCBT Set-Up 2) were chosen. The maximum fibre strains were 1.7 x 10^{-3} and 2.2 x 10^{-3}, that is in the range of the BLDT. The minimum deflection of -1mm was defined to ensure that no lift-off of the board from the support rollers could occur in the tests.

Due to machine limits, it was not possible to perform the tests at the oscillation frequency of the impacted PCB in the BLDT (280 Hz). To remain at the desired optimum machine displacement control precision the frequency was kept at 25 Hz.

A picture of the final test set-up is shown in Fig. 6. The event detector was used in the same way as for the BLDT.

EXPERIMENTAL METHOD COMPARISON

The BLDT was performed with nine samples of every PCB build-up to obtain representative results and to apply statistics. For the BLCBT, as indicated in *Board level cyclic bend test development* chapter, two different set-ups were used. Three boards for all designs and both set-ups were tested to decide which performs better. For the chosen set-up another five test repetitions were planned to apply statistics according to the BLDT evaluation.

For the BLDT, the number of drops until the first failure, detected by the event detector, was taken as evaluation parameter. Analogous, for the BLCBT the number of cycles until failure was measured.

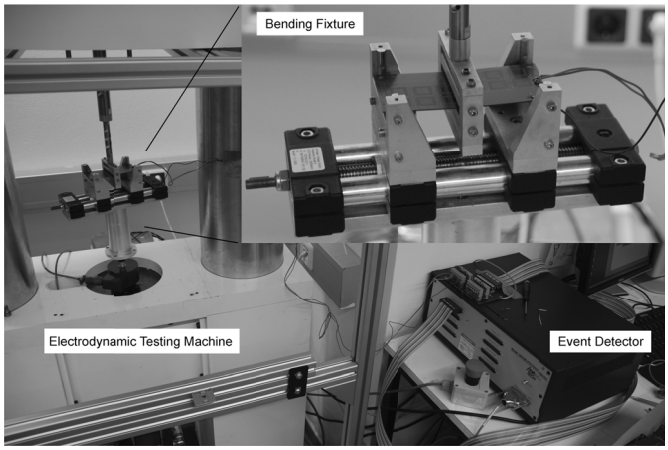

Figure 6: The test set-up of the board level cyclic bend test.

To compare the BLDT with the BLCBT the method average results for the different PCB build-ups were plotted against each other and a Pearson's r factor [7] was calculated to rate the linear correlation. A schematic representation of the method comparison is shown in Fig. 7.

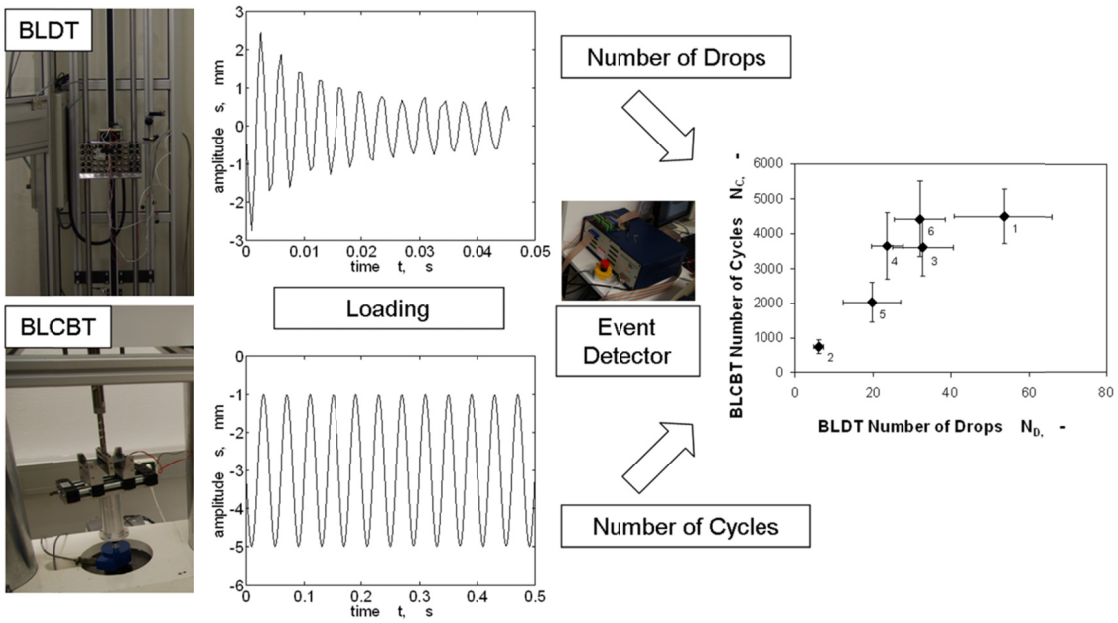

Figure 7: Schematic representation of the comparison of BLDT and BLCBT.

Furthermore, to check the correlation of the failures types introduced by the different testing methods, a failure pattern analysis was performed. Microsections of the expected failure locations were prepared and analyzed with a light microscope. It was tested if the same failure modes occur despite the different loading conditions.
Finally, as it is advantageous to use the Weibull distribution in reliability and life data analysis, similar to the BLDT analysis (e.g. [8, 9]), Weibull-parameters were determined to allow for a comparison of the methods on the basis of a statistical evaluation.
Therefore, a fictitious time-to-failure had to be calculated for all BLDT results to have a correlating parameter to the time-to-failure in the BLCBT. A conversion factor was introduced by dividing the average time-to-failure of all build-ups in the

BLCBT through the average number of drops of all PCB build-ups in the BLDT. This factor was used to calculate fictitious times-to-failure based on the number of drops until failure of the BLDT.

RESULTS AND DISCUSSION

The results of the performed BLDT are presented in Fig. 8 in terms of drops until failure. The pillars represent the average of nine measurements respectively. The results show the desired wide range of board BLDT performances for the six tested build-ups. The large gap between designs 1 and 2 results from the influence of the reinforcement in the surface layers. While design 1, having unreinforced outer layers (IL3), performed very well, design 2, built with glass fibre reinforced IL3 layers, performed worst of all designs. In design 3 a different neat epoxy resin type was used for the IL3 layers, resulting in a worse BLDT performance compared to design 1. For designs 4 and 5 the same effect, regarding the reinforcement of the IL3 layers, could be observed as for designs 1 and 2. The effect was less pronounced, apparently due to the different material manufactures. Design 6 was a low dielectric constant epoxy resin version of design 1, resulting in a BLDT performance in the range of design 3.

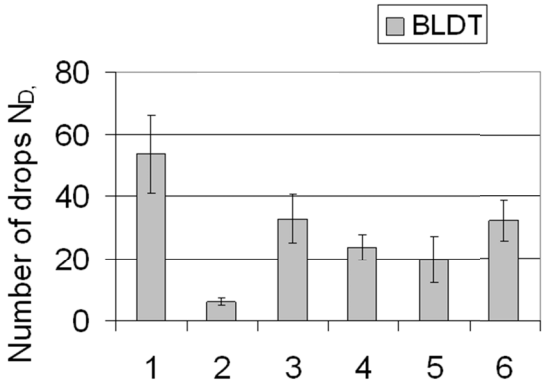

Figure 8: Results of the BLDT performed on six PCB designs. Additional to the average values the standard deviations are indicated.

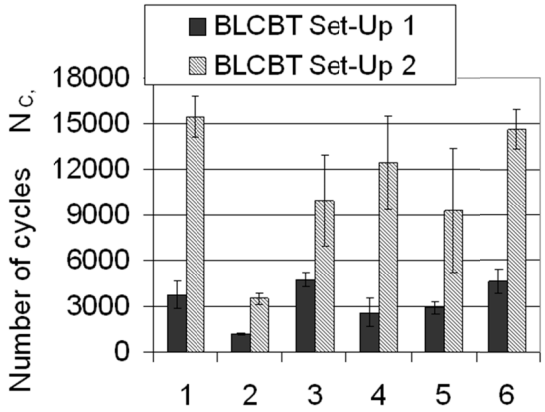

Figure 9: BLCBT results showing the amplitude dependence. Additional to the average values the standard deviations are indicated.

BLCBT with two different set-ups were performed on three specimens for every design. The average results of BLCBT Set-Up 1 and BLCBT Set-Up 2 are presented in Fig. 9 in terms of cycles until failure. As expected, set-up 2, with the application of the lower deflection amplitude, resulted in significant longer times until failure. Nevertheless, if expressed in percentage, the differences between the tested designs were very similar for the set-ups. As set-up 2 did not have an advantage regarding the measurement scatter, the faster set-up 1 was chosen for further tests.
Five more specimens were tested with set-up 1 to be able to perform a statistic evaluation of the data. In Fig. 10 the BLDT results were compared with the BLCBT results of set-up 1. The number of cycles until failure in the BLCBT was

plotted over the number of drops until failure in the BLDT. The plot is revealing a clear method correlation and the Pearson's r factor, determined as 0.87, supported the method hypothesis. However, because of existing discrepancies from the linear correlation, which can be attributed to the existing data scatter on the one hand and on the unregarded loading condition dependent material behaviour on the other hand, only significant differences in the BLDT behaviour can be expected to be reflected in the BLCBT.

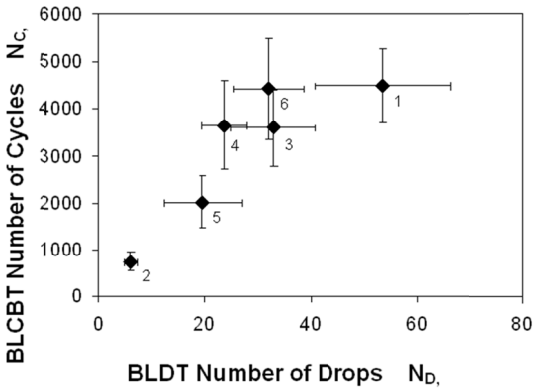

Figure 10: Comparison of the BLDT and BLCBT set-up 1 results for six PCB designs. Additional to the average values the standard deviations are indicated.

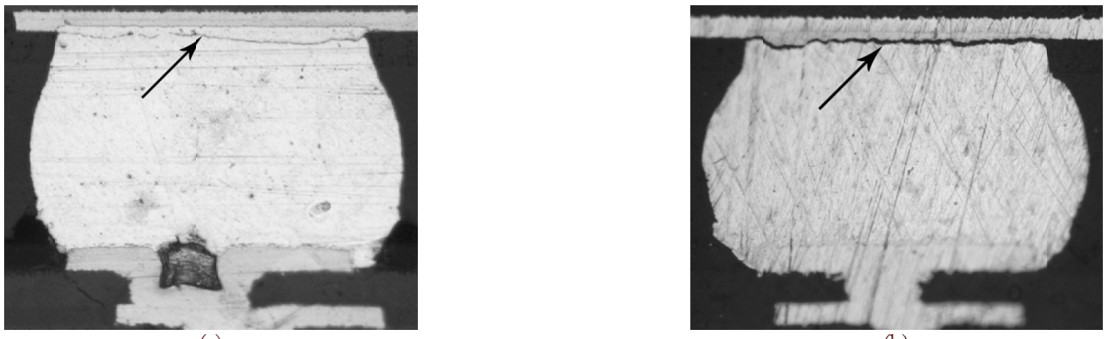

(a) (b)

Figure 11: Comparison of a) the failure of design 1 in the BLDT and b) the failure of design 1 in the BLCBT, analyzed with light microscopy.

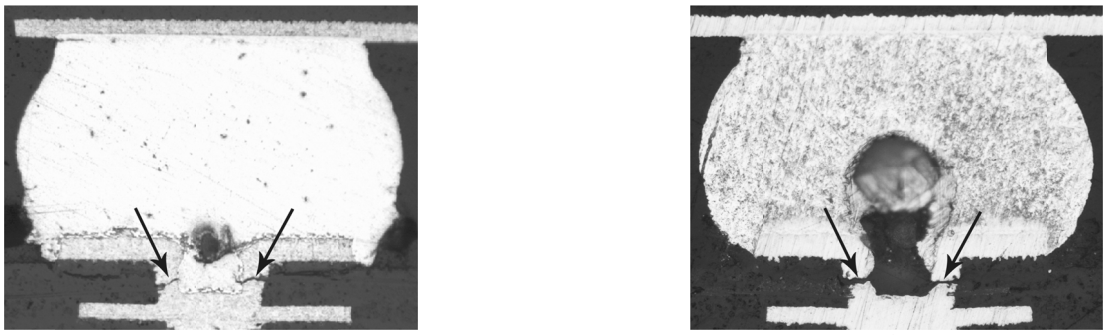

(a) (b)

Figure 12: Comparison of a) the failure of design 2 in the BLDT and b) the failure of design 2 in the BLCBT, analyzed with light microscopy.

Moreover, to verify the accordance between BLCBT and BLDT a failure pattern analysis was performed on the tested specimens. The analysis was focused on designs 1 and 2, expected to exhibit the most pronounced differences in the failure mode. In Fig. 11 and Fig. 12 the light microscopy images of identified failure locations are shown. The cross

sectional areas of the two-sided cut sphere represent the solder ball connecting the printed circuit board (at the bottom of the image) with the mounted component (at the top of the image). The detected failures are indicated by black arrows. The failures correspond to typical failure patterns mentioned in literature e.g. [4, 9-12]. In Fig. 11 the failure of design 1 in the BLDT (Fig. 11a) is compared to the failure of design 1 in the BLCBT (Fig. 11 b). A matching failure location could be observed. The solder ball was cracked close to the mounted components. In Fig. 12 the failure of design 2 in the BLDT (Fig. 12 a) is compared to the failure of design 2 in the BLCBT (Fig. 12b). Again, the failure location was the same for both test methods, but different from the design 1 location. Failure occurred in the copper interconnections in the board and not in the solder ball. Thus, it could be shown that both methods led to the same failure modes for the examined design 1 and 2, which further supports the correlation of the methods.
A statistical comparison of the BLDT and BLCBT results was based on the Weibull distribution [13].

$$y = abx^{b-1}e^{-ax^b} \tag{1}$$

The parameters a, the scale parameter, and b, the shape parameter, are given for all analyzed designs in Tab. 2. The times to failure of the BLDT are fictive values and were calculated as described in *Experimental method comparison* chapter. The performance trend in the BLDT Weibull analysis is matched to the performance trend in the BLCBT Weibull analysis for all examined designs. In Fig. 13 the difference between the Weibull distribution for designs 1 and 2 is shown graphically.

PCB Design	1		2		3		4		5		6	
Weibull Parameter	a	b	a	b	a	b	a	b	a	b	a	b
BLDT	*240.4*	*2.4*	*27.4*	*2.7*	*147.4*	*2.4*	*104.8*	*3.6*	*86.6*	*1.5*	*143.3*	*2.8*
BLCBT	*200.4*	*3.7*	*33.9*	*2.1*	*159.2*	*2.4*	*165.6*	*2.3*	*90.0*	*1.9*	*197.3*	*2.3*

Table 2: Two-parameter Weibull distributions for all tested PCB designs are compared for the BLDT and the BLCBT.

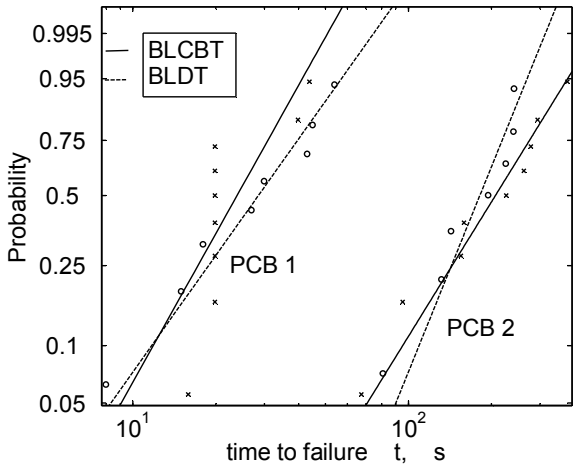

Figure 13: The graphical representation of the two-parameter Weibull distributions for designs 1 and 2. The results of both methods, the BLDT and the BLCBT are presented.

SUMMARY AND CONCLUSION

The JESD22-B111 board level drop test (BLDT) is the current state of the art to evaluate the reliability and lifetime of PCBs under impact loads. As the rather complex test set-up implicates some drawbacks such as poor reproducibility and slow test throughputs, an alternative test method was analyzed. A board level cyclic bend test (BLCBT) was evaluated. In this method, instead of repeated drops, a controlled cyclic displacement is applied on the PCBs.
The two methods were compared and evaluated for six different PCB designs. The results correlated very well and therefore the BLCBT may be used to estimate the BLDT performance. This conclusion was supported by a performed failure analysis showing that the design dependent failure modes were independent of the test method. Additionally, a

statistical evaluation based on a two-parameter Weibull distribution was performed. The statistical results supported the good approach of the two methods.
Finally, the following advantages of the BLCBT over the BLDT could be identified:

- ✓ The BLCBT testing time is significantly shorter than the BLDT testing time (The factor between the method testing times depends on the board performances. The better a board performs, the faster is the BLCBT compared to the BLDT. In our case the BLCBT was about two times faster than the BLDT. The reason for the testing time differences is an approximate break of 5 seconds between each drop in the BLDT.)
- ✓ The BLCBT can be performed considering different influence parameters (e.g. temperature, frequency or amplitude) by default. In contrast the BLDT under temperature influence is costly, as the temperature has to be applied on a large testing space. Furthermore, in the BLDT only the initial amplitude can be controlled. As this is done by adapting the impact energy, an adjustment to predefined amplitudes is difficult. The frequency in BLDT can hardly be varied at all.
- ✓ The BLCBT can be performed on basically every dynamic testing machine which is capable of applying the desired displacement and frequency.
- ✓ The BLCBT can be simulated at lower computing times than the BLDT using the Finite Element Method. Simulations of the BLDT are difficult, as the load application and the definition of the boundary conditions are challenging [14, 16]. The simplest way to simulate the BLDT is the 'Input-G method' [13, 17, 18, 20, 21]), where an acceleration signal is applied directly to the board, which is still computationally expensive.

In future analysis it is planned to generate Wöhler curves [22] to evaluate the fatigue behaviour of PCB designs. Therefore, BLCBT will be performed at different deflection levels. To determine the acting local stresses, finite element simulations are planned.
Thus, having the local failure stresses in dependence of the PCB bending amplitudes, it would be possible to plot the local failure stress over the number of cycles. This resulting Wöhler curves should help to improve the understanding and the prediction of the PCB fatigue behaviour.

ACKNOWLEDGEMENTS

The research work of this paper was performed at the Polymer Competence Center Leoben GmbH (PCCL, Austria) within the framework of the Kplus-program of the Austrian Ministry of Traffic, Innovation and Technology with contributions by the Institute of Material Science and Testing of Plastics, University of Leoben and the Austria Technologie & Systemtechnik Aktiengesellschaft. The PCCL is funded by the Austrian Government and the State Governments of Styria and Upper Austria.

REFERENCES

[1] E. H. Wong, S. K. W. Seah, V. P. W. Shim, Microelectron Reliab., 48 (2008) 1747.
[2] JEDEC Standard JESD22-B111, Board Level Drop Test Method of Components for Handheld Electronic Products, (2003).
[3] E. H. Wong, S. K. W. Seah, W. D. van Driel, J. F. J. M. Caers, N. Owens, Y. –S. Lai, Microelectron Reliab., 49 (2009) 139.
[4] J. Luan, T. Y. Tee, E. Pek, C. T. Lim, Z. Zhong, Microelectron Reliab., 47 (2007) 450.
[5] S. K. W. Shea, E. H. Wong, Y.-W. Mai, R . Rajoo, C. T. Lim, In: Proceedings of 56th electronic components and technology conference, (2006) 1003–8
[6] E. H. Wong, S. K. W. Seah, C. S. Selvanayagam, R. Rajoo, W. D. Driel, J. F. J. M. Caers, X. J. Zhao, N. Owens, L. C. Leoni, Y. –S. Lai, C. –L. YEH, J. Electron. Mater., 38 (2009) 884.
[7] J. L. Rodgers, W. A. Nicewander, The American Statistician, 42(1) (1988) 59.
[8] X. Qu, Z. Chen, B. Qi, T. Lee, J. Wang, Microelectron Reliab., 47 (2007) 2197.
[9] G. Heaslip, J. M. Punch, Electronic and Photonic Packaging, 3 (2003) 125.
[10] D. Y. R. Chong, H. J. Toh, B. K. Lim, P. T. H. Low, In: Electronics Packaging Technology Conference, (2005) 262.
[11] P. L. Tu, Y. C. Chan, K. C. Hung, J. K. L. Lai, Microelectron Reliab., 41 (2001) 287.
[12] W. H. Zhu, J. H. L. Pang, X. R. Zhang, E. Poh, Y. F. Sun, A. Y. S. Sun, C. K. Wang, H. B. Tan, In: Electronic Components and Technology Conference, (2008) 1667.
[13] O. Beucher, Wahrscheinlichkeitsrechnung und Statistik mit Matlab. Springer, Berlin Heidelberg, (2005).

[14] M. I. Sakri, S. Saravanan, P. V. Mohanram, Int. J. Comput. Methods Eng. Sci. Mech., 9 (2008) 138.
[15] Y. Wang, K. H. Low, H. L. J. Pang, K. H. Hoon, F. X. Che, Y. S. Yong, Microelectron Reliab., 46 (2006) 558.
[16] D. Yu, J. B. Kwak, S. Park, J. Lee, Dynamic responses of PCB under product-level free drop impact, Microlelectron Reliab, Article in Press (2010).
[17] T. Y. Tee, J. Luan, E. Pek, C. T. Lim, Z. Zhong, EuroSimE2004, (2004) 133.
[18] T. Y. Tee, J. Luan, E. Pek, C. T. Lim, Z. Zhong, In: Electronic Components and Technology Conference, (2004) 1094.
[19] J. E. Luan, T. Y. Tee, E. Pek, C. T. Lim, Z. Zhong, J. Zhou, EEE Transactions on Components and Packaging Technologies, 29 (2006) 449.
[20] C. –Y. Chou, T. –Y. Hung, S. –Y. Yang, M. –C. Yew, W. –K. Yang, K. –N. Chiang, Microelectron Reliab., 48: (2008)1149.
[21] J. Bai, F. Qin, T. An, In: International Conference on Electronics Packaging Technology, (2007) 187.
[22] D. Radaj, M. Vormwald, Ermüdungsfestigkeit Grundlagen für Ingenieure, Springer, Berlin Heidelberg (2007).

PAPER 3: DETERMINATION OF THE ORTHOTROPIC MATERIAL PROPERTIES OF INDIVIDUAL LAYERS OF PRINTED CIRCUIT BOARDS

P.F.Fuchs[a], M. Tonjec[a], G.Pinter[b]

[a] Polymer Competence Center Leoben GmbH, Roseggerstrasse 12, 8700 Leoben, Austria

[b] Material Science and Testing of Plastics, Department Polymer Engineering and Science, University of Leoben, Otto Gloeckel-Strasse 2, 8700 Leoben, Austria

accepted for publication in *Microelectronics Reliability* (2012)

Determination of the Orthotropic Material Properties of Individual Layers of Printed Circuit Boards

P.F.Fuchs[a], G. Pinter[b], M. Tonjec[a]

[a] Polymer Competence Center Leoben GmbH, Roseggerstrasse 12, 8700 Leoben, Austria
[b] Material Science and Testing of Plastics, Department of Polymer Engineering and Science, University of Leoben, Otto Gloeckel-Strasse 2, 8700 Leoben, Austria

Abstract

To improve the reliability of printed circuit boards (PCB), occurring failure modes have to be studied and analyzed. In order to reduce the expenses of experimental testing, finite element analysis (FEA) is used to describe the failure behaviour. Therefore, the availability of the proper material data is crucial. As the materials used in printed circuit boards, glass fibre reinforced epoxy resin and structured copper, show anisotropic material behaviour, it is necessary to determine the direction-dependent material properties. However, as only very thin layers were available of these materials, no experimental mechanical out of plane characterization could be performed. Thus, a combination of experiments, mean-field calculations and FEA simulations was used to generate the material data for both, the insulating and the conducting layers of the PCB. The generated material models were tested in board level simulations and compared to the results of simulations based on isotropic material behaviour. Significant differences were observed, approving the importance of proper material data, especially when the local stress and deformation field are important.

1. Introduction

The demands on printed circuit boards (PCB) are continuously increasing. They are used in a wide field of applications and have to endure a wide range of loads, such as e.g. impact, temperature, vibration and fatigue loads. Due to customer requirements, the boards are expected to become thinner and smaller yet should also include more complex circuits. These challenges counteract the efforts of improving the PCB reliability, which is a key factor in the industry. Thus, the build-up design and the interaction of the different integrated materials have to be optimized, which is currently done by using standardized board level tests (e.g. board level drop test [1]) for different loading conditions. The built-ups perform differently in these tests, as the global deformation behaviour influences the local stress situation. High local stresses again, can cause fracture of circuit paths and thus malfunction of the device based on the PCB. By means of the test results, the board built-ups should be optimized. A disadvantage of the board level tests is that they are quite expensive and time- consuming. Moreover, in these tests, the reasons for the different board performances are not always comprehensible, as only global failure effects and not the local failure initiation and propagation can be monitored. Thus, methods are being developed to describe the failure behaviour in detail and to predict the reliability performance without having to build and test boards. Finite element simulation models are generated, which should allow for an evaluation and understanding of different board designs. In these simulation models the boards are loaded according to the board level tests. Therefore, in order to get reliable results, it is crucial to have

proper material data. The aim of this work was to develop and evaluate methods providing this data for mechanical load cases. As the used material combinations were highly anisotropic and only available in predefined shapes, a procedure based on both, experiments and micromechanics simulations, had to be applied.

The material combinations used in a PCB result from its built up. Advanced PCB are typically multilayer PCB, consisting of several insulating layers separating the conducting layers (copper conduction paths) from each other. The insulating layers are generally glass fibre fabric epoxy composites, while the conducting layers are copper layers designed according to customer requirements. The conducting layers are formed by full copper layers, which are applied to the insulating layers and etched to obtain the requested copper geometry (copper structure). The places where the copper was removed are filled with the resin of the next insulating layer applied in the consecutive pressing process. Thus, the conducting layers can be regarded as epoxy-copper composites. The defined orientations of the reinforcements lead to the anisotropic material behaviour, which was tried to characterize in this work.

An example, showing the importance of the knowledge of the direction dependent material properties is given in Fig. 1. A typical failure in a board level drop test is indicated. The figure shows a solder ball, mounting a component on the PCB. A crack is initiated at the solder ball / copper pad / epoxy resin interface and due to propagation in the copper via resulting in PCB malfunction. The crack driving loads can be expected to be orthogonal to the crack plane, this means acting out of plane. As the glass fibre fabric has the main reinforcement effects in the in plane directions, the out of plane properties can vary significantly from the generally used in plane properties. Therefore, in order to be able to predict the proper local stress situation in an according simulation, e.g. in this case it is crucial to use the proper anisotropic data. Nevertheless, in numerous existing works about PCB simulations e.g. ([2], [3]) isotropic material models are used in default of available data.

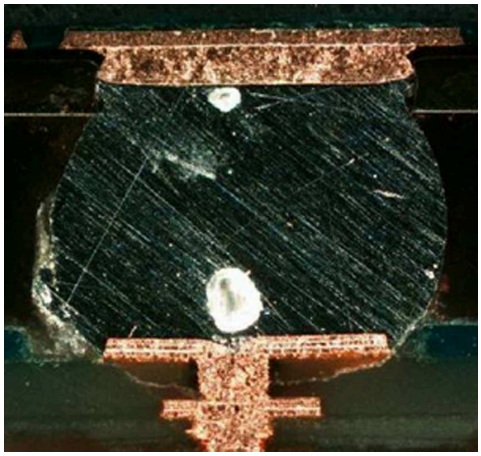

Fig. 1 Typical failure in a printed circuit board. The solder ball in the middle is connecting the component at the top with the PCB at the bottom. The crack is going through the outermost insulating epoxy resin layer.

To analyse the influence of the material models used for the individual layers, comparative test simulations of global and local deformation behaviour were performed. Therefore, differently modelled board built-ups were examined.

2. Materials

The insulating layers are defined by their matrix material and the chosen reinforcement. The matrix, the epoxy resin, can differ regarding its mechanical properties due to different filler systems. The reinforcement, usually a woven fabric, varies regarding their fabric count and the yarn definition in warp and fill direction. The specific types are classified and defined in a standard [4]. In Fig. 2, a typical microsection (50x) of a woven fabric is shown [5]. In this work two different matrix materials (epoxy resin M_1 and M_2) were characterized. Additionally, three woven fabrics types 106, 1080 and 1501 (according to the standard [4]) were analysed. The fabric count (warp x fill per cm) was 22.0 x 22.0 (106), 23.6 x 18.5 (1080) and 18.1 x 17.7 (1501) for the different types. The 106 prepregs were balanced composites (same number of fibres in warp and fill direction), while the 1080 and 1501 were not. The unbalanced prepregs were thus expected to behave different, tested in the two fibre directions. The yarn type was also diffrent for the fabric woven, being, together with the fabric count, the reason for the different resin content of the prepregs. The resin mass content was 75 %, 62 % and 46 % for the 106, 1080 and 1501 prepregs. That is, taking into account the two matrix materials with three different fabric woven respectively, in this work six different composites, expected to show a significantly different mechanical behaviour, were characterized. Additionally, the matrix material M_2 without reinforcement was analysed to evaluate the micromechanics approach. The matrix material M1 was not available, as the pure matrix materials are usually not provided by the prepreg manufactures.

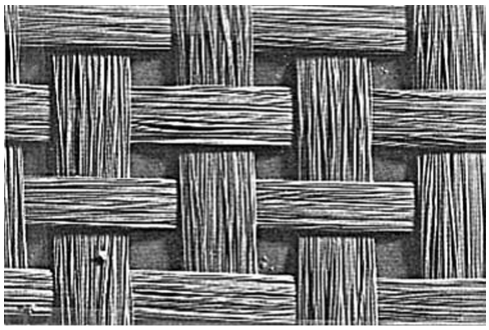

Fig. 2 Typical microsection (50x) of woven glass fabric [3].

As indicated, due to the glass fibre reinforcement, the insulating layers could not be considered as isotropic materials. The material properties depended on the loading direction. Apart from the difference between out-of-plane and in-plane, the difference between warp and fill also had to be taken into account. Three mutually orthogonal planes of symmetry could be found, why the composites did not have to be treated as fully anisotropic, but could be considered as orthotropic materials [6]. However, in contrast to unidirectional reinforced composites, the woven fabric reinforced layers are not transversal isotropic, as none of the planes of symmetry showed material isotropy.

The conducting layers for test PCB have usually a regular copper design, instead of a customer defined design, to simplify the built-up without neglecting that the actual conducting layers are not full copper. In Fig. 3, the copper design of a board level test PCB analysed in this work is shown. Considering the small size of the conducting paths (0.23 mm width), compared to the total board size (156 x 77 x 1.064mm), modelling the paths in a simulation would let exceed the model a calculable size. Thus, in this work the layers are regarded as epoxy/copper composites and an

approach to generate a homogenized material model is presented. The materials these layers consist of were etched copper foils and the matrix material filling the free volumes (epoxy resin M_1 or M_2 of the next insulation layer applied). Copper was available as applied in the actual PCB production (0.018mm thick foils). As overview, all analysed materials and their combinations are summarized in Table 1.

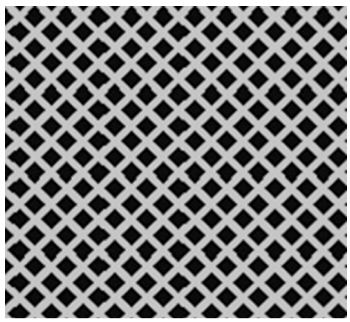

Fig. 3 Representation of a 15x15mm part of a conducting layer showing the conducting copper paths (bright) and the insulating epoxy (dark).

Table 1 Summary of all analysed layer materials including the insulating glass fibre woven reinforced epoxy prepregs, the epoxy-copper structure composites and the additionally tested pure copper and pure epoxy resin (M_2).

matrix	material reinforcement	resin content mass %	warp x fill (per cm)
M_1	*106*	75	22.0 x 22.0
	1080	62	23.6 x 18.5
	1501	46	18.1 x 17.7
	copper structure		
M_2	*106*	75	22.0 x 22.0
	1080	62	23.6 x 18.5
	1501	46	18.1 x 17.7
	copper structure		
	M_2		
	copper		

2.1. *Tensile Test Specimens*

To determine the orthotropic material behaviour of the composite layers, tensile test specimens were prepared. Two prepregs of the laminate to be analyzed were pressed together respectively. The pressing was performed according to the procedure in the actual PCB production. To measure the direction-dependant plane elasticity material parameters, specimens in warp direction (0°), in fill direction (90°) and in diagonal direction (45°) were stamped out of the plates. Except for the thickness, the specimens had the dimension of the test specimen 5A, defined in the test standard ISO 527. The thicknesses complied with the woven fabric used as reinforcement (thickness type 1501: 0.32 mm, type 1080: 0.16mm and type 106: 0.14mm). For the copper characterization, tensile test specimens according to the prepreg specimens were stamped out of thin copper foils (0.018mm). As the copper was expected to be isotropic, the cutting direction was not regarded. A 1.1mm thick plate of matrix M_2 was used to shape unreinforced epoxy tensile test specimens based on the specimen type 1BA defined in the test standard ISO 527.

2.2. *Built-up Test Boards*

To analyse the influence of the determined material parameters and the different material models used, finite element test simulations were performed. The simulations should show the effect of the material models and material types, used for the individual layers, on the global and local deformation behaviour. The simulated models were based on typical eight-layer PCB. A schematic representation of a simulated built-up is shown in Fig. 4 and the according variations are listed in Table 2.

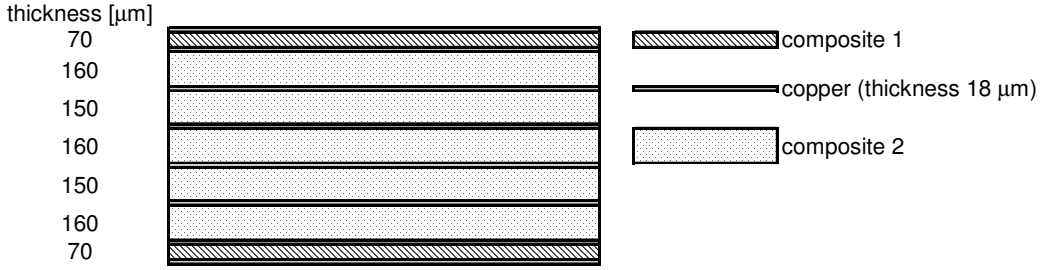

Fig. 4 Schematic representation of the PCB test boards analysed in the FEA simulations.

Table 2 PCB test board variations regarded in the FEA simulations.

	composite 1		composite 2		copper	
	prepreg	material idealization	prepreg	material idealization	layer	material idealization
board simulation 1	M_1 1080	isotropic	M_1 1501	isotropic	full copper	isotropic
board simulation 2	M_1 1080	orthotropic	M_1 1501	orthotropic	full copper	isotropic
board simulation 3	M_1 1080	orthotropic	M_1 1501	orthotropic	copper/epoxy	orthotropic
board simulation 4	M_2 1080	orthotropic	M_2 1501	orthotropic	copper/epoxy	orthotropic

3. Methods

For the insulating layers, the plane orthotropic material parameters were determined experimentally, but the missing out-of-plane parameters could not be measured, as no specimens could be manufactured from the thin laminates for this loading direction. Possible experimental methods [7] could not be applied. Thus, a micromechanics approach was used to determine the missing parameters. As indicated before, also the conducting layers were regarded as composite materials. However, an experimental characterization of these layers could not be conducted, as it was not possible to produce any specimens. The copper foil is already applied to the insulating layer when it is etched and the free volumes are filled with the epoxy resin of the next epoxy layer is applied. Thus, a homogenized material law was generated using a representative volume element (RVE) approach (e.g. [8]). The applied approaches are described in detail in the following sections.

3.1. *Experimental*

The fundamental mechanical properties of the individual insulating layers were determined by means of tensile tests. The composite layers were supposed to indicate an orthotropic primarily linear elastic behaviour, while the copper layers were supposed to behave in an isotropic non-linear way. Thus, the aim was to determine all independent orthotropic engineering constants for the composite layers and the nonlinear stress-strain behaviour for the copper layers. Additionally, the pure epoxy resin M_2 was characterized and the basic elastic properties were determined to gain

comparative data for the micromechanics calculations. Moreover, the density of the pure epoxy resin was measured (ISO 1183-1) in order to determine the composite resin volume portion on the basis of the resin mass portion (provided in the data sheet).

Tensile Test Set-Up

The tensile tests were performed on a universal testing machine (Zwick Z250, Zwick GmbH & Co. KG, Ulm, DE) based on the testing standard ISO 527-4. To determine the local strain, a digital image correlation system (Aramis, GOM mbH, Braunschweig, DE) was applied. The system used in this work was described in detail by Jerabek et. al [9]. The tested specimens, described in chapter 2.1, were fixed by manual screw grips. The load was applied with a test rate of 10 mm/min and the tests were carried out in standard climate. At least three measurements were performed for every material and the results were averaged. The test set-up is depicted in Fig. 5.

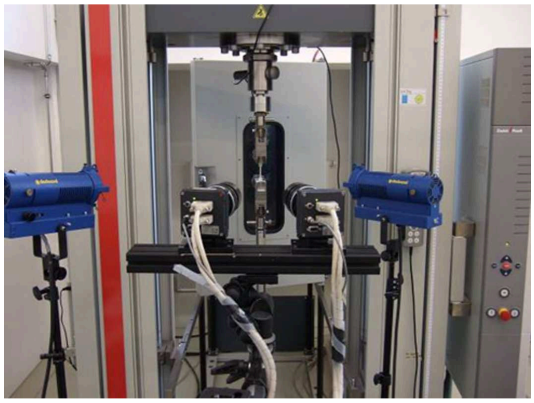

Fig. 5 Test set-up including the digital image correlation system (Aramis, GOM mbH, Braunschweig, DE) used to perform the tensile tests.

Tensile Test Data Reduction

Exemplarily test results of the digital image correlation tensile test measuremens (prepreg M_1 106) are depicted in Fig. 6. The full field distribution of the longitudinal and transversal strain is shown just before the specimen was failing. As the strain distribution was homogeneous in the parallel specimen part, the whole region with a constant cross section could be averaged to evaluate the longitudinal and transversal strains over the testing time. The according stresses were calculated from the recorded forces. That was done for 0° (direction 11), 45 ° and 90 ° (direction 22) specimens. The direction-dependent tensile moduli E_{11}, E_{45} and E_{22} were determined according to the ISO 527-4 standard. The Possion's ratio ν_{12} was calculated by averaging the negative ratio of transverse strain to longitudinal strain over the time, while the shear modulus G_{12} was obtained using the following equation [10]:

$$G_{12} = \frac{E_{45} \cdot E_{11} \cdot E_{22}}{4 \cdot E_{11} \cdot E_{22} - E_{45} \cdot (E_{22} - 2 \cdot \nu_{12} \cdot E_{22} + E_{11})} \tag{1}$$

Thus, all orthotropic material parameters of the plane elasticity E_{11}, E_{22}, ν_{12} and G_{12} were determinable with the measured results. The missing three-dimensional orthotropic engineering constants E_{33}, ν_{23}, ν_{13}, G_{23} and G_{13} could not be determined

experimentally, as no out-of-plane testing specimens could be manufactured because of the very thin prepregs.

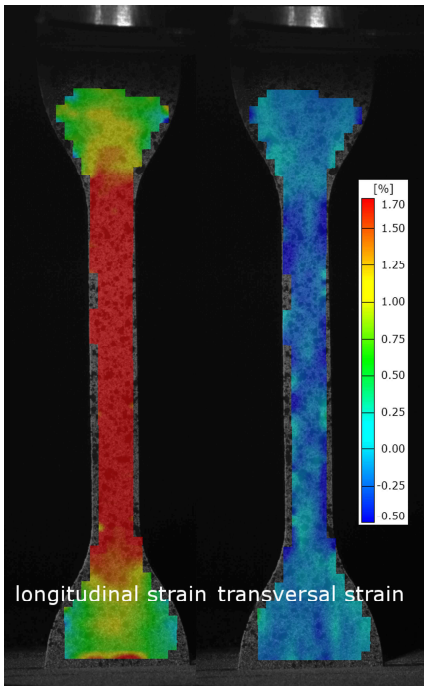

Fig. 6 Full field strain distribution measured with a digital image correlation system. The evaluation time was just before the specimen failed.

The copper and the pure epoxy matrix M_2 measurements were conducted and evaluated according to the prepreg tests. Due to the materials isotropy no different loading directions had to be taken into account. Only one tensile module and one Possion's had to be determined to define the material behaviour in the initial elastic region. However, as the behaviour of the copper and the epoxy matrix M_2 was clearly nonlinear, also the stress-longitudinal strain devolution was evaluated. The correlation between yield stress and plastic strain was prepared in tabular form for the use in an elastic plastic material law.

3.2. *Simulation*

Mean-Field Homogenization

As the three-dimensional orthotropic engineering constants of the composites could not be determined experimentally, a mean-field homogenization was used. By means of the material properties of the reinforcement (tensile modulus 73300MPa and density 2.58 g cm^{-3} for standard E-glass [5]), the resin content (producer data sheets) and the planar mechanical properties of the composite, the properties of the matrix material were back-calculated. Thus, the missing three-dimensional engineering constants could be calculated using the known material properties of the reinforcement material and the determined material properties of the matrix material. For the micromechanics calculations the software tool digimat-MF (digmat-MF 4.2.1, e-Xstream engineering SA, Louvain-la-Neuve, BE) was used and the mean-field homogenization method based on Mori-Tanaka (e.q [11], [12]) was chosen. The reinforcement was idealized as woven fibre inclusion phase [13]. The warp to weft ratio and the angle between warp and weft could be defined in the software. The warp to weft ratio was entered as listed in Table 1 and the angle was set to 90°,

according to the value in the actual prepregs. The interweaving influence could not be included in the simulations, which had to be regarded in the results interpretation.

Representative Volume Element Simulations

In order to generate a homogenized material model for the conducting layers (epoxy-copper), RVE were created and simulated. The smallest recurring entity of the regular structure (Fig. 7) was taken to represent the inhomogeneous material. Periodic boundary conditions were chosen as they were supposed to show the best results ([8], [14]). The RVE models were created using a C++ code [15]. An input file for a 10x10x10 elements cube with periodic boundary conditions was generated for the finite element software Abaqus (Abaqus 6.9, Simulia, Daussault Systèmes, Providence, RI, USA).The model was applicable for the regarded layers, as the regular copper structure (rotated in the main stress axis) could be represented. For the simulations, the material parameters were applied to the model according to the given geometry. For the RVE simulations both, copper and epoxy were modelled as linear elastic material, as the strains are assumed to stay in the elastic region (discussed in chapter 5).

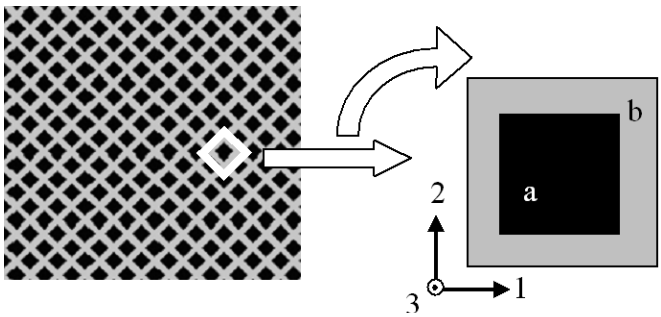

Fig. 7 The chosen representative volume element of the conducting layers. The element is representing a planar area of 1.1 x 1.1 mm (a, epoxy resin and b, copper) and is rotated in the main stress axes 1, 2 and 3.

The RVE could be treated as orthotropic, as the same planes of symmetry as for the prepregs were found. To obtain the basic mechanical material parameters of these layers, different loading situations were simulated in the finite element software. Either elongation or shear was applied and the reaction forces were determined. Thus, the orthotropic engineering constants (tensile moduli, shear moduli and Possion's ratios) could be calculated. Four loading situations, tension 22, tension 33, shear 12, and shear 23 (in Fig. 8 the loading situations are indicated), had to be regarded as E_{11} and E_{22}, G_{13} and G_{23} and ν_{13} and ν_{23} were correspondend. Thus, six independent engineering constants were determined. However, the material could not be referred to as transversal isotropic, as no plane of material isotropy was existing (A plane with isotropic material behaviour would have had only two independent engineering constants, which would have reduced the total number of engineering constants needed to describe the three-dimensional behaviour to five). The only eligible 1-2 plane could not be treated as isotropic, as e.g. a different material behaviour was observed when tested in direction 1 and a direction rotated by 45° in the 1-2 plane respectively.

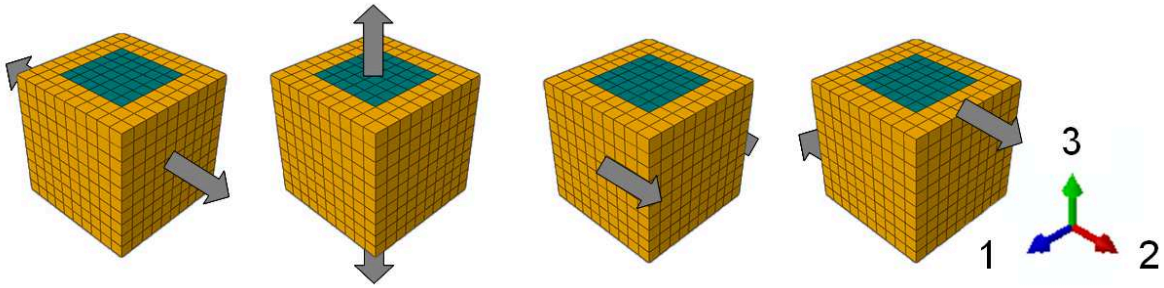

Fig. 8 Schematic representation of the RVE loading situations (from left to right: tension 22, tension 33, shear 12, and shear 32) needed to determine the orthotropic material behaviour of the conducting layers.

Board Level Test Simulations

To evaluate the influence of the usage of correct orthotropic material models on the individual layers, instead of assuming isotropic material behaviour, finite element board level test simulations (Abaqus 6.9, Simulia, Daussault Systèmes, Providence, RI, USA) were performed. In order to determine the local stresses and deformations accurately, a sub-modelling technique was used to analyse the local loading situation. In the simulations, the described PCB built-ups (2.2) were loaded according to a deflection in a BLCBT (Board Level Cyclic Bend Test) [16]. In the global model, a composite shell was used to model the composite layup. The used element type was an 8-node doubly curved thick shell element with reduced integration). The highest stresses in an insulating layer due to the three point bending load were supposed to be at the centre of the outermost epoxy layer of the board where a submodel was used to evaluate the stress situation. The submodelling technique was used to study the local region in detail. Thereby a chosen region of interest is modelled with a refined mesh and the local simulation is performed based on the results of the global model [17]. In spite of the fine mesh, the computational costs stay low, as the submodel size is very small compared to the size of the global model. The dimensions of the board in the global model were 132x77x1.064 mm and the dimensions of the submodel were 0.2x0.2x0.284 mm. The used element type for the submodel was an 8-node linear brick with reduced integration and hourglass control. The three point bending load in the global model was applied by rollers modelled as rigid parts. The support rollers were clamped, while the centre roller applying the load was just constrained in direction 1 and 2. The load was defined by the application of a displacement (3 mm in the negative direction 3) to the centre roller. The interaction between rollers and board was modelled as a frictionless hard contact. The effect of different friction coefficients was not taken into account, as the focus in this work was just a relative comparison of the results of the simulations performed with different material models. A schematic representation of the model and the indicated boundary conditions are shown in Fig. 9. As described in chapter 2.2 the material models used for the PCB simulation were varied, leading to four different cases (Fig. 4 and Table 2).

In board simulation 1, only isotropic material models were used. The material data of the prepregs M_1 1080 and M_1 1501 were chosen exemplarily for the insulating layers. The conducting layers were assumed to be full copper layers. Board simulation 2, including the direction depended material data for the prepregs, was performed to show the effect of the actual orthotropic material behaviour of the insulating layers. Board simulation 3 additionally focused on structured copper layers instead of full

copper layers, using the homogenized orthotropic material model (copper/epoxy). The results should show if the copper etching design has a significant influence on the local stress situation in the insulating layers. Finally, board simulation 4 was conducted to analyse the use of different matrix materials. The data used for the material models were the values resulting from the presented characterization methods (chapter 3), presented in chapter 4.

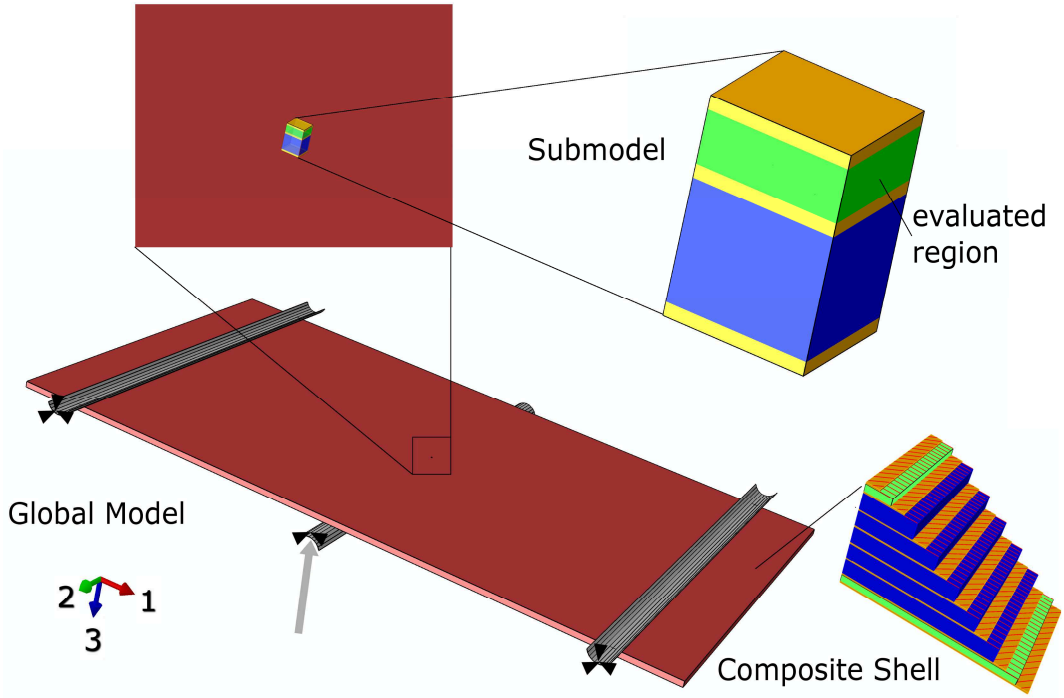

Fig. 9 Scheme of the FEA board level test simulations with the submodel used to analyse the local three-dimensional stress state. The boundary conditions of the global model are indicated.

4. Results and Discussion

The described measurement and simulation methods (chapter 3.1 and 3.2) were used to determine the anisotropic material properties of the conducting and insulating individual layers of a printed circuit board.

4.1. *Experimental Results*

Tensile Test Results

Using the described tensile test set-up and data reduction (chapter 3.1), the measurement of the composite materials resulted in the material data presented in Table 1. The influence of the different used woven fabrics is readily identifiable. A higher content of glass fibre reinforcement increases the material stiffness. A clear difference can also be observed for the different epoxy resins used. The stiffness of M_2 must be significantly higher to account for the according higher composite stiffness. The tested copper foils showed the expected elastic plastic behaviour and the pure epoxy resin M_2 test resulted in an almost linear stress-strain curve. The tensile moduli E were determined as 7150 MPa for the epoxy resin M_2 and as 50650 MPa for the copper foil. The Possion's ratio ν of the matrix material was measured as 0.35. The measurement of the transversal strain could not be performed properly on the thin copper foils, for which reason the copper Possion's ratio, 0.35, was taken

from literature data [15]. The density of the pure epoxy resin was determined as 1.6 g cm^{-3}. In Fig. 10 sample measurements of a copper foil, of an epoxy resin M_2 and of a reinforced layer M_2 1080 are compared to indicate the different material behaviours. The resultant engineering constants of all tensile tests are summarized in Table 3.

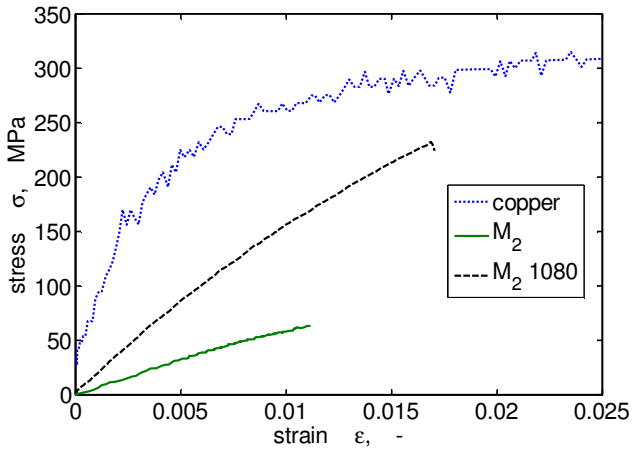

Fig. 10 Comparison of sample tensile test material behaviours of the different materials (copper, pure epoxy resin - M_2 and reinforced epoxy resin - M_2 1080) tested.

Table 3 Experimental results of the performed tensile tests.

material		$E_{(11)}$	E_{22}	$\nu_{(12)}$	G_{12}
matrix	reinforcement	MPa	MPa	-	MPa
	106	7540	7730	0.19	2393
M1	*1080*	12310	10350	0.15	2732
	1501	17360	16670	0.15	4254
	106	13360	12930	0.17	2580
M2	*1080*	17490	16240	0.16	2096
	1501	22770	20860	0.15	3850
M_2		7150		0.35	
copper		50650		-	

In the homogenized conducting layers the copper foils were assumed to be linear elastic. As the maximum strain in these layers does not exceed 0.2 % under the regarded loading situation of a BLCBT [14], the linear elastic region is not exceeded and the results should be unaffected.

4.2. *Simulation Results*

Mean-Field Homogenization

The matrix material properties were back-calculated for M1 on the basis of composite M1 106 and for M2 on the basis of composite M2 106. The composites with the highest resin content were chosen, as in these materials any possible imprecision of the reinforcement material data and the applied micromechanics approach have the least influence. The Possion's ratios of the matrix materials were assumed as 0.35 (has been verified for M_2 in chapter 4.1) and the tensile modulus of the matrix was determined iteratively. Tensile moduli of 2200 MPa for M1 and 6700 MPa for M2 were found to give the best correlations between measured (tensile tests) and simulated (mean-field homogenization) values. Compared to the tensile modulus of

M2 measured at the pure epoxy resin with 7150 MPa, the back-calculated tensile modulus was lower, but in a reasonable accordance. A reason for the discrepancy could be the unknown processing history of the resin specimens, possibly having influenced the mechanical properties. The determined matrix values were used to simulate the composite properties for the glass fibre reinforcements 1080 and 1501 as well. By comparing the obtained results (Table 4) with the measured values (Table 3) the method could be evaluated. A very good correlation for all composites could be observed for the in-plane tensile moduli. The Possion's ratios ν_{12} and the shear moduli G_{12} were also in good accordance, also when the values for the M_1 prepregs were a bit too low and the values for the M_2 prepreg were a bit too high in the simulations. A possible reason could be that interweaving could not be considered in the mean-field approach. Only straight 0°/90° fibres without physical interaction could be modelled in the micromechanics simulation, neglecting effects like deflections of the fibres due to the interlacing between warp and weft fibres, friction between the fibres or local constraints. However, based on the nevertheless good agreement for the in plane values, the out-of-plane values ν_{13}, ν_{23}, G_{13} and G_{23}, which could not be verified by experimental data, could be assumed to be applicable to describe the material. In all following test simulations the material data presented in Table 4 was used.

Table 4 Results of the mean-field homogenization for the insulating composite layers.

		E_{11}	E_{22}	E_{33}	ν_{12}	ν_{13}	ν_{23}	G_{12}	G_{13}	G_{23}
		MPa	MPa	MPa	-	-	-	MPa	MPa	MPa
M1	*106*	7710	7710	3180	0.11	0.36	0.36	1110	1080	1080
	1080	12170	10280	3770	0.09	0.36	0.37	1330	1280	1270
	1501	16660	16390	4850	0.07	0.36	0.36	1760	1660	1660
M2	*106*	13120	13120	9020	0.19	0.33	0.33	3380	3300	3850
	1080	18020	16350	10630	0.17	0.32	0.33	4020	3900	4520
	1501	25240	21320	13480	0.15	0.31	0.33	5210	5020	5870

Representative Volume Element Simulation

As described in chapter 0.0 four different loading situations (Fig. 11) were regarded and evaluated in order to describe the homogenized material behaviour of the copper structure layers. In the RVE simulations the pure epoxy resin was described by the material data generated in the mean-field approach. For copper the material data determined in the experiments was taken. Defined displacements were applied and the resulting reaction forces were used to calculate the orthotropic engineering constants (Table 5).

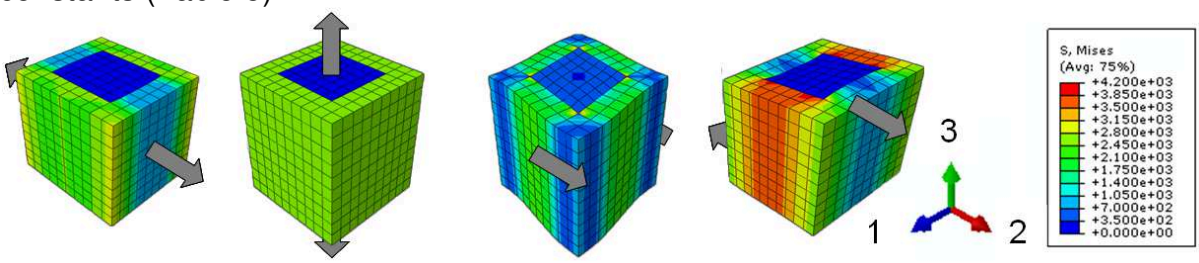

Fig. 11 Resultant stress fields (Von Mises) of the simulated RVE loading situations (from left to right: tension 22, tension 33, shear 12, and shear 32).

Table 5 Results of the RVE simulations for the copper structure layers.

		E_{11} MPa	E_{22} MPa	E_{33} MPa	ν_{12} -	ν_{13} -	ν_{23} -	G_{12} MPa	G_{13} MPa	G_{23} MPa
M_1	*copper structure*	18750	19580	26050	0.17	0.25	0.25	2460	6700	6700
M_2		23040	24510	28340	0.26	0.28	0.28	5030	8170	8170

Board Level Test Simulations

The determined material properties were used in board level test simulations in order to evaluate the influence of the different material models (used). The region of interest was the outermost insulating epoxy layer at the board centre, where in the case of a BLCBT the most critical stresses occur. Four different board designs (Table 2) were analysed and compared. In board simulation 1, only isotropic material models were applied. To describe the insulating layers and the full copper layers, E_{11} and n_{12} of the corresponding composites were used. In board simulation 2 the determined orthotropic material parameters were applied to the insulating layers. As a result, significantly higher values (up to 30 %) were observed for the in-plane stresses σ_{11} and σ_{22}, as well as for the out of plane stress σ_{33}. Thus, neglecting the direction dependent material data would result in a severe underestimation of the local stress situation. Especially the accurate determination of the deformation behaviour in the out-of-plane direction can be crucial for the simulation of PCB failures, as local cracks in printed circuit boards tend to be driven by out-of-plane loadings (Fig. 2). In board simulation 3 the orthotropic epoxy-copper structure material model was additionally used for the conducting layers. Only small effects were observed and the different material properties of the conducting layers seem to have only a very small influence on the local situation in the outermost insulating layer in the regarded load case. In board level simulation 4 a different matrix material (M_2 instead of M_1) was used. As expected, the large differences of the matrix material properties have a strong impact on the overall stress state and thus play an important role in PCB failure simulations. A summary of the local stress results of the four analysed simulation models is given in Table 6.

Table 6 Local stresses in the outmost insulating layer determined in the finite element board test simulations.

	σ_{11} MPa	σ_{22} MPa	σ_{33} MPa
board simulation 1	17.55	1.75	1.88
board simulation 2	18.42	2.28	2.38
board simulation 3	18.38	2.27	2.37
board simulation 4	28.99	6.76	6.94

5. Summary and Conclusion

The aim of this work was the determination of the anisotropic material behaviour of the layer materials used in a PCB built up and the demonstration of the importance of these material models in a PCB finite element simulation. The characterization of the direction dependent material properties of the individual layers was challenging, as at most the in-plane parameters could be determined experimentally. To find all orthotropic (the layers had three planes planes of symmetry) engineering constants, additional, non-experimental approaches were applied. The intermediate insulating layers, glass fibre woven reinforced epoxy prepregs, could be analysed by a combination of both, in-plane tensile tests and a micromechanics simulation based

on the mean field theory. The method could be verified by the agreement of the micromechanics simulation results with the in-plane experimental data of three different woven fabric reinforcements. The conducting layers, the copper structure with the epoxy resin of the overlying insulating layer filling the free volumes, were evaluated by RVE simulations based on the results of the characterization of their individual components.
The determined orthotropic material models were applied in board level test simulations and compared to simulations with isotropic material models. The stress distribution in the outermost insulating layer (in a three-point-bending load case) was evaluated, as it is the critical location for a lot of typical PCB failure patterns. Significantly higher stresses (up to 30%) in all directions were observed, using the proper orthotropic material data for the insulating layers. Thus, neglecting the direction dependent material behaviour, the local stress situation would be severely underestimated. If orthotropic material data, determined in the RVE simulations, is also used for the conducting layers (instead of assuming full copper layers), the observed stresses were almost unchanged. That is, if the region of interest is in the outermost insulating layer, the effect of the material properties of the conducting layers is very small. In a third comparison, the influence of a different matrix material in the prepregs was analysed. As expected, the resulting clearly different mechanical properties lead to a significantly different stress situation. It could concluded, that the proper determination of the direction dependent material properties is crucial for the accurate evaluation of the critical local stresses.
In ongoing work the determined material models are used to simulate the local failure behaviour in printed circuit boards. The stress intensities at predetermined cracks (corresponding to known failure patterns) are calculated to evaluate the effect of different built-ups on the local loading conditions and the board reliability.

6. Acknowledgements

The research work of this paper was performed at the Polymer Competence Center Leoben GmbH (PCCL, Austria) within the framework of the COMET-program of the Austrian Ministry of Traffic, Innovation and Technology with contributions by the University of Leoben and by the AT&S Austria Technologie & Systemtechnik Aktiengesellschaft. The PCCL is funded by the Austrian Government and the State Governments of Styria and Upper Austria.

References

[1] "Board level drop test method of components for handheld electronic products," *JEDEC Standard JESD22-B111*, no. July, 2003.

[2] T. Tee, H. Ng, C. Lim, E. Pek, and Z. Zhong, "Impact life prediction modeling of TFBGA packages under board level drop test," *Microelectronics and Reliability*, vol. 44, no. 7, pp. 1131-1142, Jul. 2004.

[3] C. Le Coq, A. Tougui, M.-P. Stempin, and L. Barreau, "Optimization for simulation of WL-CSP subjected to drop-test with plasticity behavior," *Microelectronics Reliability*, vol. 51, no. 6, pp. 1060-1068, Jun. 2011.

[4] "Specification for Finished Fabric Woven from 'E' Glass for Printed Boards," *IPC - 4412A Amendment 1*, 2008.

[5] M. W. Jawitz and M. J. Jawitz, *Materials for Rigid and Flexible Printed Wiring Boards*. 2007.

[6] A. K. Kaw, *Mechanics of Composite Materials*, Second Edi. Tayler&Francis Group, 2006, p. 457.

[7] I. Daniel, J. Luo, and P. Schubel, “Three-dimensional characterization of textile composites,” *Composites Part B: Engineering*, vol. 39, no. 1, pp. 13-19, Jan. 2008.

[8] C. T. Sun and R. S. Vaidya, “Prediction of composite properties from a representative volume element,” *Composites Science and Technology*, vol. 56, no. 2, pp. 171-179, Jan. 1996.

[9] M. Jerabek, Z. Major, and R. W. Lang, “Strain determination of polymeric materials using digital image correlation,” *Polymer Testing*, vol. 29, no. 3, pp. 407-416, May. 2010.

[10] M. E. Tuttle, *Structural Analysis of Polymeric Composite Materials*. Marcel Dekker, Inc., 2004.

[11] Y. Benveniste, “A new approach to the application of Mori-Tanaka’s theory in composite materials,” *Mechanics of Materials*, vol. 6, no. 2, pp. 147–157, 1987.

[12] H. J. Böhm, *A short introduction to basic aspects of continuum micromechanics*, vol. 80124. 2008.

[13] *Digimat Documentation*, 4.2.1 ed. e-Xstream engineering, 2012.

[14] Z. Xia, “A unified periodical boundary conditions for representative volume elements of composites and applications,” *International Journal of Solids and Structures*, vol. 40, no. 8, pp. 1907-1921, Apr. 2003.

[15] T. Antretter, “Micromechanical modeling of high speed steel,” University of Leoben, 1998.

[16] P. Fuchs and Z. Major, “Cyclic bend tests for the reliability evaluation of printed circuit boards under dynamic loads,” *Frattura ed Integrità Strutturale*, vol. 15, no. 15, p. pages–64, 2010.

[17] *Abaqus Documentation*, 6.10 ed. Dassault Systèmes, 2010.

PAPER 4: EXPERIMENTAL DETERMINATION OF COHESIVE ZONE MODELS FOR EPOXY COMPOSITES

P.F.Fuchs[a], Z.Major[b]

[a] Polymer Competence Center Leoben GmbH, Roseggerstrasse 12, 8700 Leoben, Austria

[b] Institute of Polymer Product Engineering, Johannes Kepler University Linz, 4040 Linz, Austria

published in *Experimental Mechanics*, *51*(5), 779-786 (2010)

Experimental Mechanics
DOI 10.1007/s11340-010-9370-2

Experimental Determination of Cohesive Zone Models for Epoxy Composites

P.F. Fuchs · Z. Major

Received: 26 January 2010 / Accepted: 11 May 2010

Abstract In this work, a new test set-up was applied in order to determine cohesive zone models experimentally. A high speed camera in combination with a digital image correlation system was used to record the local displacements enabling the detailed determination of crack opening values. The J-Integral method was used to calculate the cohesive stresses. The analyzed materials were composites made of glass fiber reinforced epoxy resin layers. Two different specimen geometries and the difference between warp and weft of the glass fiber mats were analyzed. As the specimen geometry didn't have a significant influence, the difference between warp and weft, regarded by the loading direction, lead to considerably different cohesive zone laws. The initial part, the linear increase to a maximum stress, was very similar, while the damage evolution was either exponential or bilinear in shape. In future work, the derived cohesive zone models will be used to perform finite element simulations on laboratory specimens and on component scale. Thus, by comparison to the measurement result, the cohesive zone models can be evaluated.

Keywords Fracture mechanics · Cohesive zone model · Digital image correlation · J-Integral method · Epoxy composite

P.F. Fuchs (✉)
Polymer Competence Center Leoben GmbH,
Roseggerstrasse 12,
8700 Leoben, Austria
e-mail: peter.fuchs@pccl.at

Z. Major
Institute of Polymer Product Engineering,
Johannes Kepler University,
Altenbergerstrasse 69,
4040 Linz, Austria

Published online: 29 May 2010

Introduction

Introduced by Barenblatt [1] and Dugdale [2] in the 1960`s, cohesive zone models (CZM) have been of growing interest recently, since they can be used for fracture simulation. Cohesive zone elements which follow the traction-separation behaviour as described by the CZM, were implemented in various FE-codes, allowing for the simulation of crack initiation and propagation. Due to new methods presented in several publications e.g. Remmers et al. [3], Zhang and Paulino [4] and Yang and Deeks [5], a crack path prediction became possible too. The advantage of the CZM models is that they can be used to describe a wide range of different damage mechanisms. For example in Yang and Cox [6] a cohesive element for the simulation of three-dimensional, mode dependent process zones is presented and used for delamination and splitting cracks in laminates. For these simulations, accurate CZM are essential but their experimental determination is still challenging. Existing experimental methods were reviewed by Sorensen and Jacobsen [7]. Two reasonable procedures were pointed out: First the direct tension experiment which was used e.g. by Ting et al. [8], with the presumption of a uniform damage evolution across the ligament, which is difficult to achieve in experiment. Second the J-Integral approach, first used by Li and Ward [9], which was chosen by Sorensen and Jacobsen for their own experimental work. Other methods (e.g. Chen et al. [10]) are semi-experimental, adapting the CZM parameters by comparing measurement results with model predictions.

In the present work, an advanced test set-up was used to experimentally determine the CZM. The approach was similar to the one used by Zhu et al. [11], but was applied on different specimen geometries and materials. The crack end opening was determined by the evaluation of high

speed camera images with a digital image correlation (DIC) system and the cohesive stresses were calculated by the J-Integral approach. The advantage of this set-up was the possibility of exact identification of the crack opening at the desired position. By means of this procedure, different specimen geometries and material influences were analyzed.

Experimental

Materials and Specimens

The analyzed materials were glass fiber reinforced epoxy resin composites. The composites were made of seven layers which were reinforced with woven glass fiber. The woven glass fibre consisted of 0° fibers and 90° fibers. The layers were pressed together applying a defined temperature and pressure profile. The specimens were cut in two different ways, resulting in both, loading in the direction of the 0° fibers and loading in the direction of the 90° fibers. Thus, possible influences of warp and weft could be identified.

Fracture tests were performed on Double Edged Notched Tension (DENT) and Center Cracked Tension (CCT) specimens. The dimension of the unnotched samples was 0.52×48×100 mm. Machined notches were cut in the specimens with the dimensions indicated in Fig. 1. Additionally, a razor blade was pressed into the machined notches to introduce a sharp precrack of 1 mm length. The total initial crack size including the machined notch and the sharp precrack resulted in 24 mm. To avoid specimen slipping, abrasive paper was glued on the specimen surface parts which were fixed in the grips.

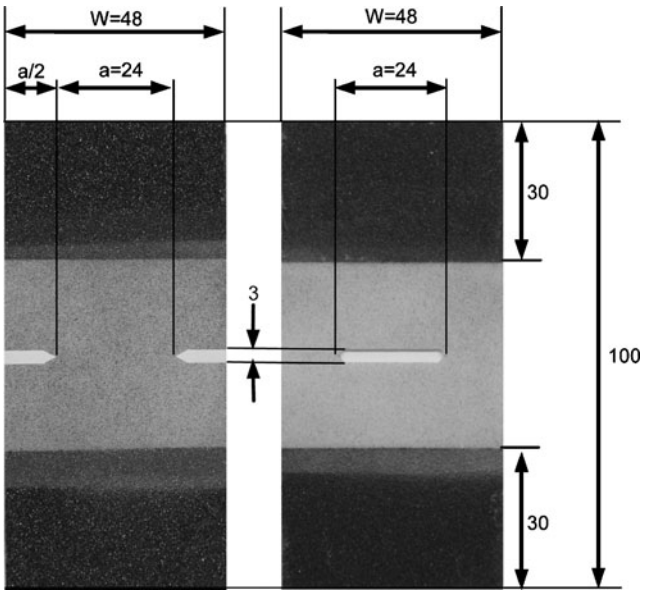

Fig. 1 Specimens used in the fracture tests [(**a**) DENT, (**b**) CCT]. The specimen parts which were fixed in the grips are covered with abrasive paper (black). A pattern of black dots was applied to a bright background for the DIC at the upper surface. The indicated dimensions are in mm

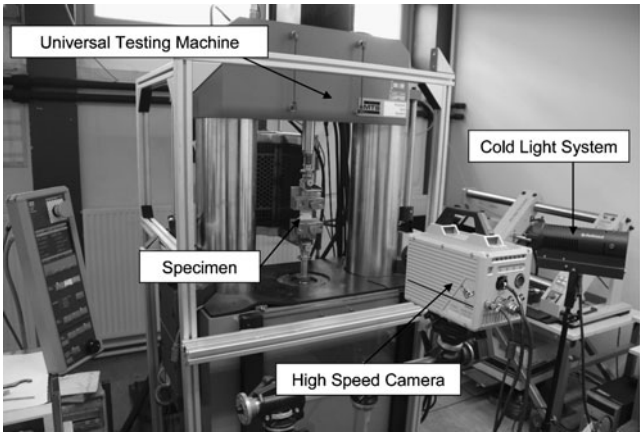

Fig. 2 Test set-up of the instrumented fracture tests including a high speed camera and a cold light system to record the fracture tests

Test Set-up

Fracture tests were performed on a universal servohydraulic testing machine (MTS 831, MTS Systems Corporation, Eden Prairie, US) with which the load and the crosshead displacement could be recorded. The testing rate was set to 100 mm/min. Local displacements in the very fast proceeding damage zone were measured with the help of an advanced high speed camera (Fastcam SA1, Photron, San Diego, US) combined with a DIC (Digital Image Correlation) system (Aramis, GOM, Braunschweig, DE). The test set-up is shown in Fig. 2.

A pattern had to be applied to the specimen surface in order to perform the DIC. A white matt grounding was applied on the surfaces and dots were produced by a black graphite spray. The pattern applied on the monitored region of the specimen is shown in Fig. 1. As the images were taken at 1000 fps with a 960×752 resolution, a strong light source was needed. A cold light system (Dedocool, Dedo Weigert Film GmbH, Munich, DE) was used in order to avoid the heating of the specimen.

Data Reduction Scheme

To determine the cohesive zone law, the J-Integral approach was used (Sorensen and Jacobsen [7], Li and Ward [9]). The J-Integral (introduced by Rice [12]) over the crack end opening δ_{end} was determined experimentally and the

cohesive stresses σ were calculated by the derivation of the curve.

$$\sigma(\delta_{end}) = \frac{\partial J(\delta_{end})}{\partial \delta_{end}} \quad (1)$$

The crack end opening could be determined precisely by the DIC system. A subset size of 21×21 and a subset overlap of 24% was chosen for the evaluation. More details about the used DIC system and technique can be found in Jerabek et al. [13].

For the J-Integral determination the correlation between the J-Integral and the strain energy release rate, valid in the field of Linear Elastic Fracture Mechanics (LEFM) was used. LEFM can only be applied when the material is linear elastic except for a small damage zone at the crack tip, whose size, $L_{0,}$ is small compared to the crack length a. In spite of the viscoelastic nature of the polymers investigated, an almost linear elastic material behaviour could be approved by the tensile test results shown in Fig. 3. The stress-strain curves increase nearly linear to a maximum value followed by a sudden decrease indicating a brittle failure. The size of the damage zone was determined from the DIC system results. Figure 4 shows the overlay of a high speed camera image and the according full-field strain evaluation of the crack tip of a DENT—90° loading direction specimen. The high speed camera image was the last frame recorded before the crack started to grow. The crack end opening, δ_{end}, at this point of time reached a value of 0.2 mm and the cohesive zone was almost completely developed. The size of the damage zone was deduced from the size of the region where a local strain concentration was observed. A local strain concentration was assumed in the area where a significant difference to the nominal strain could be measured. The nominal strain was about 0.5% and the maximum strain at the crack tip about 6%. The outer border of the damage zone was defined as the 1% strain isoline. The maximum distance between the defined outer border and the crack tip resulted

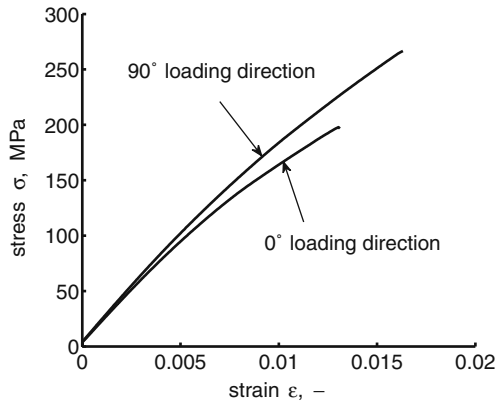

Fig. 3 Tensile test results of the material analyzed in the fracture tests

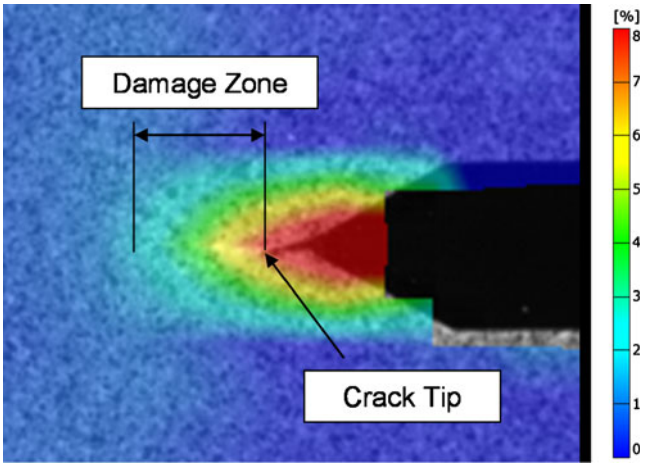

Fig. 4 The overlay of a high speed camera image and the according full-field strain evaluation of the crack tip of a DENT – 90° loading direction specimen with the estimation of the damage zone size on the crack plane

in 2.3 mm. Hence, the estimated damage zone size of 2.3 mm was small compared to the crack length of 24 mm. Thus, the conditions for LEFM were met and their application was justified to a large extent.

In the LEFM, the J-Integral, J_{el}, is correlated to the energy release rate, G, and can be calculated from the fracture tests load displacement curves.

$$J_{el} = G = \eta_e \frac{U_e}{B(W-a)}, \quad (2)$$

Where U_e is the elastic work done, B, W and a are the specimen thickness, width, and crack length respectively, and η_e is a correction factor depending on the specimen geometry. The η_e factor is discussed in Turner [14] and the according wide-range approximations used in this work were summarized by O.L. Towers [15].

However, using this approach it must be kept in mind that the applicability is correlated to the limitations of the LEFM. For further reference see Bao and Suo [16].

Results and Discussion

Determination of the Crack End Opening

The crack end opening was determined by the evaluation of the high speed camera images (The described procedure and figures refer to DENT and 90° loading direction specimens, but the concept was also used for the other specimens). By means of the DIC system, full-field strain and displacement fields were recorded over time. In Fig. 5 and in Fig. 6, the last high speed camera image, recorded before a noticeable crack growth was observed, was evaluated. Figure 5 shows the full-field strain field, where

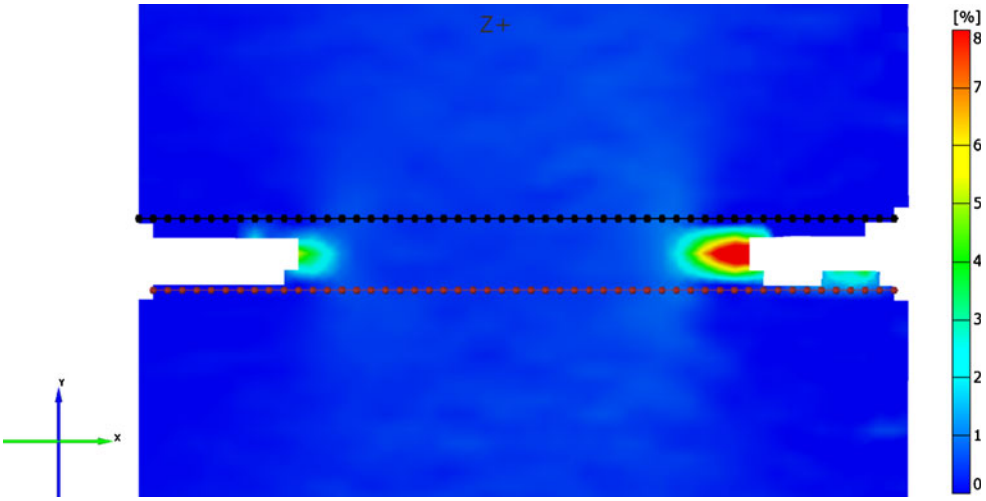

Fig. 5 The full-field strain evaluation of a DENT - 90° loading direction specimen. The according high speed camera image was the last frame recorded before a noticeable crack growth was observed. The intersection lines where the displacements were evaluated are indicated

a strong local strain concentration around the crack tips was observed. The strain concentration differed for the two crack tips due to the difficult proper parallel alignment of the specimens combined with brittle material behaviour. Consequently crack growth was not initiated simultaneously. The side where crack growth was initiated first was chosen for the determination of the cohesive zone law. The influence of the asymmetric crack growth on the cohesive zone model results is discussed in 4.3. The intersection lines indicated in Fig. 5 are parallel to the expected crack path and tangents to the damage zone at the crack tip. The displacements in Fig. 6 were evaluated along these lines. (In the figures the direction parallel to the notches is referred to as the x-coordinate and the orthogonal direction is referred to as the y-coordinate. The coordinate origin is at the specimen centre.)

Example evaluations of three chosen points of time during crack propagation are shown in Fig. 7. Additionally, the resulting high speed camera images are depicted. The measured crack end opening, $\delta_{end}{}^{m}$, was derived from the difference of the displacement values of the upper and lower intersection line at the x-coordinate of the crack tip in the unloaded state. The measured crack end opening was corrected by the subtraction of the elastic deformation between the intersection lines, δ_{el}, resulting in the actual crack end opening, $\delta_{end} = \delta_{end}{}^{m} - \delta_{el}$. The elastic deformation was derived from the difference of the displacement values of the upper and lower intersection line at the x-coordinate where the material was unaffected by the local strain concentration. This correction could only be performed until the whole area was affected by the propagated crack. This limitation has no impact on the determination of the cohesive zone law, since crack end opening values were only needed until the cohesive zone was fully pronounced. As discussed in 4.2, that happened before the correction was not practical any more. The evolution of the crack end opening over the crosshead displacement is shown in Fig. 8. Additionally the influence of small changes to the chosen initial crack tip x-coordinate is indicated. The grey area shows the quite sensitive response to an x-coordinate shift of +/− 0.5 mm. Thus, special care was taken to precisely locate the crack tip in the unloaded state.

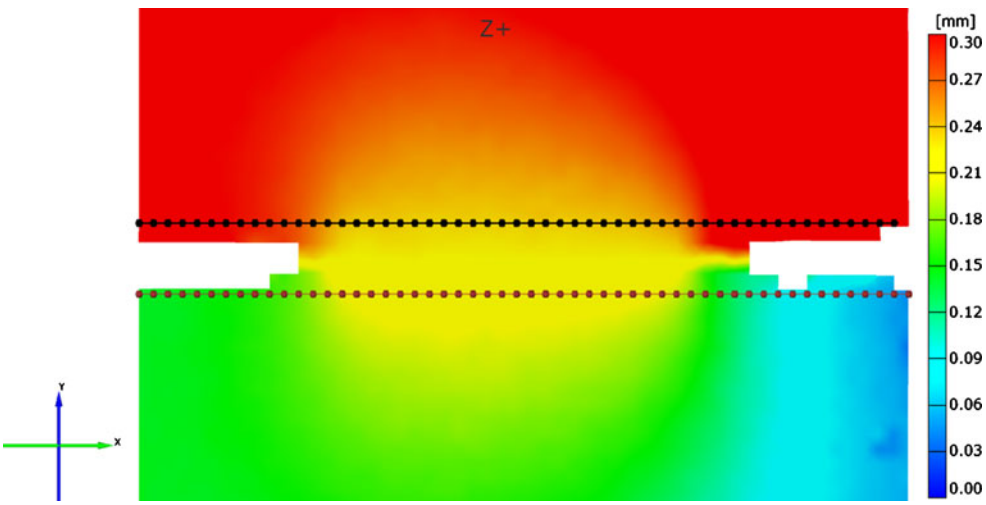

Fig. 6 The full-field displacement evaluation of a DENT - 90° loading direction specimen. The according high speed camera image was the last recorded frame before a noticeable crack growth was observed. The intersection lines where the displacements were evaluated are indicated

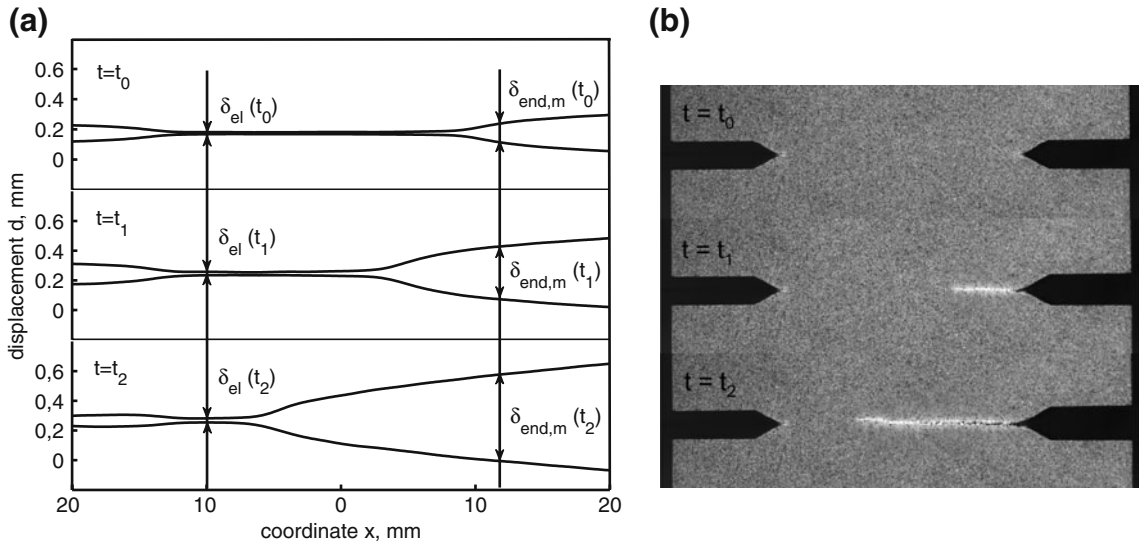

Fig. 7 (**a**) Displacement evaluations for a DENT - 90° loading direction specimen at the intersection lines. (t0, t1 and t2 are three chosen points of time during crack propagation). The change of δ_{end} and δ_{el} is indicated. (**b**) The according high speed camera images for the displacement evaluation

J-Integral Determination

The elastic work done in the fracture tests was determined from the measured force displacement curves plotted in Fig. 9. The crack extension was measured manually by visual examination of the high speed camera images. Thus, with the known geometry information and the resulting correction factors, the elastic J-Integral could be calculated using equation (2).

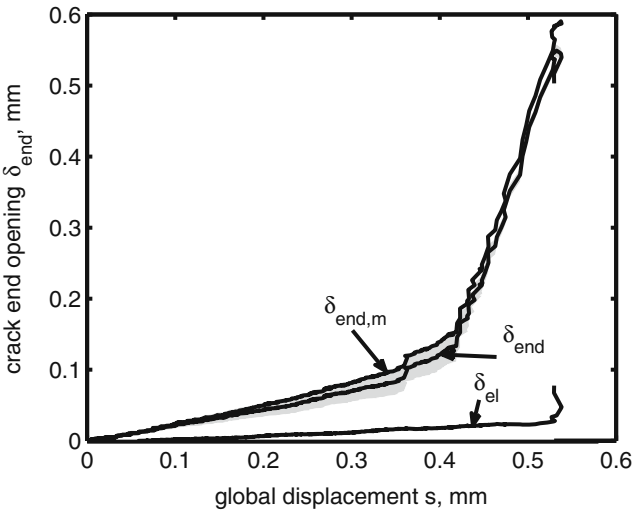

Fig. 8 The measured crack end opening, $\delta_{end,m}$, the elastic crack end opening, δ_{el}, and the actual crack end opening, $\delta_{end} = \delta_{end,m} - \delta_{el}$, over the crosshead displacement for a DENT specimen (90° loading direction). The grey area indicates the influence of small changes (+/− 0.5 mm) in the definition of the initial crack tip x-coordinate on the actual crack end opening

The derived J-Integral was plotted over the crack end opening determined in 4.1. The resulting curves are shown in Fig. 10. The curves have a sigmoidal shape reaching their maximum at about 0.2 mm crack end opening. In Fig. 10(a), the curves were compared for the different loading directions. For the 90° loading direction the plateau value was about twice as high as for the 0° loading direction. Furthermore, the plateau was reached significantly later at about 0.25 mm instead of 0.2 mm crack end opening. The comparison of the curves in Fig. 10(b) for the CCT and DENT specimens showed that the initial slope of the CCT specimen was larger reaching the same plateau value faster.

Reaching the plateau can be interpreted as a fully developed cohesive zone. The J-Integral stays constant

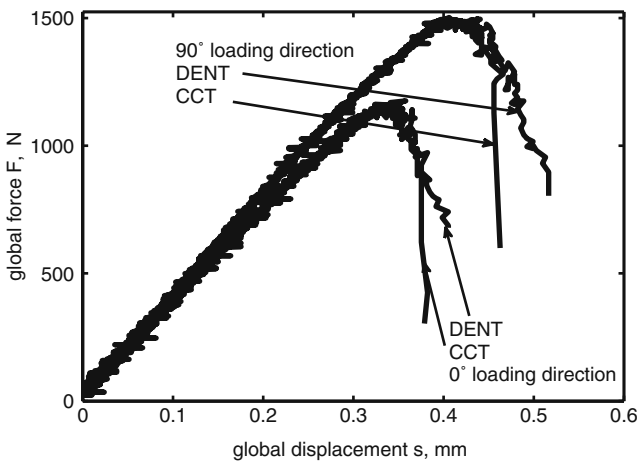

Fig. 9 Force–global displacement curves of chosen fracture tests

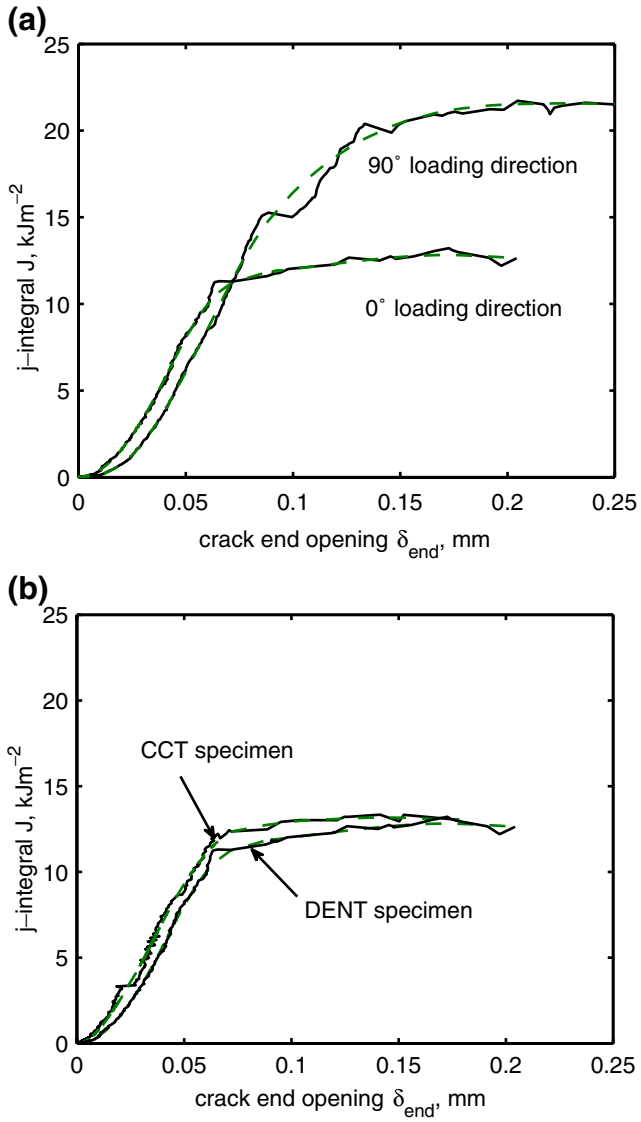

Fig. 10 The determined J-Integral-crack end opening curves. The solid lines show the measurement data and the dotted lines the fitted curves. In figure (**a**) the comparison of different loading directions is shown. Figure (**b**) depicts the comparison of different specimen geometries

and is not increased further by a growing damage zone. As a plateau value was reached in all tests, it could be concluded that the cohesive zones were fully developed at all loading directions and specimen geometries within the specimen boundaries.

Two measurements for every loading direction and specimen geometry combination were performed to check the reproducibility. Figure 11 proves the good agreement between the single measurements for DENT and CCT specimens (0° loading direction) respectively. Due to the time consuming evaluation, no further repetitions for statistical analysis were performed.

Cohesive Zone Models

The cohesive stresses were determined according to equation (1). The derivation increases the impact of measurement noise, therefore a data smoothing was performed previously. For this purpose, cubic smoothing spline fits were applied on the J-Integral-crack end opening curves, using the software Matlab (Matlab R2007b, TheMathWorks Inc., Natik, US). In Fig. 10 the fits are plotted as dotted lines in contrast to the original data plotted as solid lines. The numerical derivation of the fits leads to

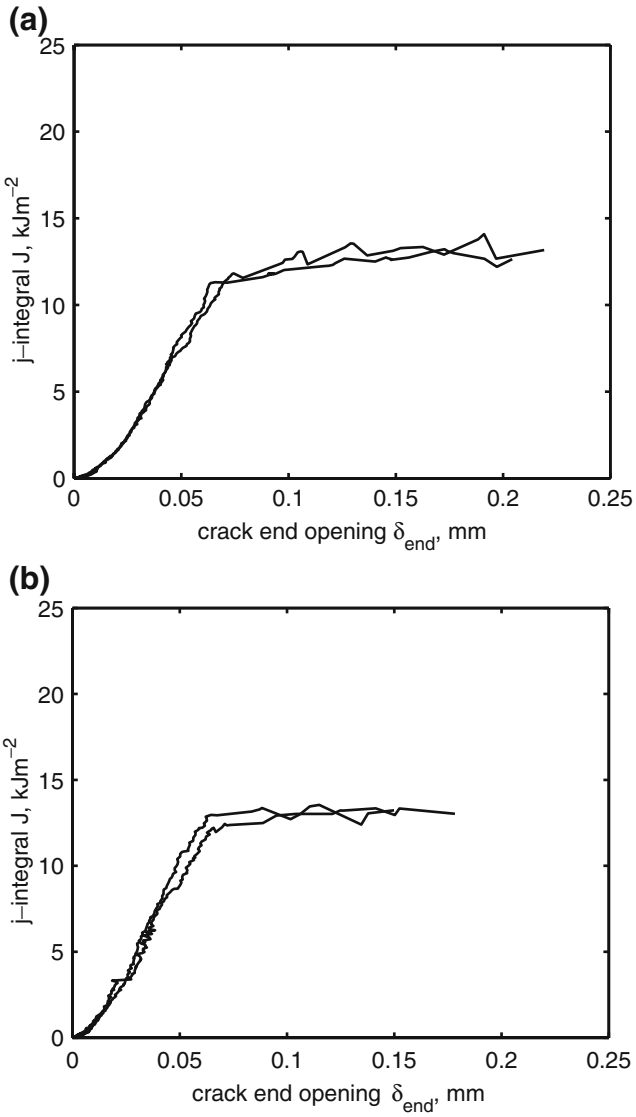

Fig. 11 The J-Integral-crack end opening measurement evaluation compared for two test specimens. The curve comparisons serve the estimation of measurement reproducibility. In figure (**a**) the comparison of two DENT 0° loading direction measurements is shown. Figure (**b**) depicts the comparison of two CCT 0° loading direction measurements

reasonable results, which were according to known cohesive zone model shapes.

The purpose of the fit was to minimise the effect of measurement noise, but it must be noted that all local effects were neglected and that the results reflect a homogenized material. This is especially important for the glass fibres. Their influence on the CZM damage zone cannot be observed explicitly but they increase the average height of the cohesive stresses.

The determined cohesive zone models are shown in Fig. 12. In Fig. 12(a), the loading directions of DENT specimens were compared. While the initial part, the linear increase and the maximum cohesive stress, was almost identical, the damage evolution was significantly different.

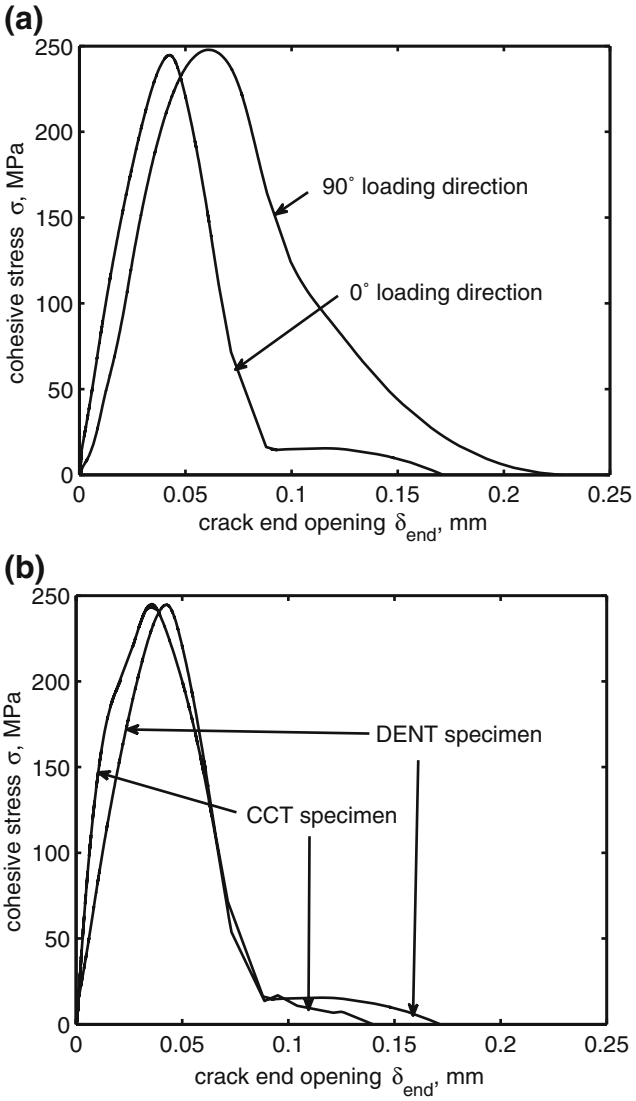

Fig. 12 The resulting cohesive zone models determined by the J-Integral approach. In figure (**a**) the comparison of different loading directions is shown. Figure (**b**) depicts a comparison of different specimen geometries

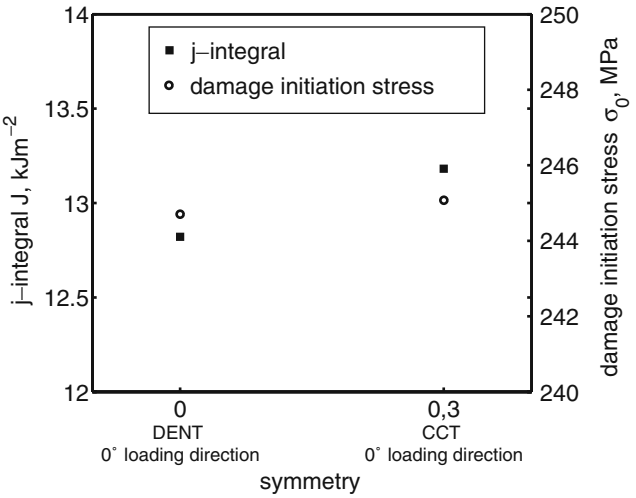

Fig. 13 An evaluation of the influence of the asymmetric crack growth on the cohesive zone model parameters. The grade of symmetry is estimated by the fraction of the crack length of the shorter crack over the crack length of the larger crack (crack lengths were measured at the point of time, when the plateau value for the J-Integral was reached)

For the 90° loading direction the cohesive stress seemed to decay exponentially in contrast to the 0° loading direction exhibiting a bilinear decay. The resulting areas under the cohesive zone models are according to the separation energy and reflecting the loading direction dependent fracture toughness. In the case of the 90° loading direction the more pronounced damage zone is indicating the higher fracture toughness. The damage initiation stress was about 250 MPa for both loading directions. The tensile strength was 198 MPa for the 90° loading direction specimen and 259 MPa for the 0° loading direction specimen. Thus, the damage initiation stresses were in a reasonable range, but the difference in the tensile strength was not reflected. In Fig. 12 (b), the results for the DENT and CCT - 0° loading direction specimens were compared. Except from a lower slope in the second part of the bilinear shaped damage evolution of the CCT specimen, no significant differences were observed.

In Fig. 13 the influence of the asymmetric crack growth is estimated. In DENT specimens cracks were only propagating from one side, while in CCT specimens cracks were propagating from both sides. Nevertheless, also in CCT specimens no perfect symmetric loading was realizable, as the cracks propagated with different velocities. In Fig. 13 a parameter, defined as the fraction of the crack length of the shorter crack over the crack length of the larger crack (crack lengths were measured at the point of time, when the plateau value for the J-Integral was reached), was used to estimate the grade of symmetry. This parameter was 0.3 for the CCT specimen and 0 for the DENT specimen. The figure shows the influence on the J-Integral and the damage initiation stress. The differ-

ences were not significant and allow the assumption, that despite asymmetric crack growth reasonable results were measured.

Summary and Conclusion

In the present work, an advanced test set-up was used to experimentally determine the CZM for glass-fiber reinforced polymeric materials. The necessary data was obtained from fracture tests. The crack end opening was measured with a high speed camera in combination with a digital image correlation system. The J-Integral was determined under the assumption of the applicability of LEFM via the energy release rate. The applicability of LEFM was experimentally verified by the estimation of the process zone size.

Using the J-Integral approach, the J-Integral was differentiated with respect to the crack end opening to determine the cohesive stresses. Due to the smoothing of the data, necessary to get rid of measurement noise, local effects were neglected, reflecting the material as homogeneous.

This method was applied to two specimen geometries (CCT and DENT) and loading directions (0° and 90°) respectively. Significant differences regarding the damage evolution were only observed for the different loading directions, but not for the specimen geometries. Depending on the loading direction, an exponential or a bilinear decrease of the cohesive stress was observed. The resulting different area under the cohesive zone model curve could be correlated to the different fracture toughness.

The results seemed reasonable, but have not been applied yet. In future work the derived results will be used in finite element simulations on laboratory specimen and on component scale. Comparisons to measurements will allow an evaluation of the cohesive zone models.

Finally, the local effects emerging from the inhomogeneous material will be discussed. The difference material properties of matrix and fibre cause an unsteady damage evolution. This effect will be analyzed in more detail in a future work to understand the resulting influences.

Acknowledgements The research work of this paper was performed at the Polymer Competence Center Leoben GmbH (PCCL, Austria) within the framework of the Kplus-program of the Austrian Ministry of Traffic, Innovation and Technology with contributions by the Institute of Material Science and Testing of Plastics, University of Leoben and AT&S GmbH. The PCCL is funded by the Austrian Government and the State Governments of Styria and Upper Austria.

References

1. Barenblatt GI (1962) The mathematical theory of equilibrium cracks in brittle fracture. Adv Appl Mech 7:55–129
2. Dugdale DS (1960) Yielding of steel sheets containing slits. J Mech Phys Solids 8:100–104
3. Remmers JJC, de Borst R, Needleman A (2008) The simulation of dynamic crack propagation using the cohesive segments method. J Mech Phys Solids 56:70–92
4. Zhang Z, Paulino GH (2004) Cohesive zone modelling of dynamic failure in homogeneous and functionally graded materials. Int J Plasticity 21:1195–1254
5. Yang ZJ, Deeks AJ (2007) Fully-automatic modelling of cohesive crack growth using a finite element-scaled boundary finite element coupled method. Eng Fract Mech 74:2547–2573
6. Yang Q, Cox B (2005) Cohesive models for damage evolution in laminated composites. Int J Fract 133:107–137
7. Sørensen BF, Jacobsen TK (2003) Determination of cohesive laws by the J integral approach. Eng Fract Mech 70:1841–1858
8. Ting SKM, Williams JG, Ivankovic A (2006) Characterization of the fracture behaviour of polyethylene using measured cohesive curves. Polym Eng Sci 46:763–798
9. Li VC, Ward RJ (1989) A novel testing technique for post-peak tensile behaviour of cementitious materials. In: Mihashi et al (eds) Fracture toughness and fracture energy. Balkema, Rotterdam, pp 183–195
10. Chen CR, Kolednik O, Scheider I, Siegmund T, Tatschl A, Fischer FD (2003) On the determination of the cohesive zone parameters for the modeling of micro-ductile crack growth in thick specimens. Int J Fract 120:517–536
11. Zhu Y, Liechti KM, Ravi-Chandar K (2009) Direct extraction of rate-dependent traction-seperation laws for polyurea/steel interfaces. Int J Solids Struct 46:31–51
12. Rice JR (1968) A path independent integral and the approximate analysis of strain concentration by notches and cracks. J Appl Mech 35:379–386
13. Jerabek M, Major Z, Lang RW (2010) Strain determination of polymeric materials using digital image correlation. Polym Test 29:407–416
14. Turner CE (1980) The ubiquitous η factor. Fract Mech, 12th conference, ASTM-STP 700:314–337
15. Towers OL (1985) Tests for fracture toughness and fatigue assessment: a compilation of stress intensity, compliance, and elastic η factors. The Welding Institute, Abington
16. Bao G, Suo Z (1992) Remarks on crack-bridging concepts. Appl Mech Rev 45:354–366

PAPER 5: LOCAL DAMAGE SIMULATIONS OF PRINTED CIRCUIT BOARDS BASED ON DETERMINED IN PLANE COHESIVE ZONE PARAMETERS

P.F.Fuchs[a], K.Fellner[a], G. Pinter[b]

[a] Polymer Competence Center Leoben GmbH, Roseggerstrasse 12, 8700 Leoben, Austria

[b] Material Science and Testing of Plastics, Department Polymer Engineering and Science, University of Leoben, Otto Gloeckel-Strasse 2, 8700 Leoben, Austria

submitted to *Engineering Fracture Mechanics* (2011)

Local damage simulations of printed circuit boards based on determined in plane cohesive zone parameters

P.F.Fuchs[a], G. Pinter[a,b], K.Fellner[a]

[a] Polymer Competence Center Leoben GmbH, Roseggerstrasse 12, 8700 Leoben, Austria
[b] Material Science and Testing of Plastics, Department Polymer Engineering and Science, University of Leoben, Otto Gloeckel-Strasse 2, 8700 Leoben, Austria

Abstract

In this work it was tried to analyse the failure pattern of a PCB under a standardized board level drop test in order to be able to evaluate the reliability and lifetime. Therefore, the fracture behaviour of the affected material was characterized. The parameters of a cohesive zone law were determined by performing a double cantilever beam test and an according simulation. The cohesive zone law was used in an enriched finite element local simulation model to predict the crack initiation and crack propagation. A good agreement between the simulated and the experimentally observed failure pattern could be shown. Using the determined location of the initial crack, the energy release rate at the crack tip could be calculated, allowing an evaluation of the local loading situation. Applying this procedure on two example PCBs, the significant influence of the chosen built ups on the local failure behaviour could be proven.

1. Introduction

The reliability and lifetime of printed circuit boards (PCBs) is a key issue in the PCB industry. The manifold use of the boards in various electronic devices exposes them to a wide range of different loads. In order to evaluate and ensure the performance of the PCBs, board level tests were introduced. In these tests common loads are reproduced and the reliability of the PCBs is analysed. In this work, the focus was set on dynamic loads, occurring e.g. when a mobile device is dropped. The industry wide standard to test the reliability under drop impact is a standardized board level drop test (BLDT) [1]. These tests have been analysed and proven to give reliable results (e.g. [2-4]). However, the experiments are time consuming and expensive. Thus, it is tried to perform preliminary finite element simulations to reduce the testing effort. These simulations are quite complex, as PCB built ups consist of significantly different interacting materials and the factor between the total board size and the crack sizes, which cause failure of the whole device (by breaking conducting paths) is less than 10-4. Numerous works (e.g. [5-7]), performed on the simulation of the local stress situation in PCBs, revealed, that the main challenge is the definition of a local loading parameter correlating with the PCB lifetime. Thus, the main aim was to develop a method, determining a proper loading parameter for the regarded failure type. While most works focus on failure in the solder ball, taking into account the equivalent plastic strain, in this work, the area of interest was the via connecting the solder ball and the according copper pad with the subjacent copper layer. A typical cross section of the regarded failure type is shown in Fig. 1. The crack started at the edge between solder ball, copper pad and insulating layer and grew towards the copper via.

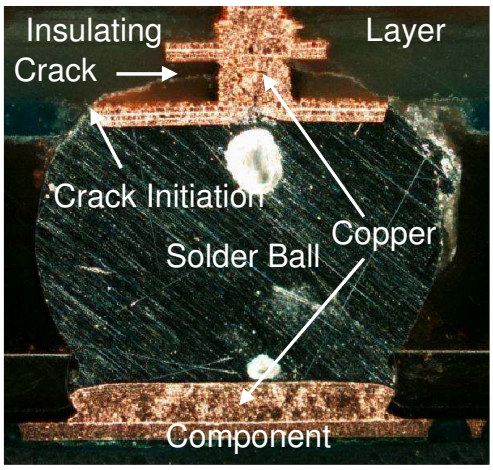

Fig. 1 Light microscopy analysis of the cross section of a typical failure pattern of a PCB tested in a board level drop test.

As the region of failure is, compared to the total board size, very small, special simulation techniques had to be applied. Furthermore, the mechanical material behaviour had to be known in detail. As the simulations should describe the local damage behaviour, also the fracture behaviour of the outermost layer had to be known. Thus, in this work the parameters of a cohesive zone law were determined for the according insulating layer, a glass fibre mat reinforced epoxy resin layer. As the cracks observed in the failure analysis of the BLDT were growing trough the matrix or along the matrix-fibre interface (without breaking the fibres), it was tried to set up a fracture test resulting in a similar in plane crack propagation. Only mode I fracture was analysed, as mode I was expected to be the dominant crack driving mode. For the determination of the cohesive zone model parameters a combination of both, experiments and simulations was applied.

2. Materials and Specimens

The experiments and simulations were performed on test PCBs, based on the recommendations for the BLDT [1]. The design of the copper layers, the ball grid area and the components position were defined according to the standard. Though, in the simulations only the most failure prone component, mounted at the centre of the printed circuit board, was regarded, in order to reduce the degrees of freedom in the model.

2.1. *PCB Built Ups*

A schematic representation of the of the analysed PCBs built ups is shown in Fig. 2. The composite layers, used as insulating layers between the copper layers, consist of glass fibre mat reinforced epoxy resin. The basic linear elastic orthotropic engineering constants of the individual layers were determined in a previous work [8] (Table 1). Two different built up variations were regarded. For both built ups composite 1 was defined as M1 1080. For PCB built up 1 composite 2 was defined as M1 1501 and for PCB built up 2 composite 2 was defined as M2 1501. For copper a nonlinear isotropic material law with a young's modulus of 50650MPa and a possion's ratio of 0.35 was used. For the solder material data from the literature was used [7].

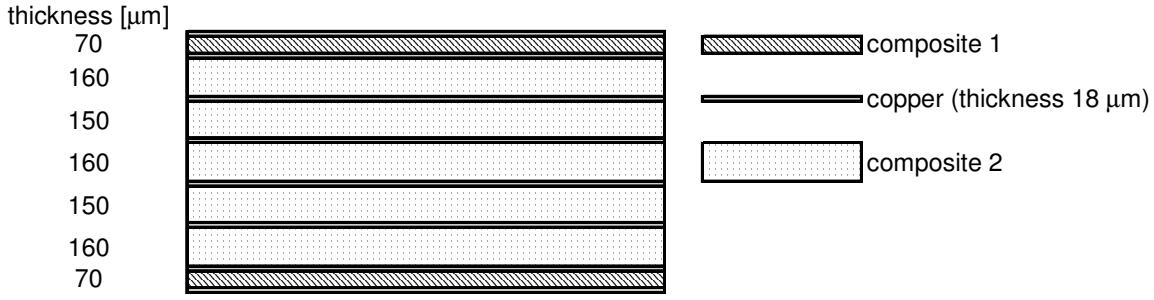

Fig. 2 Schematic representation of the analysed PCB built ups.

Table 1 Material data used to represent the insulating layers in the simulations.

		E11	E22	E33	ν12	ν13	ν23	G12	G13	G23
		MPa	MPa	MPa	-	-	-	MPa	MPa	MPa
M1	*1080*	12910	8610	5760	0.15	0.29	0.37	1960	1820	1790
	1501	15350	15050	7610	0.15	0.32	0.32	3120	2420	2420
M2	*1501*	22410	22170	16900	0.15	0.32	0.32	3030	5880	5870

2.2. *Test Specimens*

For the determination of the cohesive zone parameters test specimens were prepared to perform the according fracture tests. The material analysed was the composite used for the outermost layers, M1 1080, where the local cracks were observed. Due to the observed failure patterns described in chapter 1, it was tried to characterize in plane crack growth. Thus, in order to determine the in plane energy release rate specimens on the basis of double cantilever beam (DCB) test were chosen. The specimens were manufactured of plates pressed of two or more prepregs and three different thicknesses (0.65mm, 2mm and 5mm) were analyzed. The specimen's width, 20mm and length, at least 120mm, was defined according to the standard ISO 15024. A precrack of about 20 mm was introduced by a teflon foil, which was placed between the prepregs during the pressing program. Additionally, load blocks for the introduction of the load into the specimens were applied.

3. Experimental

The fracture tests were performed in order to be able to simulate the crack initiation and propagation. Therefore, it was tried to determine the parameters of a cohesive zone model. Experiments were performed to determine the energy release rate.

3.1. *Test Set Up*

A test set up on the basis of a DCB test was used for all specimen thicknesses (described in 2.2). The load was applied with a test rate of 10 mm/min. An optical camera (Basler A504k, Basler AG, DE) was used to record the measurement with a frame rate of 1.5 fps and a resolution of 1280x1024 to evaluate the crack propagation. In Fig. 3 the test set up for two specimens with a different thickness (0.65mm - Fig. 3a and 5 mm - Fig. 3b) is shown. The different thickness and stiffness respectively of the bending arms resulted in different load introductions. Thus, evaluating the measured data, the different loading conditions had to be taken into account.

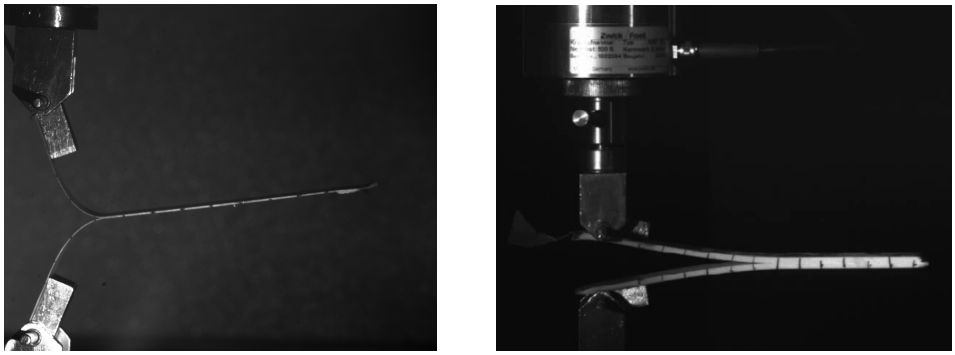

a b

Fig. 3 Fracture test set up for the 0.65mm thick specimens (a) and for the 5mm thick specimens (b).

3.2. *Data Reduction*

For the 0.65mm and 2mm specimens the energy release rate was evaluated on the basis of a T- Peel-Test [9]. The results showed significant scatter and could not be used to determine a reliable value. A possible reason could have been the difficult describable loading condition, as e.g. the peel angle could not be determined accurately. Thus, only the force-displacement curves of these measurements were used in the further work. The 5 mm specimens satisfied the ISO 15024 specimen geometry guidelines and were evaluated according to the corrected beam theory defined as method A in the standard. At least three measurements were performed for every set up and the results were averaged.

4. Simulation

Next to the experiments it was necessary to perform preliminary simulations to determine the missing cohesive zone parameters for the local stress simulation. Abaqus (Abaqus 6.10-1, Daussault Systèmes Simulia Corp., Providence, USA) was used to realize the simulations.

4.1. *Cohesive Stress Determination*

To describe the cohesive zone, the energy release rate, the cohesive stress and the function of the damage evolution have to be known. While the energy release rate could be determined experimentally and the damage evolution was predefined as linear (the influence of the chosen function was found to be rather small [10]), the cohesive stress was still unknown. Thus, the missing cohesive stress was determined by the simulation of the performed fracture mechanics experiments (Fig. 4). Different trial cohesive stresses were defined and iteratively adapted to match the simulation results, regarding the force-displacement curves, with the experimental results. The adoption of the cohesive stress was carried out using the results of the thickest specimens (5mm). The experimental results of the thinner specimens (2mm and 0.65mm) were used to evaluate the determined cohesive zone model. The extended finite element method (XFEM) with the traction-separation cohesive behaviour approach was used to simulate the DCB test.

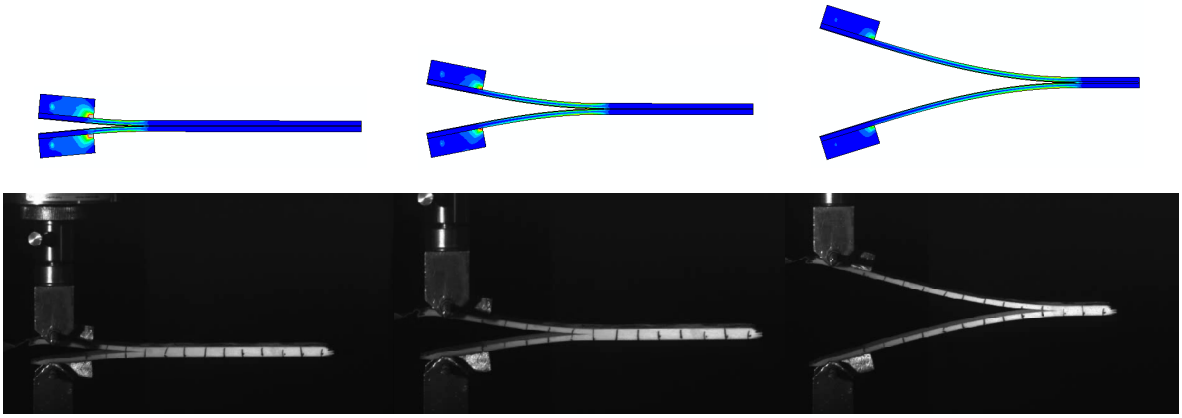

Fig. 4 The generated simulation model compared with the experiment (crack lengths: 50, 70 and 120mm).

4.2. *Local Stress Simulation*

To simulate the local stresses it was started with the analysis of a global model. The global model was realized as a quarter model of the PCB with a component mounted at the centre. The board was modelled as composite shell with layers according to the defined built ups in chapter 2.1. While the component was also modelled as composite shell, the solder balls connecting the board and the component were modelled as solids to comply with the given spherical geometry. The material data used in this simulation is described in chapter 2.1.

It was shown in a previous work that the results and the failure modes of a BLDT correlate well with the results of a BLCBT [11]. The advantage of the BLCBT, regarding a finite element simulation, is that the boundary and loading conditions are less complex and can be described properly in the simulation. In the contrary to a fixation by screws resulting in an undefined clamping state, the use of the three point bending fixture results in an explicit boundary condition. Furthermore, the computing time of a BLCBT simulation is significantly shorter than for a BLDT simulation, as instead of an acceleration only a displacement has to be applied. Thus, in this work, the global model was loaded according to a cyclic three point bending test and the loading situation of the board under the first maximum deflection (3mm) was analyzed.

A rather rough mesh was chosen for the global model to keep the computing time low. However, the actual failure sizes were very small compared to the global model. The observed crack sizes were by an approximate factor of 104 smaller than the global board size. Thus, to analyze the local stresses in the area of interest a submodel was used.

In the submodel one selected solder ball was exemplarily analyzed. The in the experiments most failure prone solder ball was chosen. The submodel was built with solid elements to correctly describe the three-dimensional stress situation. A quite dense mesh was used to get detailed results. The boundary conditions were applied with the Abaqus submodelling tool. The realization of the global model and the submodel in Abaqus is illustrated in Fig. 5.

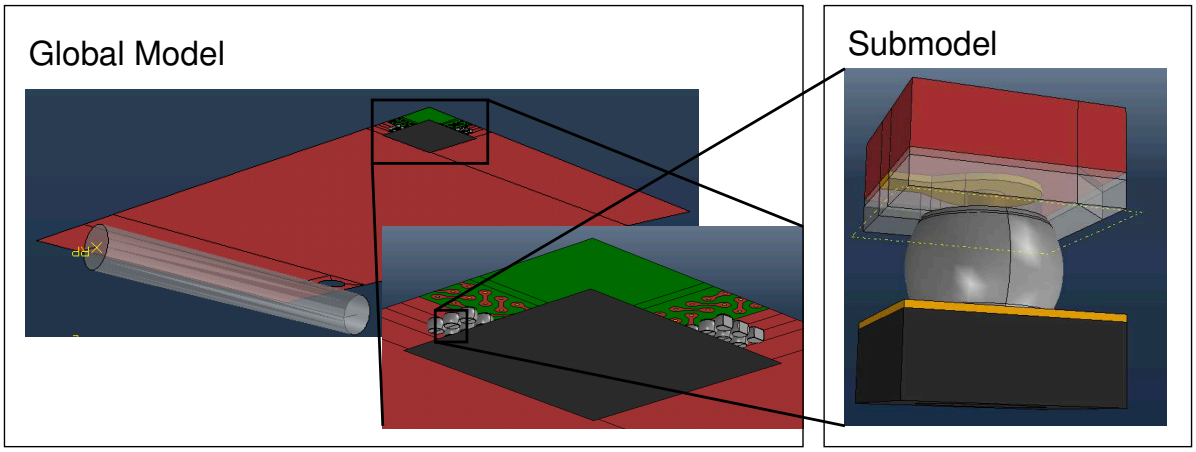

Fig. 5 The global and local (realized by a submodel) simulation model of the printed circuit board.

As the crack onset was expected to be at the re-entrant edge between solder balls, copper pad and the composite layer it was not possible to determine an exact stress state. The simulated local stress depends on the chosen mesh density for which reason it was tried to determine the energy release rate instead. Therefore fracture simulations had to be performed, which tend to be computationally expensive. In order to keep the simulation times down, the model size had to be further reduced. To do so a 'subsubmodel', a fracture simulation model, was introduced. The modelling space was defined as two-dimensional and the regarded area was narrowed down. In Fig. 6 the mises stress distribution in the cross section of the loaded submodel is shown, and the fracture simulation model is indicated by a black square. The boundary conditions of the submodel could not be applied to the fracture simulation model using Abaqus, as solid to shell submodeling is not supported by the software. Thus, the displacement of the submodel was evaluated at the border of the area, chosen for the further reduced model, and mapped to the mesh of the generated fracture simulation model using the software Matlab (The MathWorks Inc., Natick, USA).

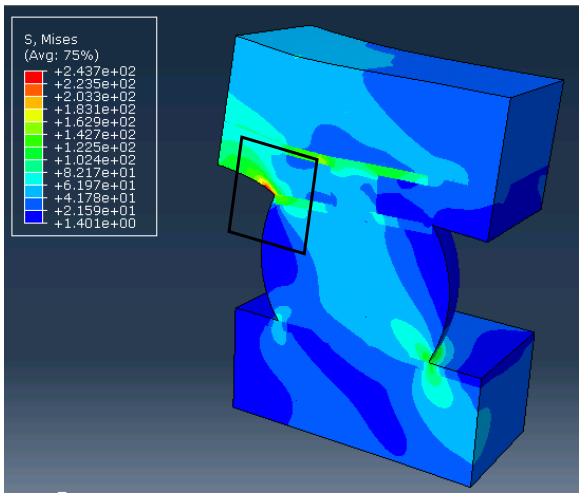

Fig. 6 Mises stress distribution in the cross section of the local submodel due to the loading conditions of a BLCBT. The area regarded in the fracture simulation is indicated by a rectangular mark.

Cohesive Zone Model Damage Simulation

In a first step, the fracture simulation model was used in an enriched finite element method (XFEM) traction-separation cohesive behaviour approach simulation

(Abaqus). The determined cohesive zone law (chapter 4.1) was used to simulate the damage behaviour of the outermost insulating layer. Thus, it was possible to predict the location of crack initiation and the direction of crack propagation.

Contour Integral Simulation

Knowing the initial crack from the cohesive zone model damage simulation it was possible to calculate the J-Integral value in a contour integral simulation. A short initial crack was predefined according to the simulated position and collapsed elements were used to model the crack tip. Thus, a parameter to evaluate the different local loading situation due to adapted board build ups could be determined.

5. Results and Discussion

5.1. *Fracture Mechanics Tests*

As indicated in chapter 3.2 for the 0.65 and 2mm specimens only the measured force-displacements curves were used for the verification of the cohesive zone law and no further data reduction was performed. The double cantilever beam specimens with a thickness of 5mm were evaluated according to the ISO 15024. The resulting energy release rates scattered between 400 and 600 J/m^2 (
Fig. 7). Possible reasons were e.g. that the specimens thicknesses were not perfectly constant due to manufacturing influences and that the crack was sometimes growing in the matrix and sometimes at the matrix fibre interface. However, the scatter stayed in a reasonable range and for the cohesive zone law the results were averaged over the crack length and over the test repetitions resulting in an average critical energy release rate, GIC, of 486 J/m^2.

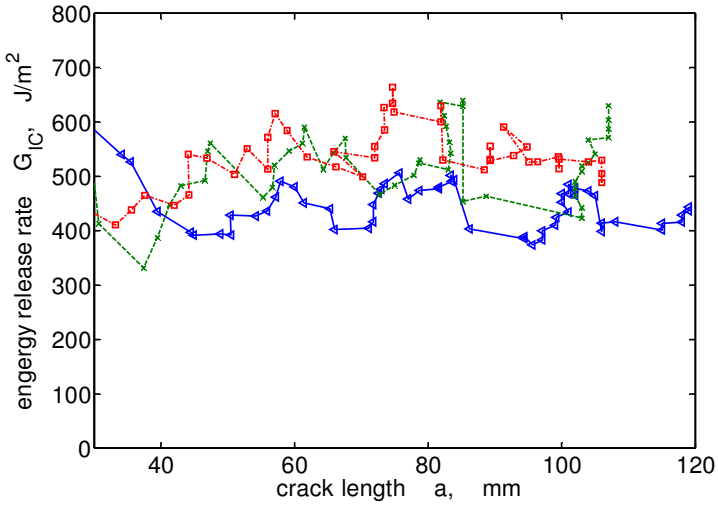

Fig. 7 The critical energy release rate G_{IC} of three DCB measurements evaluated based on the corrected beam theory over the crack length.

5.2. *Cohesive Stress Determination*

The simulations were performed according to the description in chapter 4.1. The cohesive stress was iteratively adapted in the DCB test simulations of the 5mm thick specimens. Three exemplarily results are shown in Fig. 8. The choice of the cohesive stress was observed to have an influence only on the initial slope and the reached peak force. It was found, that the cohesive zone model with an energy release rate of

0.486 J/m^2 (chapter 5.1), a linear damage evolution and a cohesive stress of 1.25 MPa proved best comparing simulation and experiment. The force-displacement curves were matching almost perfectly for the entire test time. However, the initial slope in the experiments was higher than in all the simulations. A possible reason could be an existing initial crack opening at the point of time when the experiments were started. The existing crack opening again could have been originated in the use of a teflon foil for the introduction of the precrack when pressing the specimens.

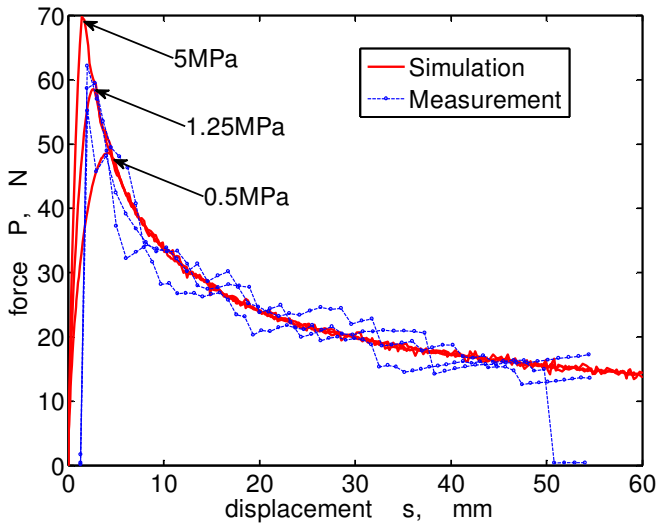

Fig. 8 Comparison of the simulated DCB test results with the experimental results. The cohesive stress of the cohesive zone law used in the simulation was adapted to match experimental results.

To evaluate the determined cohesive zone model, it was used for the simulation of the fracture tests of the thinner specimens. In Fig. 9 the simulation for the 2mm and 0.65mm specimens are compared to the experimental results. The results revealed a good correlation. Thus, it also could be shown, that the element size, which was different for the simulation models of the specimens with different thicknesses, did not have a significant influence.

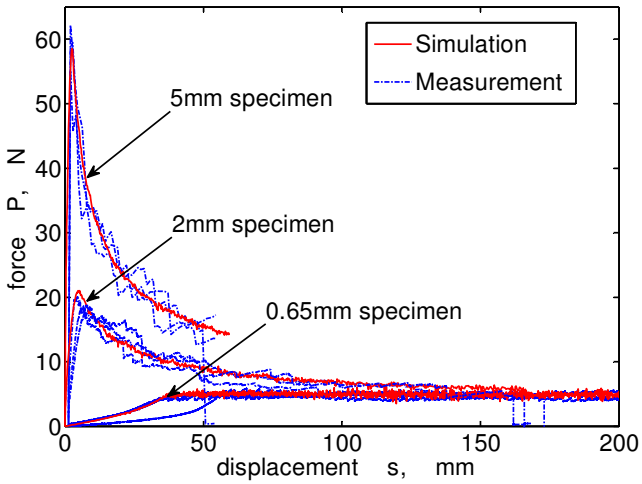

Fig. 9 Evaluation of the cohesive zone law by comparing the fracture test simulations of the 2 and 0.65mm specimens with the experimental results.

5.3. *Local Stress Simulation*

The global results of the BLCBT simulations of the PCBs built up 1 and built up 2 were used to apply the boundary conditions on the submodels. In the following two chapters the, regarding the local failure, determining results of the fracture simulation model (chapter 4.2) are presented.

Cohesive Zone Model Damage Simulation

In the fracture simulation model the cohesive zone law was used for the outermost insulating layer in an enriched finite element simulation. Crack initiation and propagation were enabled for the complete layer. The simulation result for PCB built up 1 is shown in Fig. 10. The observed crack initiation and propagation were according to the failure patterns (Fig. 1) known from the failure analysis of the BLCBT and BLDT experiments.

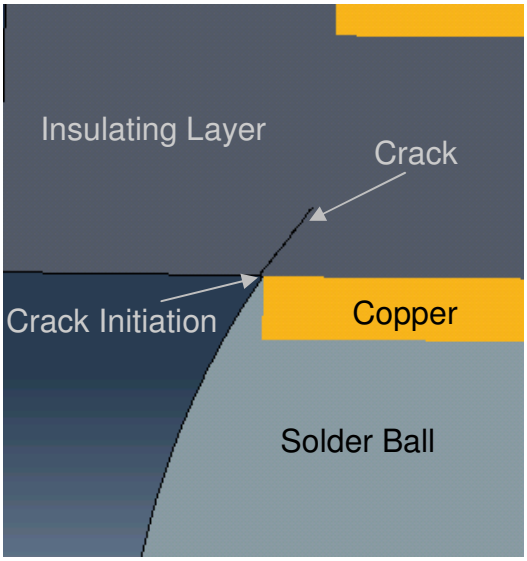

Fig. 10 Local XFEM simulation showing the crack initiation and propagation in PCB built up 1 under the global load of a BLCBT.

Contour Integral Simulation

In the contour integral simulations the prevailing energy release rate was analyzed. An initial crack, known from the failure analysis and verified by the XFEM simulation, was presumed and modelled. Around the crack tip a J-Integral value was calculated using a special mesh geometry and collapsed elements. The simulation model is shown in
Fig. 11. The simulation was performed for both, PCB built up 1 and PCB built up 2. Thus, the influence of the different inner layers on the local loading situation in the area of interest could be evaluated. The simulation resulted in a J-Integral value of 163 J/m^2 for PCB built up 1 and in 193 J/m^2 for PCB built up 2. This result can be used as an indication for the drop test reliability of the PCBs. The crack driving force was found to be lower for PCB built up 1 while the crack resistance did not change, as the outer layers (location of the local crack) were the same for both built ups. Thus, based on the simulation results, it can be expected that PCB built up 1 performs better than PCB built up 2 in a BLCBT and a BLDT respectively.

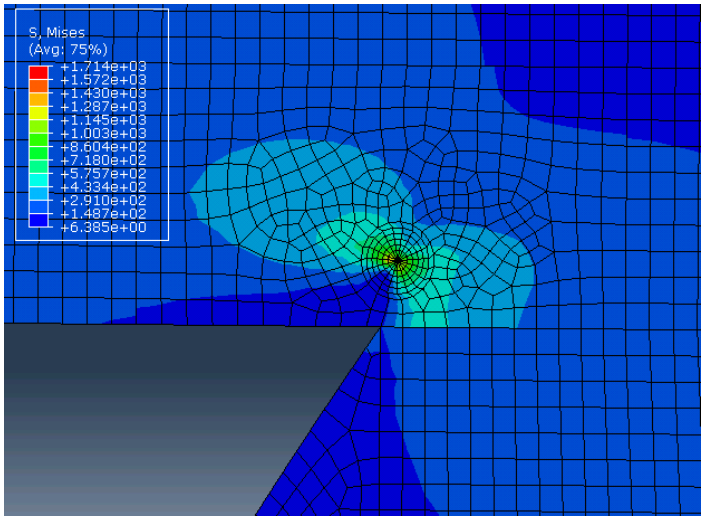

Fig. 11 Local contour integral simulation used to calculate the energy release rate at the presumed initial crack in PCB built up 1 under the global load of a BLCBT.

6. Summary and Conclusion

In this work printed circuit boards under impact loads were analysed. The parameters of a cohesive zone law of the outermost layer of a printed circuit board built up were determined to simulate the local damage behaviour. Therefore, a combination of both, experimental and simulation methods were used. With the cohesive zone law the crack initiation and propagation could be predicted applying a enriched finite element simulation. The obtained results agreed with the failure patterns observed in the experiments. Knowing the location of the crack the stress concentration at the crack tip could be calculated. Thus, it was possible to analyse the influence of the global built up on the local loading situation. Two built ups were exemplarily examined and significantly different energy release rates were calculated at the crack tip in the local failure area. Future work is focused on the verification and further use of the simulations. In order to be able to predict actual PCB built up lifetimes instead of just comparing them, it is planned to generate characteristic failure curves for the regarded failure types and materials. These failure curves are determined by performing BLCBT at different amplitudes and by simulating the according local loading conditions. The resultant curve of the energy release rate over the PCB lifetime will allow an estimation of the lifetime of a PCB built up without having to actually produce it, but just by performing the finite element simulations.

7. Acknowledgements

The research work of this paper was performed at the Polymer Competence Center Leoben GmbH (PCCL, Austria) within the framework of the COMET-program of the Austrian Ministry of Traffic, Innovation and Technology with contributions by the University of Leoben and by the AT&S Austria Technologie & Systemtechnik Aktiengesellschaft . The PCCL is funded by the Austrian Government and the State Governments of Styria and Upper Austria.

References

[1] Board level drop test method of components for handheld electronic products. JEDEC Standard JESD22-B111 2003.

[2] Wong E, Seah S, Shim V. A review of board level solder joints for mobile applications. Microelectronics Reliability 2008;48:1747-1758.

[3] Luan J, Tee T, Pek E, Lim C, Zhong Z. Dynamic responses and solder joint reliability under board level drop test. Microelectronics Reliability 2007;47:450-460.

[4] Wong E, Mai Y. New insights into board level drop impact. Microelectronics and Reliability 2006;46:930-938.

[5] Le Coq C, Tougui A, Stempin M-P, Barreau L. Optimization for simulation of wl-csp subjected to drop-test with plasticity behavior. Microelectronics Reliability 2011;51:1060-1068.

[6] Qu X, Chen Z, Qi B, Lee T, Wang J. Board level drop test and simulation of leaded and lead-free bga-pcb assembly. Microelectronics Reliability 2007;47:2197-2204.

[7] Tee T, Ng H, Lim C, Pek E, Zhong Z. Impact life prediction modeling of tfbga packages under board level drop test. Microelectronics and Reliability 2004;44:1131-1142.

[8] Fuchs PF, Pinter G, Tonjec M. Determination of the orthotropic material properties of individual layers of printed circuit boards. To Be Published n.d.

[9] Kinloch A, Lau C, Williams JG. The peeling of flexible laminates. International Journal of Fracture 1994;66:45-70.

[10] Schwalbe KH, Scheider I, Cornec A. The siam method for applying cohesive models to the damage behaviour of engineering materials and structures. 2009.

[11] Fuchs PF, Major Z. Cyclic bend tests for the reliability evaluation of printed circuit boards under dynamic loads. Frattura Ed Integrità Strutturale 2010;15:64-73.

PAPER 6: PCB DROP TEST LIFETIME ASSESSMENT BASED ON SIMULATIONS AND CYCLIC BEND TESTS

P.F.Fuchs[a], G. Pinter[b], Z.Major[c]

[a] Polymer Competence Center Leoben GmbH, Roseggerstrasse 12, 8700 Leoben, Austria

[b] Material Science and Testing of Plastics, Department Polymer Engineering and Science, University of Leoben, Otto Gloeckel-Strasse 2, 8700 Leoben, Austria

[c] Institute of Polymer Product Engineering, Johannes Kepler University Linz, 4040 Linz, Austria

submitted to *Microelectronics Reliability* (2012)

PCB drop test lifetime assessment based on simulations and cyclic bend tests

P.F.Fuchs[a], G. Pinter[a,b], Z.Major[c]

[a] Polymer Competence Center Leoben GmbH, Roseggerstrasse 12, 8700 Leoben, Austria
[b] Material Science and Testing of Plastics, Department Polymer Engineering and Science, University of Leoben, Otto Gloeckel-Strasse 2, 8700 Leoben, Austria
[c] Institute of Polymer Product Engineering, Johannes Kepler University Linz, 4040 Linz, Austria

Abstract

The aim of this work was to predict the performance of printed circuit boards (PCB) in a board level drop test (BLDT). The applied methodology was based on results of a board level cyclic bend test (BLCBT) and an according finite element simulation of the test. A function, describing the relation between a local loading parameter, determined in the simulation model for different deflection amplitudes of the BLCBT, and the according cycles to failure, measured in the experiments, was modelled. The method was evaluated by comparing the predicted results of two additional PCB built-ups with experimentally determined lifetimes. The determined lifetimes agreed very well, although the differences between the analysed PCB types were not very clear. Applying the known correlation between the BLCBT and the BLDT, the predicted results for the BLCBT could be used to estimate the BLDT performance.

1. Introduction

Printed circuit boards (PCB) are the linking part in all electronic devices. They bring together all applied components and connect them through a complex structure of conducting paths. They are used in almost every product, including electronic systems. Nowadays mobile devices represent one major area of application of rising interest. Related research is focused on small, high performance gadgets with an increasing number of features. Thus, the PCB industry faces some demanding challenges. Multilayer boards with multiple thinner layers (boards with up to 22 layers are state of the art), lower conducting path sizes and smaller via diameters are increasingly sought after. These developments are counteracting the effort of ensuring the reliability of the devices and necessitate an optimized design, based on improved understanding of material behaviour.

The range of loads, PCB have to endure during their lifetime is - due to their large field of applications - wide spread. E.g. for mobile devices, impact loads are of special interest, as they are especially prone to be dropped. These impact loads are considered within this work. The current industry-wide standard to evaluate the drop performance of PCB is a board level drop test (BLDT) [1]. Thereby, an instrumented drop of a defined test board is repeated, till a failure is detected. The number of drops till failure is used as an indicator for the drop test reliability. An accelerated test, a board level cyclic bend test (BLCBT) [2], applying a sinusoidal load continuously, has been developed as an alternative. The advantage of this method, next to shorter testing times, is very precisely defined boundary conditions, compared to those used in a BLDT test. This simplifies the finite element (FE) simulation of the experiment, which is crucial for the presented approach.

However, the experimental methods exhibit the drawback of being both time consuming and expensive. PCB producers have to design, produce, assemble (has often to be done externally) and repeatedly test (to achieve a relevant statistical statement) the PCB. Between design completion and a first reliability estimation, there are rather long waiting times. Therefore, there is an effort to accelerate the reliability and lifetime estimation by performing FE simulations. The prediction of both the global and local deformation and damage behaviour has been tried in several works (e.g.[3], [4], [5], [6], [7] and [8]); moreover, attempted to be set in correlation with the PBC reliability. So far, several promising results and complimentary correlations between simulation results and experimentally observed lifetimes were established and presented. However, in order to accurately describe a correlation between the simulation results and the fatigue lifetime, a number of different board designs, covering a representative range of the PCB lifetimes, had to be analysed in the BLDT. Here, a method, allowing the generation of a correlation curve by testing just one PCB design, is presented.
The predominant number of failures in PCB during a BLDT or BLCBT is allocated at or near the vicinity of the solder bumps, connecting the board with the mounted components. Typical failure patterns are depicted in Fig. 1. The failure type depends on the PCB built-up and design.

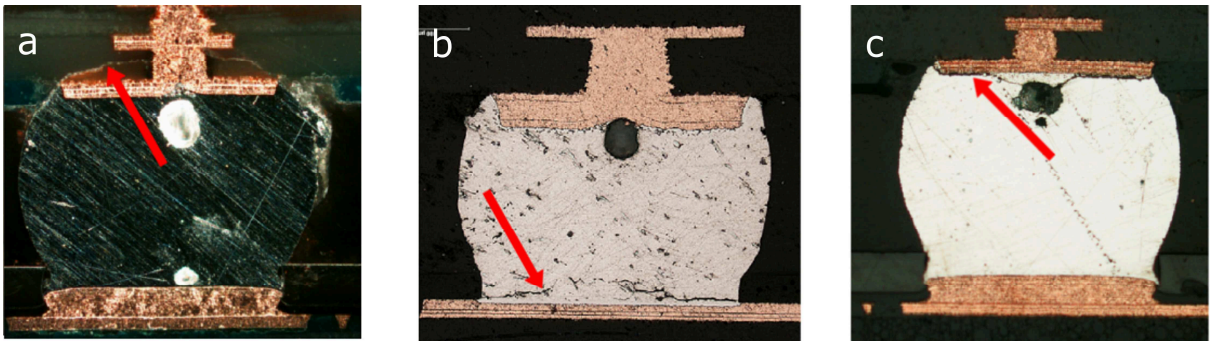

Fig. 1 Typical failure patterns of PCB during a BLDT or BLCBT: a) Failure in the outermost epoxy layer, b) Failure in the solder bump, close to the component, c) Failure at the interface between solder bump and copper pad.

The challenge posed by FE simulations, is the determination of a critical loading parameter, which is associated with the lifetime of the PCB. The globally applied load cannot be used as a loading parameter, since the local conditions produced the biggest impact on damage behaviour. Thus, using the finite element models, loading parameters, describing the local situation, were determined. Depending on the failure type, different approaches have been applied. For example: for failure type b (solder bump - Fig. 1b), the maximum equivalent plastic strain in the solder and for failure type c (interface between solder bump and copper pad -.Fig. 1c), the maximum peel stress at the solder copper pad interface have been used in published works ([4] and [5]). For failure type a (outermost epoxy layer - Fig. 1a), a parameter based on a fracture mechanics concept has been proposed [9]. The tested PCB in this work showed a type b failure; henceforth, it was tested with the maximum equivalent plastic strain. However, the presented method should be applicable independently of the failure type, as long as the failure mode can be modelled in an adequate way.

2. Materials and Specimens

Three different PCB built-ups have been analysed in this work. The test boards were eight layer PCB (eight copper layers with insulating epoxy intermediate layers), with

five mounted components (Fig. 2). The design and mounting of the components was based on the recommendations of the JEDEC standard for the BLDT[1]. The components were ball grid area packages (type: 288 Ball BGA with 4 Rows of Balls, pitch: 500µm, pad diameter: 350µm and solder material: 96.5Sn/3.0Ag/0.5Cu (SAC305)) with dimensions of 12x12x0.65 mm. The dimensions of the boards were 132x77x1.064 mm. The boards had a symmetric design and the outermost epoxy layers were unreinforced, while the inner epoxy layers were reinforced with fabric, woven from 'E' glass. The reinforcement was according to the standardized types described in the IPC-4412A specification [10] (The defined types 7628 and 1501 were used). The three boards differed just by the epoxy matrix used for the inner intermediate layers. These board built-ups shall now be referred to as PCB 1, 2 and 3. The epoxy resin of the outermost layers was defined as material M_I and the epoxy resins of the inner layers were designated as material $M_{II\text{-}PCB1}$, $M_{II\text{-}PCB2}$ and $M_{II\text{-}PCB3}$ (according to the PCB types respectively). A schematic representation of the cross section of the boards is given in Fig. 3.

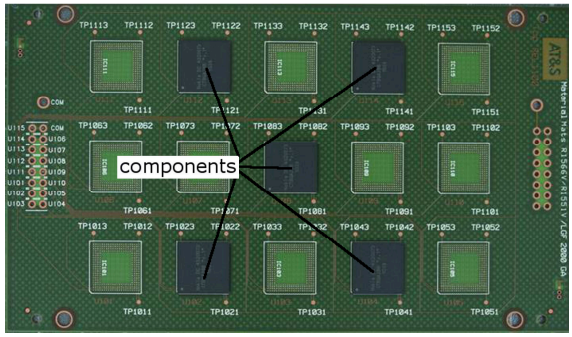

Fig. 2 Top view of a tested PCB, showing the board with the five mounted components.

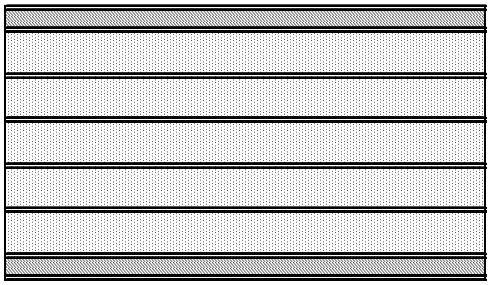

Fig. 3 Schematic representation of the cross-section of the tested PCB, showing the multilayers built-up.

The material properties of the individual epoxy layers and copper were determined by in-house measurements, based on methods described in an earlier work [11]. The material models used for solder and ceramic were adopted from literature [12] and [13]. The reinforced epoxy layers were described by linear elastic orthotropic material data, while the pure epoxy resin layers, the copper (paths and vias) and the solder were described by a an isotropic elastic plastic material model (.

Table 1). E_{11}, E_{22} and E_{33}, the direction dependent Young's moduli, ν_{12} ν_{13} and ν_{23}, the Possion's ratios and G_{12}, G_{13} and G_{23}, the shear moduli, are the necessary engineering constants for the definition of a linear orthotropic material model. For the definition of an isotropic material model, the linear region is sufficiently described by one Young's modulus, E, and one Possion's ratio, ν. Additionally, for the elastic

plastic models, the yield stress over the plastic strain also had to be defined. The correlation was described in tabular form.

Table 1 The material data applied in the finite element simulations for the different materials used.

part	*material*	*matrix resin*	*content*	$E_{(11)}$	E_{22}	E_{33}	$\nu_{(12)}$	ν_{13}	ν_{23}	G_{12}	G_{13}	G_{23}	*material model used*
			%	GPa	GPa	GPa	-	-	-	GPa	GPa	GPa	
component	ceramic		-	112.4			0.28						isotropic linear elastic
solder bump	SAC 305		-	37.9			0.35						isotropic elastic plastic
vias and pathes	copper		-	50.6			0.35						isotropic elastic plastic
outermost layer	resin	M_I	100	2.8			0.37						isotropic elastic plastic
inner layer	prepreg	$M_{II\text{-}PCB1}$	45	19.3	19.1	8.0	0.10	0.34	0.34	3.0	2.8	2.8	orthotropic linear elastic
			42	22.6	18.2	8.4	0.11	0.33	0.35	3.2	3.0	3.0	orthotropic linear elastic
		$M_{II\text{-}PCB2}$	45	21.9	21.7	10.8	0.12	0.33	0.33	4.1	3.9	3.9	orthotropic linear elastic
			42	25.2	21.0	11.4	0.13	0.32	0.34	4.4	4.2	4.1	orthotropic linear elastic
		$M_{II\text{-}PCB3}$	45	23.2	23.0	12.6	0.13	0.32	0.32	4.9	4.6	4.6	orthotropic linear elastic
			42	26.5	22.4	13.3	0.14	0.31	0.33	5.2	5.0	4.9	orthotropic linear elastic

3. Methods

The aim of this work was to generate a function correlating the PCB lifetime with a predictable local loading parameter. Therefore, experiments (BLCBT) were realized at different deflection amplitudes (in order to describe a representative range of different local loading conditions) for PCB type 1, and the times to failure were recorded. The broken boards were analysed and the failure mode was determined. Based on the failure mode, a local loading parameter was calculated for every tested deflection amplitude, using FE simulation models. Thus, the requested correlation between the local loading parameter and the time to failure (of the specified failure mode) could be modelled. By simulating the local loading parameter of PCB type 2 and 3, the resulting model could be used to predict their lifetime. The experiments and simulations are described in detail in the subsequent chapters.

3.1. *Experimental*

The BLCBTs were performed on an electro dynamic testing machine (Bose ElectroForce 3450, Bose Corporation, Eden Prairie, US). A three point bending fixture was used to apply the load. The board was placed centred on the support rollers and tape was used to avoid shifting of the board. Due to the set-up, only positive deflection values could be applied. A picture of the experimental set-up is shown in Fig. 4. The deflection was applied sinusoidal with a frequency of 25 Hz and a bearing distance of 105mm. The time to failure was measured simultaneously for all five components using an event detector (256STD, Analysis Tech, Wakefield, US), recording the resistance of the daisy chains going through the connections (solder bumps) between board and components respectively. Failure was defined as a resistance greater than 1000 ohms, lasting for 1 microsecond or longer. A more detailed description and discussion of the experimental set-up has been published before [2].

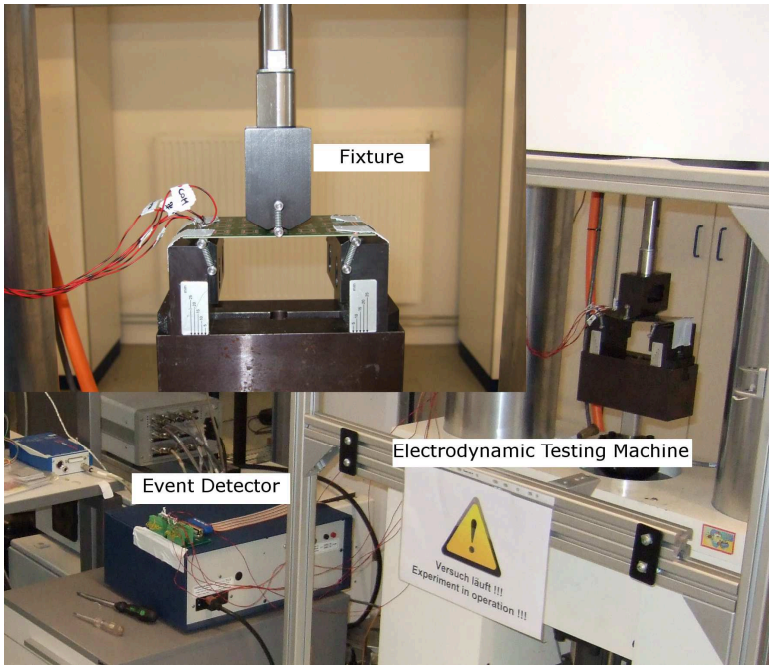

Fig. 4 The test set-up of the BLCBT, showing the three point bending fixture with a mounted PCB, the testing machine and the event detector.

As indicated before, different deflection amplitudes were applied to cover the range of different local loading conditions (usually originating from different PCB built-ups), while testing only one PCB design. The deflection was cycled between a minimum deflection of 1mm (to avoid a lift-off of the PCB from the support rollers) and a maximum deflection of 1mm, plus the deflection amplitude for all measurements. The deflection amplitudes were chosen, aiming for the generation of a representative number of interpolation points for a curve, describing the local failure parameter over the lifetime. At least three repetitions were performed for every amplitude of the BLCBT for PCB 1. For validation, PCB 2 and PCB 3 were tested only on one amplitude level. A 2mm amplitude set-up was selected, as the according maximum deflection (3mm) was close to the maximum deflection in a BLDT. In Table 2, the performed measurements are listed.

Table 2 The chosen BLCBT deflection amplitude values for measurements of the different PCB types.

amplitude	*repetitions*		
mm	PCB 1	PCB 2	PCB 3
1	3	-	-
1.75	3	-	-
2	8	8	8
2.75	3	-	-
3	3	-	-
3.5	3	-	-
4	3	-	-

Additionally to the BLCBT, also BLDT (eight repetitions per PCB type) have been performed, to verify the agreement of the test results. The BLDT were conducted according to the JEDEC standard [1]. The broken boards of both test methods were analysed using light microscopy. Micro sections of the expected failure locations were prepared and the failure modes were identified.

3.2. *Simulation*

The local loading parameters in the BLCBT experiments were determined using a finite element simulation model. The software Abaqus (Abaqus 6.10-1, Daussault Systèmes Simulia Corp., Providence, USA) was utilized to realize the simulations. One challenge was due to the local failures, causing PCB malfunction, being very small compared to the total board size (crack sizes of ~ 50 µm vs. a board length of 135 mm) Thus, in order to obtain the required resolution of the stress and deformation in the area of interest, a sub-modelling technique was applied. Doing so, a global model was simulated and the resultant displacement field devolution was used to drive a sub-model (a defined local area), by applying the corresponding displacement boundary conditions on the sub-model - global model interfaces. The advantage of the sub-modelling technique is a detailed solution, obtained for a local region, without excessively higher computing times. A relatively coarse mesh, keeping the computing times low, is used for the global model, while a refined mesh can be employed for the sub-model, as the sub-model size is very small compared to the global model size. In Fig. 5, an illustration of the global model (the applied boundary conditions are indicated) and the sub-model is shown.

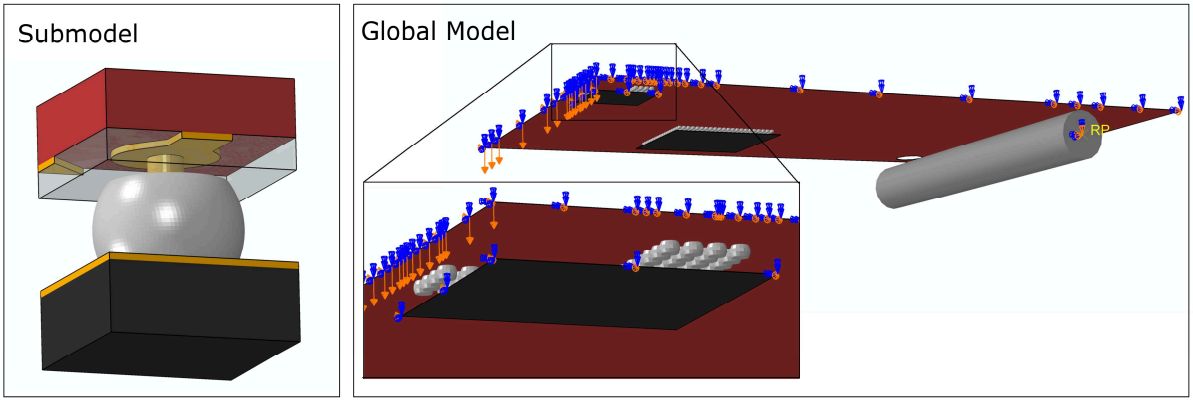

Fig. 5 Illustration of the global and the local model (sub-model). In the global model, the boundary conditions for a BLCBT load are indicated.

The BLCBT global simulation model was realized via a PCB quarter model, taking advantage of the existent symmetries. The board and the component of the global model were generated using shell elements. To account for the layer wise built-up, a composite layup section, including the single layers and the according material models, was assigned to the board. The solder bumps were integrated as solids to comply with the given spherical geometry. The interfaces between board, solder bumps and components were represented by tie constraints. A rigid cylinder, with an interaction definition against the board, accounted for the support rollers. The load application was conducted, applying a displacement along the centre line (contact line between fin and board in the experiment).

Evaluating the global model results, the solder bump, bearing the highest loads, was determined. This solder bump, with the associated part of the board and the mounted component (see Fig. 5), was chosen for the sub-model analysis. The sub-model was modelled with solid elements in order to obtain the three-dimensional stress and strain distribution field. The load was applied, exploiting the results of the global model. As failures in the solder bump were analysed in this work, the equivalent plastic strain (discussed in chapter 1) was chosen as local loading parameter. The

maximum value found in the solder bump was evaluated via the board deflection. In Abaqus, the variable PEEQ is used for the equivalent plastic strain, and it is evaluated by the following equation:

$$\bar{\varepsilon}^{p} = \int_{0}^{t} \sqrt{\frac{2}{3}\dot{\varepsilon}^{p} : \dot{\varepsilon}^{p}}\, dt \qquad (1)$$

where $\bar{\varepsilon}^{p}$ is the equivalent plastic strain and $\dot{\varepsilon}^{p}$ the plastic strain rate. A cross section of the sub-model, representing the equivalent plastic strain distribution, is shown in Fig. 6.

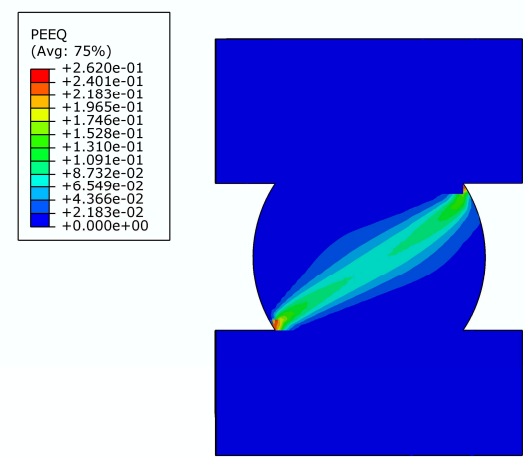

Fig. 6 Equivalent plastic strain distribution in the critical solder bump for a BLCBT deflection of 5mm calculated, using the sub-model of PCB 1.

In Table 3, the computation times for the global model and the sub-model for an Intel® Core™ i7-930 @ 2 x 2.80 GHz computer with 12 GB RAM are indicated. Reasons for the difference are the increased number of degrees of freedom (more solid elements) and the higher percentage of elements with an elastic plastic material behaviour.

Table 3 Computation times for the local and the global model.

	Number of shell elements	*Number of solid elements*	*Computation time (min)*
Global model	~ 120 000	~ 15 000	~45
Local model	-	~ 210 000	~ 2800

3.3. *Lifetime Modelling*

Using the experimental results (times to failure for different deflection amplitudes) and the corresponding simulation results (equivalent plastic strains in the solder bump) of PCB 1, a lifetime prediction curve was generated. The results (equivalent plastic strain over lifetime) were fitted, using a Manson-Coffin equation, a common model to describe low cycle fatigue of metals [14]. The Manson-Coffin equation is a power-law equation between cycle life and plastic strain:

$$N = C/(\varepsilon^{p})^{c} \qquad (2)$$

where N is the number of cycles of +- ε^{p}, ε^{p} is plastic strain, c is the exponent and C is the proportionality constant. In this work, the equivalent plastic strain was utilized for ε^{p}. Using the Manson-Coffin fit the lifetime of PCB 2 and PCB 3 was predicted.

Therefore, the according simulation results, the equivalent plastic strains, were substituted in the equation. Finally, the predicted results were compared with the experimental results.

4. Results and Discussion

The experimental results and the simulation results obtained, applying the methods described in chapter 3, are presented in this section. Furthermore, a lifetime prediction, based on these results, is shown and verified by comparison to both, BLCBT and BLDT results.

4.1. *Experimental Results*

The times to first failure in the BLCBT (first disconnection, detected at one of the five components mounted), varied between 100 and 3000 s for the different deflection amplitudes applied. Only PCB, tested with the 1mm amplitude set-up did not fail in the considered time range (>100000 s). Additionally, significant differences between the times to failure of the five components mounted on one PCB were observed. As expected, the centre component, enduring the highest loads, failed first. The other components (diagonally arranged) broke later or not at all. Especially at lower amplitudes, no failures were detected at the diagonal components; consequently, the results were based only on the first failures. For PCB 1, all amplitudes were tested, while for PCB 2 and PCB 3 only the 2mm amplitude was regarded. The results (mean values) are presented in Table 4. The data scatter is shown and discussed in chapter 4.3.

Table 4 Results of the BLCBT for the different deflection amplitudes, chosen for the PCB types respectively.

amplitude	*cycles to failure*		
mm	PCB 1	PCB 2	PCB 3
1	>2500000		
1.75	54317		
2.00	18939	15806	13635
2.75	8375		
3.00	4442		
3.50	3350		
4.00	1550		

The broken PCB from the BLCBT were analysed via a light microscope. Therefore, micro sections were prepared, starting at the outermost rows of the BGAs. If no failure was found, the next rows were micro-sectioned and analysed. However, almost all errors were found to be at the corners of the outermost rows of the BGA. The failure mode observed was always failure type b (described in chapter 1), regardless of the testing amplitude and the PCB type. A representative cross-section is shown in Fig. 7. The crack initiates and propagates in the solder close to the component. Based on these results, the maximum equivalent plastic strain in the solder was elected as local loading parameter, as it was known to correlate well with the low cycle fatigue lifetime of metals (chapter 3.3).

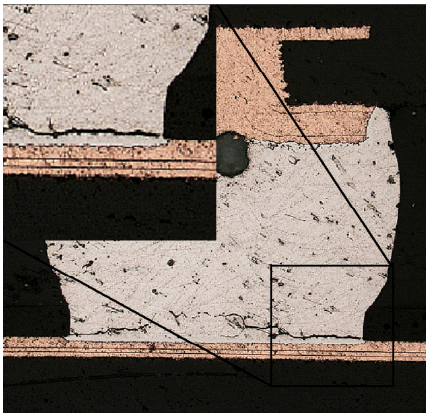

Fig. 7 Cross section of a solder bump of PCB 1, tested in a BLCBT. The crack is initiating and growing in the solder.

The experimental results of the BLDT were used for comparison only and are shown in chapter 4.3. The analysis of the PCB, which failed in the BLDT, revealed the same failure type and failure position (solder bumps at the corner of the outermost row) as the analysis of the BLCBT PCB.

4.2. *Simulation Results*

As described, the simulations of the BLCBT were performed stepwise. First, a global model was analysed. The rather coarse mesh only allowed a preliminary prediction, but could be used to determine the critical solder bumps. The solder bumps at the corner of the outermost row of the centre component were found to undergo the highest equivalent plastic strains. That was in complete agreement with the failure analysis, as these solder bumps were the first to fail. In Fig. 8, the equivalent plastic strain distribution of the solder bumps of the centre component in the global model is shown. Based on the global model results, a sub-model simulation of the critical solder ball was performed. In the sub-model simulations, a precise maximum equivalent stress of the solder was evaluated. The maximum values were found in the solder, close to the component (see the equivalent plastic strain distribution in Fig. 6), as expected, knowing the failure patterns from the experiments. The results for PCB1, PCB 2 and PCB 3 over the deflection are depicted in Fig. 9. Small but clear differences were observed. Due to the alteration of the matrix material of the inner layers in PCB 2 and PCB 3, the global deformation behaviour and thus the local loading conditions were changing.

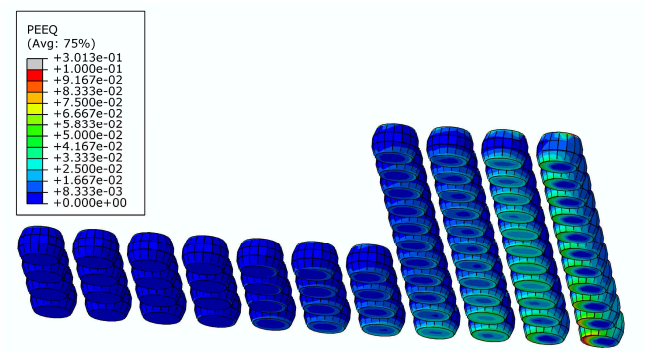

Fig. 8 Equivalent plastic strain distribution of the solder bumps of the centre component for a BLCBT deflection of 5mm calculated in the global model.

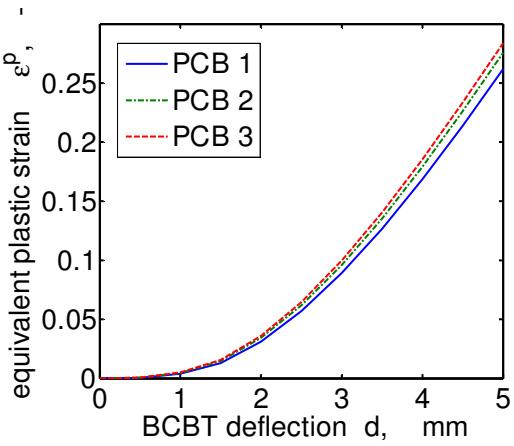

Fig. 9 Maximum equivalent plastic strain in the critical solder bump over the BLCBT deflection calculated in the sub-model for PCB 1, 2 and 3.

4.3. *Lifetime Analysis*

Using the results of the BLCBT experiments and the BLCBT simulations, a lifetime curve was modelled. The equivalent plastic strains of PCB 1 over their according lifetimes were fitted with the Manson-Coffin equation, resulting in values of 2.34+-0.46 for the exponent c and 73.17+-63.83 for the proportionality factor C (equation 2). The exponent c is known from literature to be, dependent on the material, around 2.0 [14], which is in agreement with the determined value. In Fig. 10, the experimental results of PCB1 are depicted together with the Manson-Coffin fit. An arrow indicates the 1mm deflection amplitude BLCBT results (no failure in the considered time range). The fitted Manson-Coffin equation corresponds with the results very well, particularly, as expected (the Manson-Coffin equation was developed for low cycle fatigue), the lower cycle fatigue range. Getting to the higher cycle range (> 40.000 cycles), the experimental data indicated a flattening of the strain lifetime devolution and the arrival at a steady level, which cannot be reproduced by the Manson-Coffin equation, limiting its range of application. However, typical PCB fail within the well described low cycle fatigue range. In Fig. 11, the results were plotted on double - logarithmic axes and additionally - in order to evaluate the prediction quality of the fit - the experimental results of PCB 2 and 3 (measured with a 2mm deflection amplitude) were added. The horizontal lines in the figure indicate the standard deviation of the measurement results. To approve the prediction method, the results should lie on the line of the Manson-Coffin fit. With respect to the mean values, a very good agreement was observed. The experimental results followed the predicted trend and were close the values calculated with the Manson-Coffin equation. However, taking into account the standard deviations, it has to be concluded, that the differences between the different board types were not significant. Therefore, the good correlation between the yet available experimental and the predicted results cannot be regarded sufficient to approve the method. Nevertheless, also the BLDT results (Table 5) agreed very well with the 2mm deflection amplitude results from the BLCBT, further supporting the applicability of the prediction procedure. When the BLDT results are compared with the BLCBT results, only the relative differences between the PCB types can be taken into account, as the loading type (cycles and dropstop failure respectively) is different. To compare the results, a linear correlation, based on the rate between the cycles to failure in the BLCBT and the time to failure in the BLDT of PCB1, was assumed.

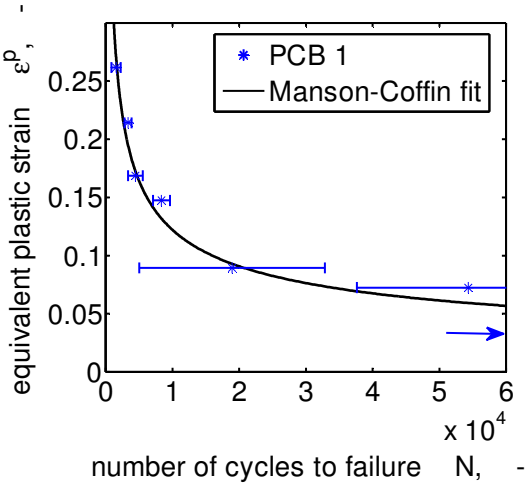

Fig. 10 The local loading parameter (equivalent plastic strain) over the number of cycles to failure for PCB1, with a fit of the Manson-Coffin equation. An arrow indicates the equivalent plastic strain, which does not lead to failure in the time range considered (> 250000 cycles).

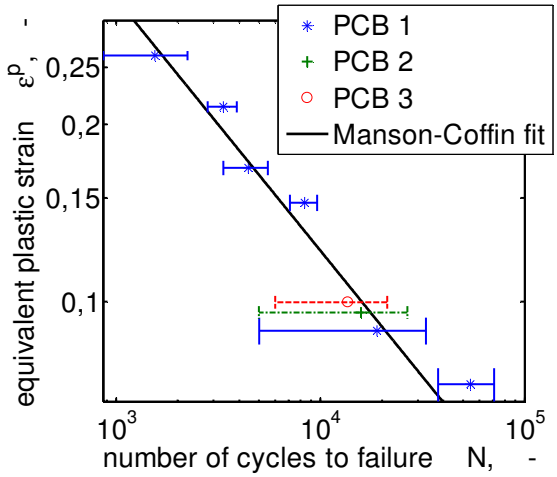

Fig. 11 The local loading parameter (equivalent plastic strain) over the number of cycles to failure for PCB 1 with a fit of the Manson-Coffin equation on a double logarithmic scale. Additionally, the results of PCB 2 and 3 are plotted to illustrate the good prediction quality.

Table 5 Comparison of the BLCBT and BLDT prediction and experimental results. For the BLCBT, the 2 mm deflection amplitude results are given.

		drops/cycles to failure		
		PCB 1	PCB 2	PCB 3
BLCBT (prediction)		20811	17614	16046
BLCBT (experiment)	mean	18939	15806	13635
	stdev	13923	10800	7634
BLDT (prediction)		636	538	490
BLDT (experiment)	mean	579	506	478
	stdev	268	256	234

5. Summary and Conclusion

The purpose of this work was to define an improved prediction methodology for the performance of PCB in a BLDT. Therefore, a lifetime prediction curve, based on BLCBT results, has been generated. The BLCBT was chosen, as its results are correlating with the BLDT results and it had the advantage, that different loading conditions are easily adjustable by changing the deflection amplitudes. Thus, adapting the BLCBT set-up, the lifetime range of interest could be covered, testing only one PCB type. Compared to other approaches, where different appropriate built-ups have to be defined, produced and tested, in order to cover the lifetime range, this poses an important saving of time and costs. Furthermore, the BLCBT is easy to be reproduced in a finite element simulation, enabling the calculation of a local loading parameter, correlating with the lifetime. This local loading parameter is needed; as failures in PCB are very small compared to the total board size and mainly depend on the local conditions. Thus, a simulation model was needed to accurately determine a parameter, describing the local situation. In this work, the failures were observed to initiate and propagate in the solder bump, connecting the board with the mounted components. Therefore, the maximum equivalent plastic strain of the critical solder bump, known to correlate with the low cycle fatigue life of metals, was used as local loading parameter. The experimental results of the BLCBT (lifetimes at different deflection testing amplitudes) and the simulation results (equivalent plastic strain according to the different deflection amplitudes) of one PCB type were utilized to model an equivalent plastic strain and lifetime correlation. A Manson-Coffin equation was fitted and used to predict the BLCBT lifetime of two other PCB types (differing by the materials used for the inner layers of the multilayer board). The results showed a very good agreement between the predicted values and the experiments (performed to evaluate the method), even if the differences between the PCB boards were not very big. Additionally, conducted BLDT also showed a very good correlation and approved the approach.

6. Acknowledgements

The research work of this paper was performed at the Polymer Competence Center Leoben GmbH (PCCL, Austria) within the framework of the COMET-program of the Austrian Ministry of Traffic, Innovation and Technology with contributions by the University of Leoben and by the AT&S Austria Technologie & Systemtechnik Aktiengesellschaft. The PCCL is funded by the Austrian Government and the State Governments of Styria and Upper Austria.

References

[1] “Board level drop test method of components for handheld electronic products,” *JEDEC Standard JESD22-B111*, no. July, 2003.

[2] P. F. Fuchs and Z. Major, “Cyclic bend tests for the reliability evaluation of printed circuit boards under dynamic loads,” *Frattura ed Integrità Strutturale*, vol. 15, pp. 64-73, 2010.

[3] X. Qu, Z. Chen, B. Qi, T. Lee, and J. Wang, “Board level drop test and simulation of leaded and lead-free BGA-PCB assembly,” *Microelectronics Reliability*, vol. 47, no. 12, pp. 2197-2204, Dec. 2007.

[4] C. Le Coq, A. Tougui, M.-P. Stempin, and L. Barreau, “Optimization for simulation of WL-CSP subjected to drop-test with plasticity behavior,” *Microelectronics Reliability*, vol. 51, no. 6, pp. 1060-1068, Jun. 2011.

[5] T. Tee, H. Ng, C. Lim, E. Pek, and Z. Zhong, “Impact life prediction modeling of TFBGA packages under board level drop test,” *Microelectronics and Reliability*, vol. 44, no. 7, pp. 1131-1142, Jul. 2004.

[6] T. Tee, H. Ng, and Z. Zhong, “Board level solder joint reliability analysis of stacked die mixed flip-chip and wirebond BGA,” *Microelectronics and Reliability*, vol. 46, no. 12, pp. 2131-2138, Dec. 2006.

[7] T. Tee, H. Ng, D. Yap, X. Baraton, and Z. Zhong, “Board level solder joint reliability modeling and testing of TFBGA packages for telecommunication applications,” *Microelectronics Reliability*, vol. 43, no. 7, pp. 1117-1123, Jul. 2003.

[8] E. H. Wong, S. K. W. Seah, W. D. van Driel, J. F. J. M. Caers, N. Owens, and Y.-S. Lai, “Advances in the drop-impact reliability of solder joints for mobile applications,” *Microelectronics Reliability*, vol. 49, no. 2, pp. 139-149, Feb. 2009.

[9] P. F. Fuchs, G. Pinter, and K. Fellner, “Local damage simulations of printed circuit boards based on determined in plane cohesive zone parameters,” *to be published*.

[10] “Specification for Finished Fabric Woven from ‘E’ Glass for Printed Boards,” *IPC - 4412A Amendment 1*, 2008.

[11] P. F. Fuchs, G. Pinter, and M. Tonjec, “Determination of the orthotropic material properties of individual layers of printed circuit boards,” *to be published*.

[12] H. Ma, “Characterization of lead-free solders for electronic packaging,” Auburn University, 2007.

[13] C.-Y. Chou, T.-Y. Hung, S.-Y. Yang, M.-C. Yew, W.-K. Yang, and K.-N. Chiang, “Solder joint and trace line failure simulation and experimental validation of fan-out type wafer level packaging subjected to drop impact,” *Microelectronics Reliability*, vol. 48, no. 8-9, pp. 1149-1154, Aug. 2008.

[14] S. S. Manson and G. R. Halford, *Fatigue and durability of structural materials*. ASM International, 2006, p. 456.